Wave Induced Loading and Stability of Rubble Mound Breakwaters

Hald, Tue

Publication date:
1998

Document Version
Publisher's PDF, also known as Version of record

Wave Induced Loading and Stability of Rubble Mound Breakwaters

Tue Hald

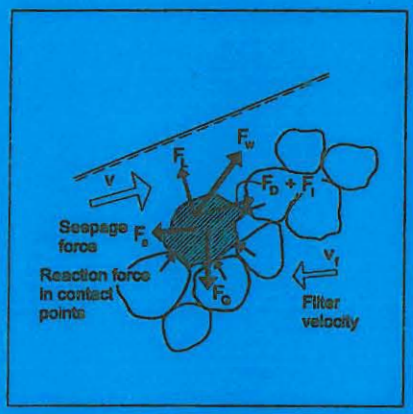

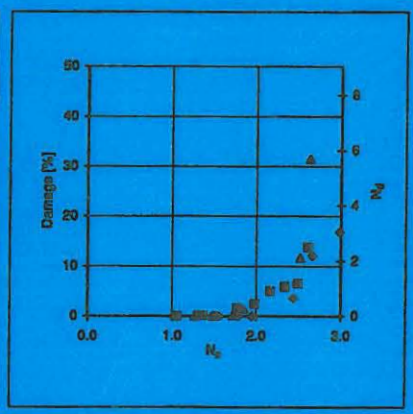

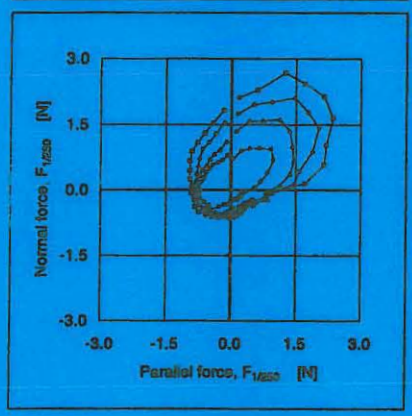

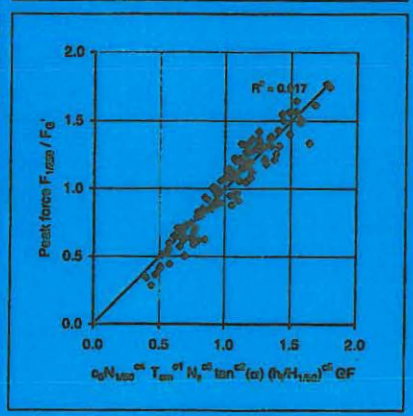

Hydraulics & Coastal Engineering Laboratory
Department of Civil Engineering
Aalborg University

June 1998

Hydraulics & Coastal Engineering Laboratory
Department of Civil Engineering
Aalborg University
Sohngaardsholmsvej 57
DK–9000 Aalborg, Denmark

ISSN 0909–4296
SERIES PAPER No. 18

Wave Induced Loading and Stability of Rubble Mound Breakwaters

by

Tue Hald

July 1998

Published 1998 by
Hydraulics & Coastal Engineering Laboratory
Aalborg University

Printed in Denmark by
Centertrykkeriet, Aalborg University

ISSN 0909–4296
SERIES PAPER No. 18

Preface

The present thesis *Wave Induced Loading and Stability of Rubble Mound Breakwaters* is submitted as one of the requirements for obtaining the degree of Ph.D. according to Order No. 989 of 11 December 1992 from the Danish Ministry of Education. The thesis is defended publicly 20 November 1998 at Aalborg University.

The study was supported by the Danish Technical Research Council (STVF) as part of the frame work programme Marine Techniques 2 (Marin Teknik 2) and was carried out in the period from Marts 1995 to July 1998 at Aalborg University (AAU). Associate Professor Peter Frigaard, Department of Civil Engineering, Aalborg University, acted as supervisor during the study.

During a 5 month stay at SINTEF Civil and Environmental Engineering, Department of Coastal and Ocean Engineering, Trondheim, model tests were carried out and analyzed. Special thanks to Alf Tørum, SINTEF for making the stay possible and to Tore Holm–Karlsen, Norwegian Coast Directorate for making it financial possible.

Last but not least the author wishes to thank his colleagues and the technical staff within the department.

Aalborg, July 1998.

Tue Hald.

Contents

List of Symbols

a_P	:	Slope parallel acceleration of water in runup wedge
A	:	Cross sectional area of armour stone at right angles to $\bar{v}$
A_e	:	Average eroded area
b	:	Middle side length of box fitting a stone
b_{50}	:	Average value of middle side length of box fitting a stone
C_a	:	Viscous force coefficient for internal flow forces
C_b	:	Drag force coefficient for internal flow forces
C_c	:	Inertia force coefficient for internal flow forces
C_D	:	Drag coefficient for external flow forces
C_L	:	Lift coefficient for external flow forces
C_M	:	Inertia coefficient for external flow forces
D_{15}	:	Unit cube length exceeded by 85% by weight of a sample
D_{85}	:	Unit cube length exceeded by 15% by weight of a sample
D_{n50}	:	Equivalent cube length $D_{n50} = (\frac{W_{50}}{\rho_m})^{\frac{1}{3}}$
E	:	Wave envelope
E_{max}	:	Maximum wave envelope
f	:	Frequency
$f(\cdot)$	:	Function of
f_p	:	Peak frequency
F	:	Force
F_D	:	Drag force
F_f	:	Internal flow force
F_G	:	Gravity force
F'_G	:	Submerged weight
F_I	:	Inertia force
F_L	:	Lift force
F_N	:	Normal force
F_m	:	Average force
F_p	:	Hydrostatic pressure force
F_P	:	Parallel force
F_w	:	Resulting wave induced force
F_s	:	Seepage force or resulting internal force

$F_{1/n}$	:	Average force of highest $1/n$ of the forces in a record
g	:	Gravity
GF	:	Groupiness factor
GF_{max}	:	Maximum groupiness factor
$GF(t)$	:	Groupiness factor function
h	:	Water depth
h_b	:	Water depth at breaking
h_t	:	Water depth at toe
H	:	Regular wave height
H_b	:	Breaking wave height
H_m	:	Average wave height
H_{m0}	:	Significant wave height based on spectral estimate
H_{max}	:	Maximum wave height
H_{max0}	:	Deep water maximum wave height
H_n	:	Average height of the highest n waves in a record
H_s	:	Significant wave height
H_{s0}	:	Deep water significant wave height
H_{zdc}	:	Zerodown-crossing wave height
$H_{1/n}$	:	Average height of highest $1/n$ of the waves in a record
$H_{n\%}$	:	Wave height exceeded by n % of the waves in a record
$H^2(t)$	:	Instantaneous wave energy
i	:	Hydraulic pressure gradient
K	:	Stability coefficient
K_D	:	Stability coefficient in the Hudson formula
KC	:	Keulegan-Carpenter number
l	:	Longest side length of box fitting a stone
l_{50}	:	Average value of longest side length of box fitting a stone
L	:	Regular wave length
L_0	:	Deep water wave length based on regular waves
L_m	:	Wave length based on T_m
L_{m0}	:	Deep water wave length based on $\frac{g}{2\pi}T_{m0}^2$
L_p	:	Wave length based on T_p
L_{p0}	:	Deep water wave length based on $\frac{g}{2\pi}T_{p0}^2$
n	:	Porosity
N_d	:	Number of stones moved in a down-slope row
$N_{\%D}$	:	Percentage damage
N_m	:	Number of moved stones
N_{ms}	:	Damage level equivalent number of moved stones
N_s	:	Stability number
N_z	:	Number of zero crossing waves
P	:	Permeability coefficient in Van der Meer's formulae
R_d	:	Rundown level
Re	:	Reynolds number
R_u	:	Runup level

s_m	:	Wave steepness defined as $\frac{H_s}{L_m}$
s_p	:	Wave steepness defined as $\frac{H_s}{L_p}$
s_{m0}	:	Deep water wave steepness defined as $\frac{H_{s0}}{L_{m0}}$
s_{p0}	:	Deep water wave steepness defines as $\frac{H_{s0}}{L_{p0}}$
S	:	Damage level
$S(f)$	:	Spectral density
t	:	Shortest side length of box fitting a stone
t_{50}	:	Average value of shortest side length of box fitting a stone
T	:	Regular wave period
T_{02}	:	Average period based on spectral estimate
T_m	:	Average period
T_{m0}	:	Deep water average period
T_{om}	:	Dimensionless period defined as $T_m\sqrt{\frac{g}{D_{n50}}}$
T_p	:	Spectral peak period
T_{p0}	:	Deep water spectral peak period
T_s	:	Significant period
Ur	:	Ursell number
v	:	Velocity of water in runup wedge
v_P	:	Slope parallel velocity of water in runup wedge
v_f	:	Bulk/filter velocity of the water outflow
V	:	Volume of armour stone
W_{15}	:	Unit mass exceeded by 85% of the stones
W_{50}	:	Average unit mass
W_{85}	:	Unit mass exceeded by 15% of the stones
z	:	Depth below SWL
$\bar{z}_i(x)$	:	Average profile
α	:	Slope angle
Δ	:	Relative reduced unit mass density $\Delta = \frac{\rho_m}{\rho_w} - 1$
η	:	Elevation
η_{max}	:	Maximum elevation
η_{min}	:	Minimum elevation
ϕ	:	Internal friction angle
γ	:	Peak enhancement factor
μ	:	Average value
ρ	:	Correlation coefficient
ρ_m	:	Unit mass density
ρ_w	:	Water density
σ	:	Standard deviation
θ	:	Direction of force
θ_S	:	Shields parameter
ξ	:	Surf similarity parameter
ξ_m	:	Surf similarity parameter based on T_m

Summary

Wave Induced Loading and Stability of Rubble Mound Breakwaters

The present state of knowledge when designing coastal structures has improved in the recent years. However the available design methods concerning especially rubble mound structures are characterized by a number of empirical and semi–empirical formulae making model tests inevitable and even when conducting model tests very large variability in e.g. the degree of stability is observed.

This background motivated the investigations conducted in the present study. The objective was to investigate and clarify which wave parameters are important for the hydraulic stability of the armour layer on typical rubble mound breakwaters. Furthermore, it was intended to quantify the influence on the stability of each parameter. Focus was put on the wave induced loading on single armour stones and the relation to the stability.

Based on existing litterature the state of physical understanding of the processes related to the hydraulic stability was discussed. Further, governing parameters influencing the stability were identified and their influence quantified to retrieve the state–of–the–art. Model tests were conducted at SINTEF with scale models of prototype breakwaters and both the wave induced loading and the stability were investigated. At Aalborg University model tests with an idealized model of a rubble mound breakwater were conducted and formed the basis for a detailed parametric investigation of the wave induced loading.

Based on analyses of the experimental data wave–force models were derived containing the direct influence of the investigated parameters on the wave induced forces. Comparison with results of stability investigations and commenly used stability formulae show good correlation with simple stability formulae based upon the derived force models.

Summary in Danish

Bølgeinducerede kræfter og stabilitet af stenkastningsmoler

Indenfor de seneste år er metoderne til design af kystnære konstruktioner blevet forbedret væsentligt. Med hensyn til specielt stenkastningsmoler er designmetoderne dog stadig karakteriseret ved et antal empiriske og halvempiriske formler, hvilket betyder at fysiske modelforsøg er uundgåelige. Til trods for at der udføres modelforsøg, kan der stadig observeres store udsving i f. eks. graden af stabilitet fra forsøg til forsøg.

Denne baggrund danner grundlaget for de undersøgelser der er blevet udført og beskrevet i nærværende rapport. Formålet var at undersøge og klarlægge hvilke bølgeparametre, der har betydning for den hydrauliske stabilitet af dæklaget på typiske stenkastningsmoler. Desuden var det hensigten at kvantifisere indflydelsen af hver enkelt parameter på stabiliteten. Vægten var koncentreret omkring bølgeinducerede kræfter på enkelte dæksten og disses sammenhæng med stabilitet.

Udfra eksisterende litteratur er graden af fysisk forståelse af de processer, der har forbindelse med den hydrauliske stabilitet, klarlagt. Desuden er de parametre der har betydning for stabiliteten identificeret og deres indflydelse kvantifiseret. På SINTEF blev der udført modelforsøg med skalamodeller af prototypemoler, og både de bølgeinducerede kræfter samt stabiliteten blev undersøgt. Et detaljeret model–parametrisk studie af de bølgeinducerede kræfter blev udført på baggrund af en række model forsøg udført på Aalborg Universitet med en idealiseret model af en stenkastningsmole.

Baseret på de eksperimentelle data blev bølge–kraft modeller opstillet for kraften i udvalgte retninger indeholdende den direkte indflydelse af de undersøgte bølgeparametre. Udfra de opstillede modeller blev simple stabilitetsformler udviklet og en sammenligning med resultater fra udførte stabilitetsundersøgelser samt almindelige anvendte stabilitetsformler viser at der opnås en god beskrivelse af stabiliteten.

CHAPTER 1

Stability of Breakwaters

1.1 The Rubble Mound Breakwater

Rubble mound breakwaters have throughout the history provided protection to mankind against the violent forces of the surrounding sea. Their applications are versatile, being used for the enclosure of harbour basins, in providing safe berthing facilities and for the protection of land (dikes) and beaches (offshore breakwaters).

Because of the various applications of rubble mound breakwaters at various sites, large variations in applied construction materials and environmental loading appear. Although appearing different, the cross section of the rubble mound breakwater have several points of resemblance, see Figure 1.1. The innermost

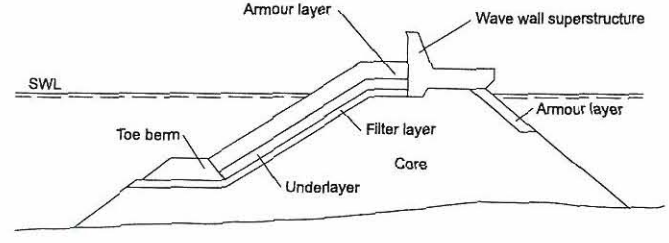

Figure 1.1: Example of typical rubble mound breakwater cross section.

part, termed the core, constitutes the major part of the breakwater. The core is a mound made of quarry run or gravel from the sea bed which in it self is not

able to resist wave attack and requires protection.

The armour layer is the outer seaward layer providing the protection against the major part of the exerted wave forces by a number of units sufficiently large and heavy to remain in position under wave attack. Normally, rock units are used, but if heavier units are needed or if natural sources of rock are not available, the units are made of concrete. On the leaside a rear armour layer is constructed to protect the breakwater against possible overtopping and wave disturbances from the harbour basin.

To provide a safe basis for the armour layer a toe berm is constructed and to improve the foundation for the armour layer one or more filter layers are placed between the core and the armour layer. Another purpose of the filter layer(s) is to prevent the finer materials in the core from being washed out through the gaps between the armour units.

In cases where access on the top of the breakwater is required or a reduction in the amount of overtopping is desired a crown wall is constructed.

Until the late 1960's the rubble mound breakwaters were exclusively used close to the coast and a fair amount of experience was available and natural sources of material were abundant for these situations. But as the construction of larger vessels and oil tankers was in progress a strong need for safe berthing facilities in deeper water arose and to fulfill these needs, the traditional near–coast structures were extended to deeper water simply by scaling. Hereby heavier equipment and artificial units were required and optimization of the costs for saving materials was necessary.

The dominating loads on breakwaters are due to waves interacting with the structure. Because the waves are irregular and of stochastic nature the waves are described by characteristic parameters, such as the significant wave height H_s defined as the mean of the highest one–third of the waves, rather than by individual wave parameters. With good accuracy the waves in deep water are described by the socalled Rayleigh distribution and thus the characteristic parameters are sufficient, but the transformation of the waves from deeper water into more shallow water involves refraction, shoaling and breaking processes which changes the character of the waves. As a result the largest waves break, making the distribution of the individual waves in shallow water differ from the Rayleigh distribution, and also the waves become more asymmetric. Obviously, the loads exerted by the waves and the succeeding response of the breakwater also change from deep to more shallow water.

To illustrate which governing design conditions existing rubble mound breakwaters are exposed to, the wave characteristics of the most important rubble mound breakwaters in Spain are shown in Figure 1.2. To distinguish between

the different wave conditions the following criteria are used:

- Breaking limit criterion:
$$\frac{H_s}{h} > 0.55$$
- Non–breaking criterion:
$$\frac{H_s}{h} < 0.35$$
- Shallow water criterion:
$$\frac{h}{L_0} < \frac{1}{20}$$
- Deep water criterion:
$$\frac{h}{L_0} > \frac{1}{4}$$

where h is the water depth.

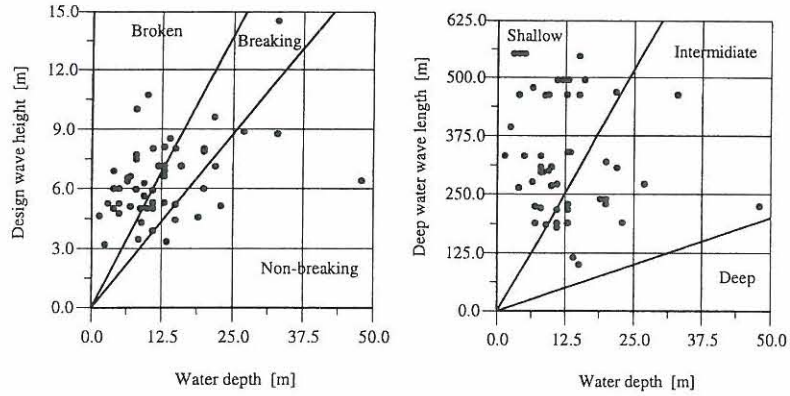

Figure 1.2: Wave characteristics of rubble mound breakwater build in Spain (From M.O.P.U. 1988).

Generally, the main part of the breakwaters are constructed in shallow water with breaking wave or close to breaking wave conditions. Only a few rubble mound breakwaters are constructed in deep water and in non-breaking conditions. This fact underline the importance of accurate design criteria in more shallow water.

1.2 Breakwater Failure Modes

The wave conditions at the location of the breakwater eventually leads to failure of the entire breakwater structure when a single structural component of the breakwater is not able to withstand the exerted wave forces or to fulfill its function. Thus, failure implies any partial or total collapse of one or more structural component leading to global collapse of the structure as a whole, but also

situations, when for instance the acceptable wave penetration into the harbour area is exceed, are considered as failure.

Because the rubble mound breakwater consists of several structural components different failure modes occur. Figure 1.3 outlines the possible failure modes for a typical rubble mound breakwater configuration including different soil and block layers, a berm and a crown wall.

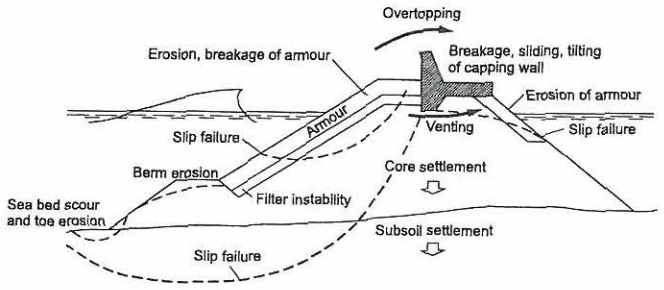

Figure 1.3: Possible failure modes for a rubble mound breakwater. From Burcharth (1993).

Due to the complexity of the rubble mound breakwater and the wave conditions many design concepts and design formulae have been developed until now for the different failure modes. Until the mid 1980's the Shore Protection Manual (1977, 1984) has been the state–of–the–art when designing breakwaters, but the inadequacy of the recommendations herein is clearly reflected by the vast amount of published research within rubble mound breakwaters during the last two decades.

Especially the hydraulic stability of the main armour layer on the seaward face has been subjected to research for many years in order to obtain a reliable design method, i.e. a method to determine the adequate stone weight of the single units in the armour layer to obtain a stable armour layer as a whole. This is not without due cause since the main armour layer usually constitutes the single most expensive part of the rubble mound breakwater as the layer has to protect the breakwater against the major part of the exerted forces. In some cases the construction costs of the armour layer constitutes up to 50% of the total construction costs but is most often about 20%.

1.3 Hydraulic Stability of Armour Layers

Different failure modes can be connected to the armour layer. The armour layer can fail as a whole where either the armour layer slides on the filter layer or becomes instable due to failure in a slip circle through both the armour layer and other parts of the breakwater. This type of failure is possible when the down-rush of one big wave is able to exert a force exceeding the friction between layers or in a slip circle, making this failure mode likely to occur only in case of a steep slope. Because of the seldom occurrence, this failure mode has not been paid much attention. Failure by instability of single units occur, when the dislocating force is greater than the stabilizing force. This type of failure mode is often decisive when designing a rubble mound armour layer.

It should be straight forward to assume, that a relation between the exerted wave loads and the stability of the armour layer would be of major interest, but the normal approach to the problem has simply been to relate easy accessible wave parameters, e.g. wave height and period, directly to the single unit weight. The design tools are physical model tests and/or empirical or semiempirical formulae based on model tests and prototype observations. The most important hydraulic stability formulae proposed are shown in Table 1.1. All shown formulae are modified from their original form to include the equivalent cube length D_{n50} instead of unit mass W_{50} in order to give some consistency in the comparison.

Generally all the stability formulae are of the type:

$$N_s = \frac{H_n}{\Delta D_{n50}} = K f(\cdot)$$

where:

N_s	:	Stability number.
H_n	:	Characteristic wave height.
Δ	:	Relative reduced unit mass density, $\Delta = \rho_m/\rho_w - 1$.
D_{n50}	:	Equivalent cube length, $D_{n50} = (W_{50}/\rho_m)^{\frac{1}{3}}$.
$f(\cdot)$	:	Function of.
K	:	Empirical coefficient determined by the parameters not accounted for in the stability equations.

Researcher(s)	Modified form
Castro (1933)*	$\frac{H}{\Delta D_{n50}} = \left\{ K_1 (\cot\alpha + 1)^2 \sqrt{\cot\alpha - \frac{2}{\rho_m}} \right\}^{\frac{1}{3}}$
Iribarren (1938)	$\frac{H}{\Delta D_{n50}} = K_2^{\frac{1}{3}} (\cos\alpha - \sin\alpha)$
Mathews (1948)*	$\frac{H}{\Delta D_{n50}} = \left\{ K_3 \frac{H}{T} (\cos\alpha - 0.75 \sin\alpha)^2 \right\}^{\frac{1}{3}}$
Epstein, Tyrrel (1949)*	$\frac{H}{\Delta D_{n50}} = K_4^{\frac{1}{3}} (\tan\varphi - \tan\alpha)$
Hickson, Rodolf (1951)	$\frac{H}{\Delta D_{n50}} = \left(K_5 \frac{H}{T} \right)^{\frac{1}{3}} \tan\left(45° - \frac{\alpha}{2}\right)$
Hudson, Jackson (1953)	$\frac{H}{\Delta D_{n50}} = K_6^{\frac{1}{3}} \frac{(\tan\varphi \cos\alpha - \sin\alpha)}{\tan\varphi}$
Larras (1952)*	$\frac{H}{\Delta D_{n50}} = K_7^{\frac{1}{3}} (\cos\alpha - \sin\alpha) \frac{\sinh \frac{4\pi z}{L}}{\frac{2\pi H}{L}}$
Beaudevin (1955)*	$\frac{H}{\Delta D_{n50}} = \left\{ K_8 \left(\frac{\cot\alpha - 0.8}{1.12 - 0.15\cot\alpha} \right) \right\}^{\frac{1}{3}}$
Hudson (1958)	$\frac{H}{\Delta D_{n50}} = (K_D \cot\alpha)^{\frac{1}{3}}$
Goldschtein, Kononenko (1959)*	$\frac{H}{\Delta D_{n50}} = (K_8 \tan^{1.83}\alpha)^{\frac{1}{3}}$
SN-92-60 (1960)*	$\frac{H}{\Delta D_{n50}} = \left(K_9 \frac{H}{L} \sqrt{1 + \cot^3\alpha} \right)^{\frac{1}{3}}$
Svee (1962)	$\frac{H}{\Delta D_{n50}} = K_{10}^{\frac{1}{3}} \cos\alpha$
Rybtchevsky (1964)*	$\frac{H}{\Delta D_{n50}} = \left(K_{11} \frac{H}{L} \right)^{\frac{1}{3}} \cos\alpha \sqrt{\cot\alpha}$

Table 1.1: Selected hydraulic stability formulae for rock armour layer.

continued

Researcher(s)	Modified form
Iribarren (1965)*	$\frac{H}{\Delta D_{n50}} = K_{12}^{\frac{1}{3}} (\tan\varphi \cos\alpha - \sin\alpha)$
Metelicyna (1967)*	$\frac{H}{\Delta D_{n50}} = K_{13}^{\frac{1}{3}} \cos(23° + \alpha)$
SPM (1977)	$\frac{H_s}{\Delta D_{n50}} = (K_D \cot\alpha)^{\frac{1}{3}}$
Losada, Giménez-Curto (1979)	$\frac{H}{\Delta D_{n50}} = \{A(\xi - \xi_0) \exp(B(\xi - \xi_0))\}^{-\frac{1}{3}}$
SPM (1984)	$\frac{H_{\frac{1}{10}}}{\Delta D_{n50}} = (K_D \cot\alpha)^{\frac{1}{3}}$
Hedar (1986)	$\frac{H_b}{\Delta D_{n50}} = \left(\frac{6}{\pi}\right)^{\frac{1}{3}} \left\{ \frac{B f_1(\gamma) \cos\alpha}{A(\frac{h_b}{H_b} + 0.7)(\tan\varphi + 2)} \right\}$
Medina, McDougal (1988)	$\frac{H_s}{\Delta D_{n50}} = \frac{1.86}{1.27} \sqrt{\frac{2}{\ln N_z}} (K_D \cot\alpha)^{\frac{1}{3}}$
Van der Meer (1988)	$\frac{H_s}{\Delta D_{n50}} = \begin{cases} 6.2\, \xi_m^{-0.5} P^{0.18} \left(\frac{S}{\sqrt{N_z}}\right)^{0.2} \\ \xi_m^P \sqrt{\cot\alpha}\, P^{-0.13} \left(\frac{S}{\sqrt{N_z}}\right)^{0.2} \end{cases}$

Notation:

H_n	:	Wave height	T	:	Regular wave period
L	:	Regular wave length	ξ_n	:	Surf similarity parameter
N_z	:	Number of waves	h_b	:	Water depth at breaking
z	:	Depth below SWL	D_{n50}	:	Equivalent cube length
Δ	:	Relative reduced unit mass density	ρ_m	:	Unit mass density
			α	:	Slope angle
φ	:	Internal friction angle	S	:	Damage level
γ, P	:	Permeability factors	$f_1(\gamma)$	:	Permeability function
K_x, A, B	:	Empirical coefficients	*	:	From PIANC (1976)

Table 1.1: Selected hydraulic stability formulae for rock armour layer.

Taking a look on the different design formulae in Table 1.1 large differences in the complexity and the influence of the different parameters is observed although several points of resemblance.

Several of the stability formulae considered are derived on a theoretical basis considering the forces acting on a single unit and followingly calibrated using model test with regular waves, only the formulae by Beaudevin (1955) is purely empirical. E.g Iribarren (1938, 1965) is based on sliding and Svee (1962) is based on lifting of the single units. Later tests with irregular waves justified the use of the significant wave height H_s in the Hudson formulae (1958) instead of the regular wave height H. This recommendation in SPM (1977) is still videly used in design today. However, in SPM (1984) H_s was replaced by the average of the highest 10% of the waves $H_{\frac{1}{10}}$. All formulae are derived with non–breaking waves and does not include the water depth h. This is included by Hedar (1986) suggesting the use of the breaking wave height H_b and water depth at breaking h_b. Moreover, the influence of permeability was also included.

By the use of irregular waves the importance of the duration of wave attack became important and Medina and McDougal (1988) extended the SPM (1984) recommendations to include the number of waves by assuming the waves to be Rayleigh distributed.

The influence of the wave period was included directly by Mathews (1948), Hickson and Rodolf (1951), Larras (1952), SN–92–60 (1960) and Rybtchevsky (1964) from which it can be seen that the unit size increases continuously with increasing period. Also Hudson was aware of the influence from the period, because the tests by Hudson and Jackson (1953) were carried out in a way which ensured that the worst wave conditions were tested. The design formula by Hudson (1958) is the most widely used due to its simplicity and today all formulae that resembles this are termed the Hudson–type stability formulae.

Later, Losada and Giménez–Curto (1979) included the effect of the wave period in the surf similarity parameter. In short, this parameter qualitatively describes the kinematics of waves breaking on a constant slope and from the stability formulae of Losada and Giménez–Curto minimum stability is observed for collapsing breakers. Depending on the type of breaking Van der Meer (1988) derived separate empirical formulae for plunging breakers and for surging breakers.

Despite the complexity of the stability formulae a large scatter between the damage predicted by the formulae and model test results still exists as illustrated in Figure 1.4.

This significant scatter in the model tests is mainly due to the stochastic response of the breakwater and the rather crude characterization of the waves. In Figure 1.4 the prediction by SPM (1977) makes no distinction between breaking

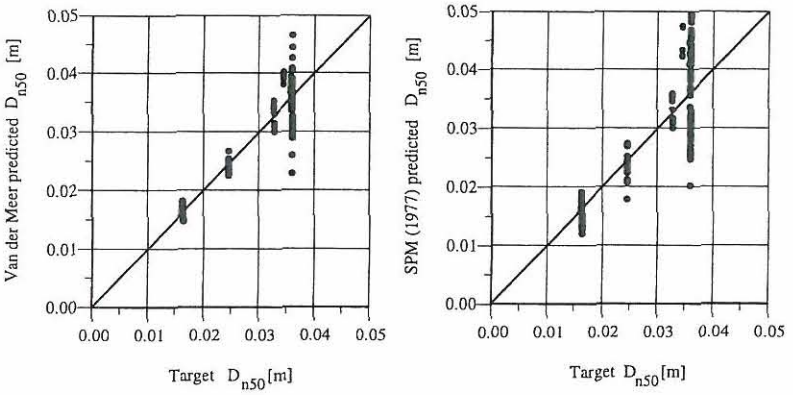

Figure 1.4: Example of scatter seen in the Van der Meer and the Hudson–type stability formulae in relation to model test results. Data from Van der Meer (1988) and Thompson and Shuttler (1975).

and non–breaking waves and waves of different periods whereas the prediction by Van der Meer (1988) does. Neither of the predictions take into account the different sea bed slopes and water depths. Moreover, the natural wave grouping, i.e. the succession of the individual waves in a wave train, is different in each of the conducted tests. Any information regarding wave grouping is omitted in the stability formulae although the breakwater responds differently to different types of grouping, e.g. Johnson et al. (1978) and Burcharth (1979).

1.4 The Design Situation

The majority of rubble mound structures are constructed in the near-coastal areas, i.e. normally in shallow water where the sea bed configuration influences the wave heights and kinematics. The available design methods concerning the design of rubble mound structures are characterized by a number of empirical or semi-empirical formulae making model tests inevitable. Even when model tests are conducted very large variability in e.g. the stability between individual model test is observed. All together, to obtain a reliable structure able to resist the design loads during its lifetime, very conservative safety factors must be employed with increased economical costs in consequence.

The large variability is motivated by three major sources:

- The varying character of the incident waves determined by the sea bed configuration and the interaction with the structure.
- The stochastic nature of the incident waves.
- The stochastic structural response of the rubble mound structures.

With background in the large experience in building mound breakwaters and the major research efforts especially during the last two decades to find reliable design tools, one major question still arises: *Why is it so difficult to design breakwaters?*

In Figure 1.5 the physical processes involved when designing a rubble mound breakwater and the related characterization of each process are outlined.

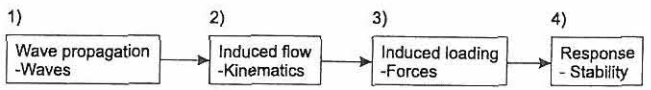

Figure 1.5: Basic scheme of the physical processes related to the hydraulic stability of a rubble mound breakwater under wave attack.

Considering the design formulae for the armour layer easy accessible wave parameters, e.g. wave height and period, have been used to characterize the waves and to design the armour layer. Hereby both the induced flow and loading are neglected. In deep water this approach works reasonable well because the wave heights are described very well by one distribution, namely the Rayleigh distribution.

In shallow water strong shoaling, refraction, and breaking can cause rather different wave kinematics and change both the wave height and the energy distribution. Because the wave load on the structure is determined by the kinematics of the incident wave, a breaking wave causes a different load than the load from a non-breaking wave of equal height. Consequently, the degree of instability and asymmetry of the incident waves becomes of importance making the deep water approach inadequate. Consequently in order to reduce the scatter other parameters such as groupiness, skewness and/or steepness must be included.

In common to both the deep water and the shallow water situation is the lack of a clear physical relationship between the processes outlined in Figure 1.5, i.e. between the wave parameters, the wave kinematics which actually determines the load, and the succeeding structural response. Thus, to obtain a more accurate prediction of the structural response, relevant wave parameters must be defined on basis of the structural response of the structure.

1.5 Objectives

The overall objectives of the present project is to investigate and clarify which wave parameters are important for predicting the structural response of coastal structures. Furthermore, it is intended to quantify the influence on the stability of each parameter. Derived wave parameters are to be applied in failure mode formulae.

Due to the videly use of rubble mound structures as coastal protection emphasis is put on this specific class of coastal structures. Furthermore, even when the prediction of the structural response is based on more complex formulae containing several information on the wave action, e.g. the Van der Meer formula, a large scatter still prevail.

In the following the scope of the thesis is outlined.

In chapter 2 a qualitative description of the four aspects related to the hydraulic stability (c.f. Figure 1.5) is given. The purpose is to reveal the state of physical understanding. Focus is put on the describing the wave induced flow and the hereby exerted wave forces. Also the significance of refraction, shoaling, and wave breaking on the characteristics of the shallow water wave field is discussed, i.e. changes in the wave height distribution and the wave form.

Chapter 3 is more concentrating on describing the commonly used approach when designing the armour layer, i.e. the direct link between the waves and the stability, c.f. 1) and 4) in Figure 1.5. Selected formulae for the hydraulic stability are studied in order to identify governing variables and comparison to different wave parameters is made to clarify and retrieve the influence.

In chapter 4 the direct correlation between the wave forces and the stability is investigated by physical model tests conducted at SINTEF, Trondheim with scale models of prototype breakwaters. The stability investigations were performed using different cross sections with different types of armour stone placements. A single cross section was selected for investigating the character of the wave forces over the slope.

To investigate the influence of different wave parameters in more detail, model tests with an idealized structure were conducted at Aalborg University. A simplified model of a rubble mound slope with strain gauge mounted stones was used in order to obtain a measurable response to individual waves and to make the tests reproducible. This detailed parametric study of the wave induced loading to different wave conditions is described in chapter 5.

Chapter 6 is devoted to a comparison between the common approach described in chapter 3 and the results obtained in chapter 5 relating the wave parameters to the exerted forces. Hereby a validation of the wave–force model can be made.

Chapter 7 will conclude the thesis.

CHAPTER 2

Hydraulic Stability Related Physics

The purpose of the present chapter is to uncover the state of physical understanding of the processes: wave propagation, wave induced flow, wave induced loading and structural response, and the link between these processes.

Primarily, the characteristics of the waves in both deep and shallow water are described. Secondly, the induced kinematics and forces related to the wave action on the slope are discussed. Finally, special attention paid to the identification of the character of the most damaging force and the related mode of damage.

2.1 Wave Propagation onto The Structure

2.1.1 Deep Water Waves

In deep water the shape and height of the waves are not influenced by the sea bed and the waves are normally being defined as deep water waves in terms of the ratio between water depth h and wave length L_0. Accordingly, deep water waves exists if:

$$\frac{h}{L_0} > \frac{1}{4} \tag{2.1}$$

Generally, the waves are stochastic in nature and it is necessary to characterize the waves by some characteristic parameter values. These properties are derived from the wave energy spectrum defining the distribution of energy over

the frequencies included in the wave train and the wave height distribution, see Figure 2.1 and 2.2.

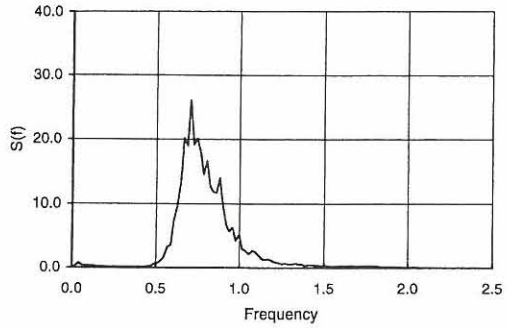

Figure 2.1: Typical deep water wave energy spectrum.

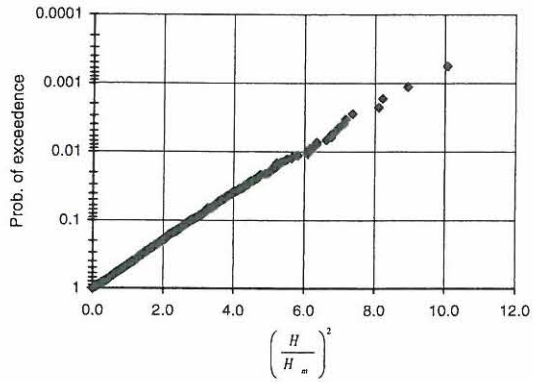

Figure 2.2: Typical deep water wave height distribution.

The waves are reproduced in accordance with a specified spectrum and the succession of the individual waves in the wave train is determined by the distribution of the phases associated with each frequency. Each phase is treated as independent random variables with a uniform probability density on the interval $[0;2\pi]$ leading to a Gaussian distributed surface elevation. If the spectrum is considered narrow–banded and the surface elevation is Gaussian distributed the wave heights follow the Rayleigh distribution with good accuracy.

In a natural wave train, group formations of high waves occur from time to time. This phenomenon is two–fold characterized by the spectrum shape and

the distribution of phases and must be described by two independent measures. Herein, the spectrum shape in terms of the peak enhancement factor γ and the groupiness factor GF are applied. The Groupiness factor is a global measure of the variance contained in the square of the wave height function, see enclosure 1:

- In the shape of the wave spectrum some group formation is inherent due to wave–wave interactions, e.g. a narrow–banded spectrum will contain a higher number of waves within each group than a broad–banded (see Elgar et al. (1985)). If two infinite long (and Gaussian distributed) wave trains of different spectral shape are considered the Groupiness factors are identical, i.e. the expected value of $GF \equiv 1$.
- However, within samples of a wave train with a given spectral width, different Groupiness factors can occur. This is a result of small deviations of the actual applied phases from the pure uniform distribution. When deviating from the uniform distribution also the wave height distribution will differ from being Rayleigh distributed, e.g. a higher degree of grouping will result in higher waves than prescribed by the Rayleigh distribution (see Mase et al. (1983)).

The notation for the most common used characteristic parameter values are given below. Whenever possible the recommendation given by IAHR (1987) in the "List of Sea State Parameters" are followed:

H	Wave height.
H_s	Significant wave height; The average of the highest one third of the waves. No distinction is made between frequency H_{m0} and time $H_{1/3}$ domain estimates.
$H_{1/n}$	Average height of highest $1/n$ of the waves in a record.
H_n	Average height of the highest n waves in a record.
$H_{n\%}$	Wave height exceeded by n % of the waves in a record.
H_{max}	Maximum wave height.
T	Wave period.
T_p	Spectral peak period.
T_m	Average period. No distinction is made between frequency T_{02} and time domain $\overline{T}$ domain estimates.
L	Wave length.
L_m	Wave length based on T_m.
L_{m0}	Deep water wave length based on $\frac{g}{2\pi}T_{m0}^2$.
s_m	Wave steepness defined as $\frac{H_s}{L_m}$.
γ	Peak enhancement factor.
GF	Groupiness factor.
N_z	Number of waves.

The above definitions applies to both deep and shallow water and in order to be able to differentiate between the two situations the deep water waves are indexed by a nought, e.g. H_{s0}.

2.1.2 Finite and Shallow Water Waves

During the wave propagating from deep water toward finite water, shoaling and possibly breaking takes place. As a result the waves become more non–linear and some energy transformation between the frequencies in the spectrum takes place.

Experience from various site specific model tests indicate that the following typical ranges signify wave breaking:

$$0.5 < \frac{H_s}{h} < 0.7 \tag{2.2}$$

Furthermore shallow water waves are defined if:

$$\frac{h}{L_0} < \frac{1}{20} \tag{2.3}$$

The shoaling and breaking processes influence both the wave energy spectrum as well as the wave height distribution, see Figure 2.3 and 2.4.

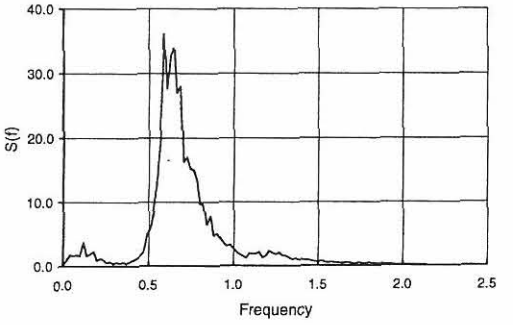

Figure 2.3: Typical shallow water wave energy spectrum.

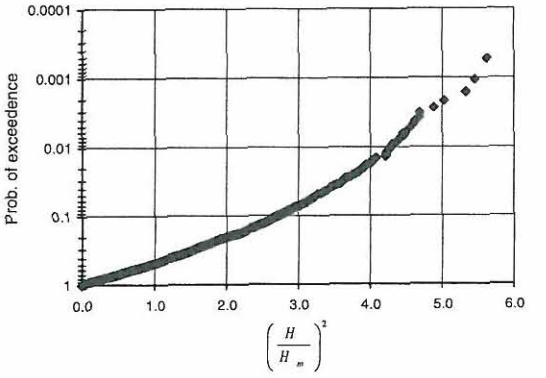

Figure 2.4: Typical shallow water wave height distribution.

Regarding the wave spectrum, energy is increased in the lower frequency area and at twice the peak frequency of the spectrum. These energy components are termed sub– and super harmonic, respectively, and occur as a result of non–linear interactions between the individual wave components of the spectrum.

Eventually when wave breaking occur the total amount of energy in the spectrum reduces. Unfortunately no simple models are able to take this into account in a proper way due to the complicated varying sea bed topography.

The wave breaking also influences the wave height distribution in that there exists relatively fewer large waves. As shown by Thornton and Guza (1983) the

deviations from the Rayleigh distribution occur for waves higher than $H_{1/10}$, i.e. the average of the highest 1/10 of the waves. For higher waves Klopman and Stive (1986) proposed based on a limited number of data a modified Glukhovskiy distribution in which the parameter H_s/h was included.

Only a few investigations concerning wave grouping characteristics in finite and shallow water exists even though the shoaling and breaking processes changes the shape of the spectrum and possibly also the phase distribution. Mase and Iwagaki (1984) report some effects of shallow water on the wave grouping in both natural and simulated wave data: In shoaling water the groupiness become smaller. List (1991) confirm this observation.

The Ursell number Ur is one of the most popular parameters for identification of shallow water and classification of the waves, as it represents both the rate of dispersion and the ratio of wave non–linearity:

$$Ur = \frac{H}{h}\left(\frac{L}{h}\right)^2 \tag{2.4}$$

If $Ur << 1$ the wave height is very small, so the non–linear terms are negligible, and the waves become linear. In case $Ur >> 1$ the waves are very long compared to the water depth thus having an almost constant velocity distribution over the depth. If $Ur = O(1)$ the waves are classified as the socalled Boussinesq type.

2.2 Flow on and inside The Structure

Eventually when the waves face the structure slope wave breaking will be triggered causing the water to rush up and down the slope, see Figure 2.5. The maximum level reached during uprush is termed the runup level R_u, and the minimum level reached during downrush is termed the rundown level R_d.

On the impermeable or less permeable slopes the up– and downrush will only take place in the outermost porous part of the structure causing the highest possible velocities. An increased permeability will reduces the flow velocities in the armour layer because larger proportion of the flow takes place inside the structure.

The wave action will also cause a rise of the internal water level, as indicated in Figure 2.5, leading to a complex internal flow field. The internal water level rise is a result of both a larger inflow period and inflow surface during uprush than during downrush.

The most critical flow field occurs in a zone around and just below SWL where

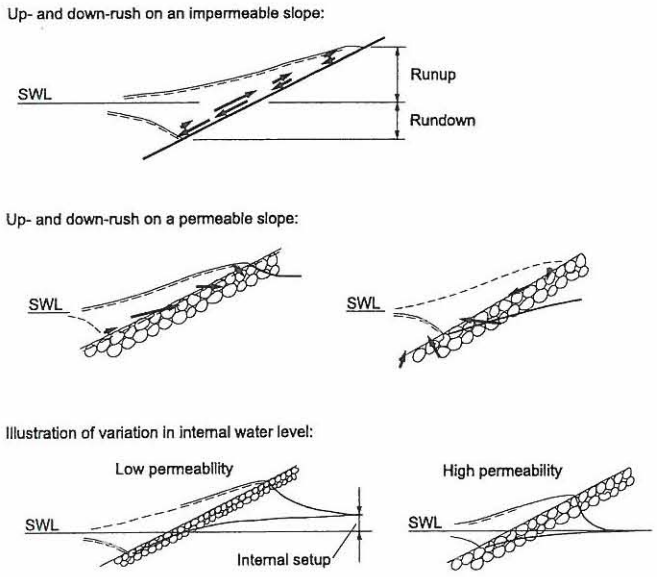

Figure 2.5: Illustration of up– and downrush on a slope. From Burcharth (1993).

the downrush interacts with the uprush from the succeeding wave. Hereby the most sudden changes in both the magnitude and the direction of the velocity occur. It is also in this region the largest velocities are produced.

Depending on the type of breaking and the structural characteristics the up– and downrush produces different situations with different kinematic characteristics as described in the following.

2.2.1 Breaking on The Slope

The type of breaking on the slope can be characterized by the surf similarity parameter

$$\xi = \frac{\tan\alpha}{\sqrt{\frac{H}{L_0}}} = \frac{\tan\alpha}{\sqrt{\frac{H}{\frac{g}{2\pi}T^2}}} \tag{2.5}$$

Typically, three forms of breaking occur on steeper slopes. For steep waves on a mild slope plunging breakers occur, characterized by the crest of the wave curling forward and impinging onto the wave trough, see Figure 2.6. For less steep waves on steeper slopes surging breakers occur, characterized by a narrow or nonexisting surf zone and high reflection and uprush, see Figure 2.6. The third type of breakers exists in the transition between plunging and surging and is called collapsing waves.

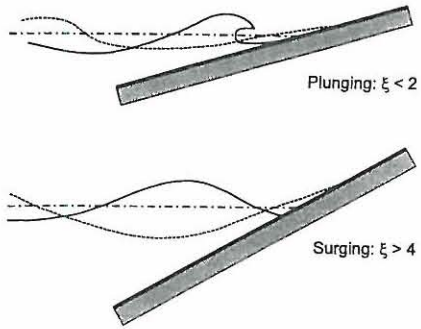

Figure 2.6: Two types of breaking waves on a steep slope.

As the wave breaking is closely connected to the kinematical wave characteristics it seems obvious also to use the surf similarity parameter to describe the effects of breaking on the velocities and accelerations on the structure slope.

In Figure 2.7 the maximum water particle velocity and acceleration on the slope as function of the surf similarity parameter is shown.

From Figure 2.7 the collapsing breaker ($2 < \xi < 3$) is identified as the situation when simultaneous high velocities and accelerations occur. In the collapsing breaker being the transition between plunging and surging breakers similarities to the flow under the two extremes are present.

The plunging breakers generally produce large acceleration due to the abrupt wave form change when the crest impinges onto the wave trough. The uprush level (as well as the downrush level) reached by the plunging breakers are opposite the surging breakers significantly lower.

The surging breakers generally feature large uprush accompanied by minor velocities during the up- and downrush and somewhat weaker accelerations under the

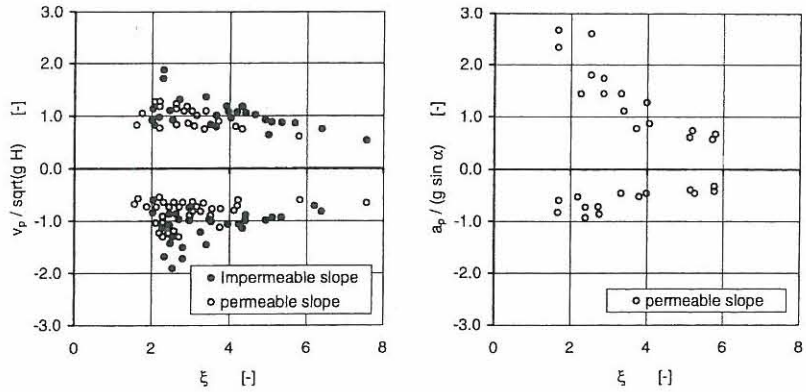

Figure 2.7: Effects of type of breaking on the water velocity and acceleration on the slope. (a) Change of maximum water particle velocity and (b) Change of maximum water particle acceleration. Data from Sawaragi et al. (1983).

front of the advancing wave crest than for the collapsing breakers. The amount of inflow and outflow through the surface of the structure slope is strong under the surging breaker.

Bruun and Johannesson (1974), Gunbak (1976) and Sawaragi et al (1982) applied the term resonance to describe the conditions on the slope matching the collapsing breaker. Bruun and Johannesson (1974) defined resonance as the situation when the downrush period is equal to the wave period so that every downrush meets the succeeding breaking wave at the lowest position of the downrush.

2.2.2 Up- and Downrush Velocities

No theory to estimate wave kinematics on a permeable rubble mound on which wave breaking takes place is available. Therefore only experimental data and rough estimates of the maximum velocity can be discussed.

A first approximation of the slope parallel velocity can be found by setting the potential at the maximum uprush level equal to the potential at SWL:

$$v_P = \sqrt{2gR_u} \tag{2.6}$$

Hudson (1958) derived the Hudson formula by assuming the runup level to be

proportional to the wave height, thus $v_P \approx \sqrt{2gH}$. From Figure 2.7 this assumption seems to be a good approximation in most situations on the rubble mound structure.

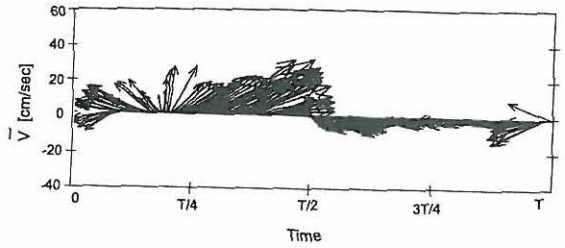

Figure 2.8: Variation of velocity vector during one wave period at position of armour stone displacement. After Melby and Kobayashi (1996).

The results by Sawaragi et al. (1983) referred in Figure 2.7 only show the magnitude of the peak velocities. Sawaragi et al. (1983) also concluded that maximum generally occur below SWL. Among others Tørum (1992) and Melby and Kobayashi (1996) investigated the variation of the velocity in several locations below SWL during one up– and downrush cycle. In the investigations by Melby and Kobayashi (1996) reported velocities were measured at the location of observed armour stone motion. An example of a velocity vector time series over one wave period measured approximately $h/3$ below SWL is shown in Figure 2.8. Large variations in magnitude and direction are observed and furthermore a large vertical velocity is observed just below the steep wave front. The shown velocity characteristics are not solely due to the external flow but also a contribution from the internal flow.

2.2.3 Internal Flow Velocities

The internal flow field have been investigated in both physical and numerical models and no simple models are able to predict the corresponding velocities. In Figure 2.9 illustrations of typical internal velocity fields during up– and downrush are given. The calculated velocities are based on a numerical FE–scheme solving the equations of momentum and continuity.

Figure 2.9 clearly depicts the complexity involved. Most interesting are the conditions around the lowest level of wave retreat where an outward directed internal jet of water occur causing high flow gradients near the structure surface. At this point the external flow also produces maximum velocities. Whether the produced flow is able to move any armour stone or not depend on the magnitude of the corresponding forces.

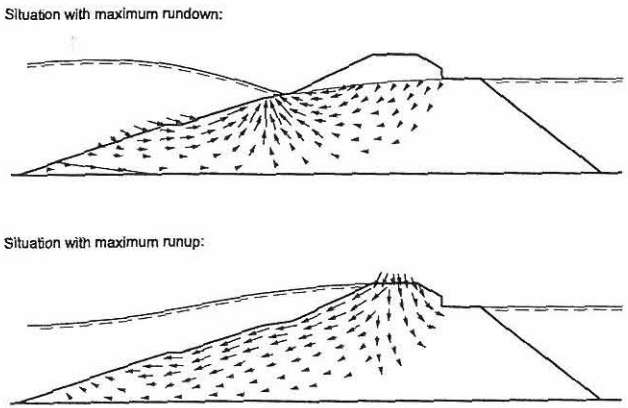

Figure 2.9: Typical internal velocity field at the time of maximum runup and rundown on a slope. From Barendes (1988).

2.3 Hydrodynamic and Gravitational Loading

The forces acting on an armour stone on the slope are schematized in Figure 2.10.

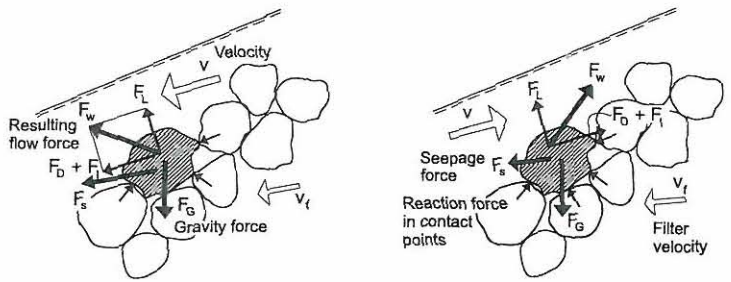

Figure 2.10: Illustration of forces on an armour stone.

As a result of the flow over the slope all forces except the gravity force can vary in size and direction with time. Depending on the type of failure mode that occurs the different forces will either act stabilizing or destabilizing.

The buoyancy force remains constant while the stone is submerged but changes to zero while the free surface passes over the stone. The gravity force F_G can be expressed as $\rho_m g D_{n50}^3$. As the buoyancy acts vertically upwards the submerged weight F'_G can be expressed as $(\rho_m - \rho_w) g D_{n50}^3$.

The resulting wave induced force F_w can be interpreted as the vectorial sum of a drag force F_D, a lift force F_L and an inertia force F_I, i.e. $\overline{F}_w = \overline{F}_D + \overline{F}_L + \overline{F}_I$.

As a result of outward directed flow and the internal water level rise a seepage force F_s arise.

The forces acting at the contact points with neighbouring stones are constant when no wave action and settlements take place but will change during wave action. In case the forces are directed into the mound large contact forces will be mobilized. However for forces directed away from the mound the contact forces will be severely limited.

2.3.1 External Flow Forces

The resulting wave induced force F_w can be considered as the net force resulting from the integration of the pressure on each point of the stone. However such an approach is only possible in very few cases and a simpler approach has to be used.

Applying the classical Morison equation the wave induced forces on a single resting armour stone can be expressed as:

$$F_D \approx C_D \rho_w A v|v| \tag{2.7}$$

$$F_L \approx C_L \rho_w A v|v| \tag{2.8}$$

$$F_I \approx C_M \rho_w V \frac{dv}{dt} \tag{2.9}$$

where

ρ_w	:	Density of water.
A	:	Cross sectional area of armour stone at right angles to $\bar{v}$.
V	:	Volume of armour stone.
v	:	Velocity of water.
C_D, C_L, C_M	:	Drag, lift and inertia coefficients depending of stone shape, Reynolds number Re and Keulegan–Carpenter number KC.

Originally, the Morison equation was used for describing forces on a vertical cylinder and the velocity was taken as the undisturbed velocity. For a stone

embedded in an armour layer the situation is different; The stone is in a boundary layer and partly sheltered by other stones influencing both the flow kinematics and the added mass.

However, the Morison formulation has a fairly sound physical background and several experiments have been conducted deriving drag and inertia coefficients.

Iwata et al. (1985) measured drag and inertia coefficients on a rounded rubble stone embedded in a two–layer rock armoured rubble mound slope. Both horizontal and vertical forces were measured verifying that the vertical force was governed by the lift force whereas the horizontal force was composed of both drag and inertia forces of comparable sizes. Drag and inertia coefficients were found to be in the order of 0.5.

Tørum (1992,1994) analyzed slope normal and parallel forces measured on a single stone in a berm breakwater as Morison type forces. Concerning the slope parallel force, the drag and inertia coefficients were found to be approximately 0.35 and 0.2, respectively. The variation with varying Keulegan–Carpenter number is shown in Figure 2.11. Attempts were made to model the normal force but the force was not purely lift dominated and no consistent coefficients were found.

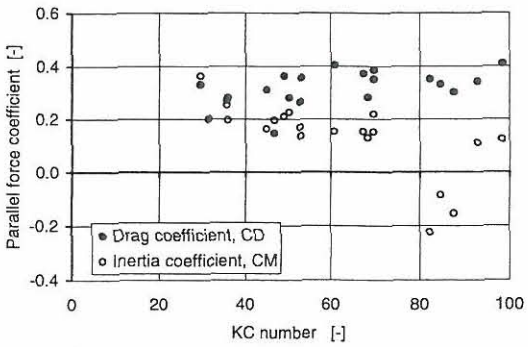

Figure 2.11: Variation of drag and inertia coefficients for parallel force. Data from Tørum (1994).

The variation of the resulting force along the slope was investigated by Sigurdsson (1962) and Sandström (1974) using spheres on a slope exposed to regular waves. Similar investigations were undertaken by Juhl and Jensen (1989,1990) using horizontal cylinders and irregular waves and comparable results obtained. An example of the results obtained by Sandström (1974) is presented in Figure 2.12 showing that the largest forces occur just below SWL.

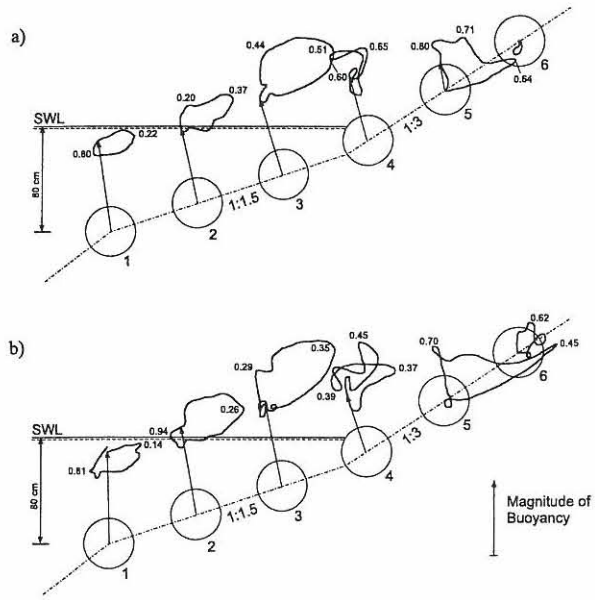

Figure 2.12: Example of force hodographs along the slope. Small numbers signify time in sec. a) $H = 7\,cm$ and $T = 0.8\,sec$, b) $H = 7\,cm$ and $T = 1.0\,sec$. After Sandström (1974).

2.3.2 Internal Flow Forces

A contributing term to the total normal force is possibly the seepage force F_s caused by the internal water flow out of the structure. The seepage force experienced by an armour stone is due to both the build up of hydrostatic pressure as well as the internal flow out of the structure, i.e. $\overline{F}_s = \overline{F}_p + \overline{F}_f$. The individual terms contributing to the seepage force may be expressed as, see Madsen (1974):

$$F_p \approx \frac{V}{1-n}\frac{\partial p}{\partial x} \tag{2.10}$$

$$F_f \approx \rho_w g \frac{V}{1-n} i \tag{2.11}$$

$$i = C_a v_f + C_b v_f |v_f| + C_c \frac{\partial v_f}{\partial t} \tag{2.12}$$

where:

$\frac{\partial p}{\partial x}$	:	Pressure gradient.
n	:	Porosity of core material.
V	:	Volume of armour stone.
i	:	Hydraulic pressure gradient.
v_f	:	Bulk/filter velocity of the water outflow.
C_a, C_b, C_c	:	Viscous, Drag and inertia force coefficients depending of stone shape, size, porosity, Reynolds number and Keulegan–Carpenter number.

Eq. (2.12) is also known as the extended Forchheimer equation by Polubarinova–Kochina (1952).

The viscous, drag and inertia terms have been evaluated in different flow regimes but only a few with special reference to wave induced flow in rubble mound structures. By oscillatory water tunnel tests Andersen (1994) and Burcharth and Andersen (1995) investigated the variation of the coefficients in the relevant Re and KC–range and expressions were derived for each individual coefficient. Normally, only the drag term is of importance and the viscous and inertia terms are omitted. A more detailed discussion of the importance of the three components for a wide range of coastal wave conditions is given by Gu and Wang (1991). Roughly, the drag coefficient C_b is in the order of $1.0/D_{n50} - 3.0/D_{n50}$ $[s^2/m^2]$ for a porosity of 0.4 and a Keulegan–Carpenter number of around 10.

The most important factor influencing the seepage force is the porosity (or the permeability). This, however, cannot be derived directly from eq. (2.11) and eq. (2.12) but is included in the force coefficients. From Günbak (1976), a high hydrostatic pressure build up takes place if the permeability is low. In this case the flow force is low since only small internal water level fluctuations are allowed.

For a high permeability the situation is reversed because the internal water level tend to follow the up– and downrush more closely.

The importance of the seepage force is very uncertain. The stone may start moving due to the seepage force but this motion changes the force as the local flow conditions changes. Barends and Hölscher (1988) analyzed the effect of porous flow and concluded that in the initial stage the stone is being lifted. If no other flow mechanisms occur the stone will remain in position. This, however, is not the case of a breakwater subjected to waves.

2.4 Loading Required for Armour Stone Motion

2.4.1 Displacement Mechanisms

In Figure 2.13 different types of failure mechanisms are depicted.

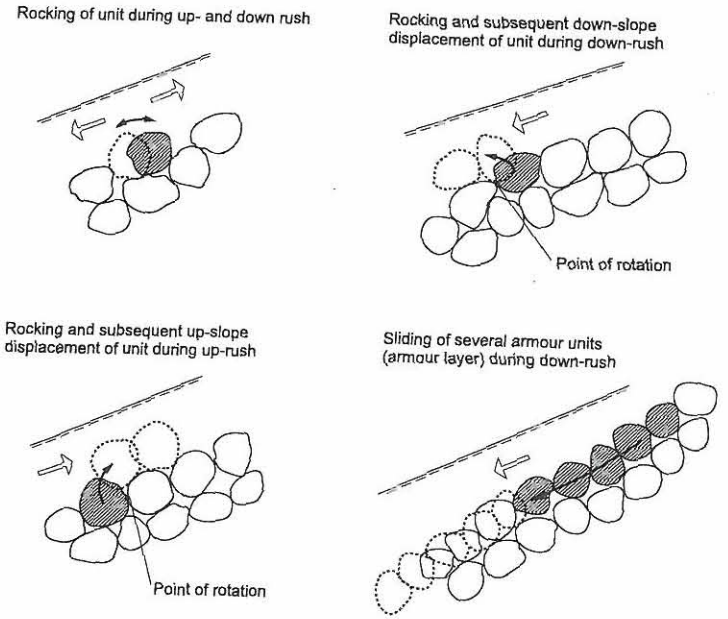

Figure 2.13: Typical armour layer failure modes. After Burcharth (1993).

Generally, it is accepted that the fluctuating pressure due to up– and downrush causes settlements in the armour below SWL and the armour stones become more closely packed. Above SWL the armour stones become less compact and may be drawn right out of the layer and following roll down during the downrush (or up during uprush if the slope is sufficiently mild). The loosened stones around SWL are more likely to displace than any other and Figure 2.14 demonstrates a typical damage distribution curves based on model tests conducted with irregular waves. Kobayashi et al. (1990a) identified, based on numerical simulations, that the initiation of damage is most likely to occur $0.75H$ below SWL.

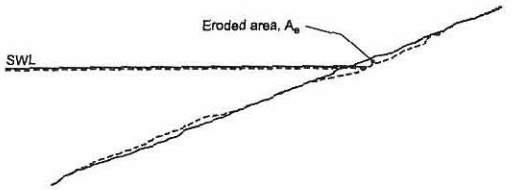

Figure 2.14: Typical measured damage distribution curve.

After the stone is being drawn out of the layer, rolling is the most dominant mode of motion. However, only very few observations of the incipient stone motion exists. Melby and Kobayashi (1996) report observations of rubble stone motions under regular waves. Accordingly, once loosened the armour stone would be drawn almost vertically out under the steep wave face during uprush followed by down slope rolling during the succeeding downrush. This was most pronounced under severely plunging or collapsing waves and the situation is more or less equal to the resonance situation previously described.

2.4.2 Character of Damaging Force

Iribarren (1938, 1965) considered sliding of the armour stone to be the dominant mode of motion, see Figure 2.15.

Neglecting the inertia force the criterion for stability is expressed:

$$F_D + F'_G \sin\alpha \leq \tan\phi(F'_G \cos\alpha - F_L) \tag{2.13}$$

By inserting the expressions for F_D, F_L, F'_G and $v \approx \sqrt{2gH}$ the criterion write into the following form:

$$\frac{\rho_w H}{(\rho_m - \rho_w)D_{n50}} \leq K(\tan\phi\cos\alpha - \sin\alpha) \tag{2.14}$$

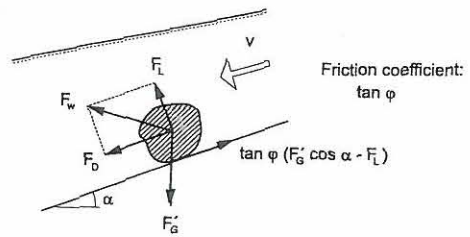

Figure 2.15: Idealized model of forces on armour stone during downrush.

Hedar(1960) supported the findings of Iribarren. Although considering rotation to be the dominant mode of motion Hedar reached the same stability criterion during downrush as Iribarren. Furthermore, Hedar found during uprush that the term $-\sin\alpha$ in eq. (2.14) changed to $+\sin\alpha$. However, Hudson (1958) abandoned the Iribarren formulation and developed an equation based on a simple quantitative force ratio between driving and resisting forces:

$$\frac{F_D + F_L}{F'_G} \approx \frac{\rho_w D_{n50}^2 v^2}{(\rho_m - \rho_w) g D_{n50}^3} K \tag{2.15}$$

where the velocity was approximated by $\sqrt{2gH}$ and the dimensionless function K was found by model tests to depend on $\cot\alpha$. In the formulation by Hudson the direction of the wave induced force is neglected.

Sigurdsson (1962) made measurements on sphere armour and the results showed that a possible displacement mechanism was a large force component normal to the slope. This could act simultaneously with a slope parallel force. Svee (1962) used this to develop a formula based on lifting only considering the normal force and assumed that the parallel force was transmitted from one stone to another down to the toe.

Latest transport formulations based on a Shield criterion have been used in both numerical and analytical approaches, e.g. Kobayashi et al. (1990b,c) and Cornett (1995). Basically, the Shield criterion approach is identical to Iribarren and from the definition of the Shield parameter θ the relation to the stability number N_s is found:

$$\begin{aligned} \theta &\equiv \frac{v^2}{\Delta g D_{n50}} \\ &\approx \frac{\sqrt{2gH}^2}{\Delta g D_{n50}} = \frac{2H}{\Delta D_{n50}} \end{aligned} \tag{2.16}$$

The obvious discrepancies between the different stability formulations might be explained by Bruun and Johannesson (1974). In a review of the hydraulics of rubble mound structures, two different situations that may produce sufficiently large destructive forces are discussed. One situation is when downrush velocities are maximum, producing high drag and lift forces. The other situation occur when downrush velocities, even if they are lower than the maximum velocities, join with suction (lift) forces occurring in the trough of a breaking wave. Simultaneously severe seepage may occur.

Cornett (1995) measured slope normal and parallel forces on panels of stones in regular waves and found that the direction of the peak force in all tested conditions varied between the normal direction and $\pm 45°$. This indicate a good correlation between the maximum induced force and the related mode of motion described by Melby and Kobayashi (1996). Comparing damage profiles and wave induced forces along the slope Araki and Deguchi (1998) also concluded that an upward directed force was able to lift up the rubble stones.

In conclusion, some confusion related to the identification of the most damaging force exist. However, the previous discussion indicate that a force component normal to the slope is required to displace any stone. This force occur simultaneous with a down slope directed force occurring during downrush or a somewhat smaller upslope directed force occurring in the socalled resonance situation.

CHAPTER 3

Hydraulic Stability Assessment

The common approach of relating characteristic wave parameters to the armour stone weight has evolved in a vast amount of published research in this area. However, the influence of the different parameters is not clear and uncertainties still exists.

Based on the discussion of the different involved physical phenomena in chapter 2 a list of relevant governing parameters is compiled. Secondly, based on a literature study the influence of the different governing parameters on the hydraulic stability is discussed. It is intended to clarify and retrieve the state-of-the-art.

3.1 Governing Parameters

The various stability formulae in Table 1.1 and the discussion in chapter 2 revealed the most important parameters governing the hydraulic stability of the armour layer and the wave induced loading on the armour stones. These governing parameters can be divided into two types: Structural and hydraulic parameters, and are summarized below. The structural parameters describe the geometry of the breakwater and characteristics of constituent material whereas the hydraulic parameters describe the wave action on the breakwater.

Main hydraulic parameters are:

- Wave height H
- Wave period T

- Duration of wave attack, characterized by the number of waves N_z
- Spectral shape γ
- Groupiness GF
- Water depth $h(x,t)$
- Water density ρ_w.

Main structural parameters are:

- Armour stone diameter D_{n50}
- Armour stone grading D_{85}/D_{15}.
- Armour stone shape and surface roughness.
- Armour stone density ρ_m.
- Slope angle $\cot\alpha$
- Crest height
- Permeability, porosity
- Armour layer thickness
- Placement pattern
- Internal friction angle

The great number of independent variables make it imperative to limit the lists above. Most of the structural parameters have larger influence on the stabilizing forces and does not influence the wave induced forces significantly. Of the listed parameters these are armour stone density, layer thickness, placement pattern and internal friction angle. Only the armour stone diameter, the slope angle, the crest height and the permeability have major influence on the induced loading. However, on rubble mound breakwaters no or only a little amount of overtopping is normally allowed leaving the influence from the crest height insignificant (see Van der Meer (1988)). Furthermore, the permeability is to certain degree influenced by e.g. the layer thickness making it difficult to separate the parameters completely.

If only the most important parameters are retained, a failure function describing

the hydraulic stability of the armour layer can be found based on dimensional considerations:

$$f(H, T, N_z, \gamma, GF, h, \cot\alpha, \text{permeability}, D_{n50}) = 0$$

There is no known mathematical relationship determining the failure function. Therefore, to determine correct similitude relationships the variables must be described in a dimensionless way.

3.2 Dimensionless Products

Dimensional analysis indicate that the functional relationship $f(\cdot)$ can be expressed:

$$f(\frac{H}{\Delta D_{n50}}, \frac{H}{L}, \frac{\tan\alpha}{\sqrt{\frac{H}{L_0}}}, \frac{h}{L}, \frac{h}{H}, N_z, \gamma, GF, \cot\alpha, \text{permeability}) = 0$$

Following a short discussion on each dimensionless product is made.

The stability number $\frac{H}{\Delta D_{n50}}$ appears in all of the present stability formulae and is a combination of two dimensionless products, the $\frac{H}{D_{n50}}$ and the relative mass density Δ. In fact the stability number is some measure of the ratio between the driving and the stabilizing forces as discussed in paragraph 2.4.2. E.g. if the driving force increases the stability number increases and a larger stone diameter is required to obtain the same degree of stability. On the other hand if two structures with different stability numbers are considered the structure having the highest stability number is most stable since it is able to resist a larger force.

The influence of wave period is included in the wave steepness and the surf similarity parameter describing the wave form and shape. According to chapter 2 different types breaking occur on the slope depending on the slope angle and steepness. In the surf similarity parameter these parameters are combined.

The effect of water depth is mainly on the highest waves in a wave train as described in chapter 2. Hence the two dimensionless terms $\frac{h}{L}$ and $\frac{h}{H}$ used to distinguish between the wave conditions in different water depths can also be used to describe the conditions of the wave attack on the breakwater.

The remaining parameters $N_z, \gamma, GF, \cot\alpha$ and permeability are in it self dimensionless and does not need any normalization.

3.3 Influence of Governing Parameters

3.3.1 Wave Height

The far most dominant parameter affecting the stability is the wave height as can be observed from the list of various stability formulae in Table 1.1. From here stability formulae showing different influence of the wave height have been selected and listed in Table 3.1. In order to be able to identify the influence, the equivalent cube length D_{n50} is used as a measure of stability.

Researcher(s)	$D_{n50} \propto$
Iribarren (1938, 1965)	H
Mathews (1948)	$H^{\frac{2}{3}}$
Larras (1952)	H^2
Hudson (1958)	H
SPM (1977)	H_s
SPM (1984)	$H_{\frac{1}{10}}$
Van der Meer (1988)	Plunging waves : $H_s^{0.5}$ Surging waves : $H_s^{1.0+0.5P}$ where $P = 0.1$ - 0.6

Table 3.1: Influence of wave height from selected stability formulae.

As seen from the Table 3.1 large deviations in the influence of wave height is present. The linear relationship suggested by Iribarren (1938, 1965) and Hudson (1958) is the far most used relation and has been supported by several researchers. This relationship has its background in the assumption that the wave force on the stone depends linearly on the wave height. Others, e.g. Mathews (1948) have deviated from this assumption in order to include the effect of wave period. Van der Meer (1988) indicated that the influence of wave height is different for plunging and surging waves, which suggests that different mechanisms are responsible for producing damage. This approach is fundamentally different from previous work and might resolve some previous discussions.

As indicated in Table 3.1 which wave height parameter that is suitable for characterizing stability when using irregular waves is also discussed. The SPM changed their suggestion from H_s to $H_{\frac{1}{10}}$ and later it has been suggested to use $H_{\frac{1}{30}}$ (Vidal et al. (1995)) and $H_{\frac{1}{20}}$ (Jensen et al. (1996)). However, these parameters does not take into account the duration of the wave attack and Vidal et al. (1995) proposed to use the wave height parameter H_n. Jensen et al. (1996) suggested that H_{250} was a suitable choice. Basically this discussion is not related to which

influence the wave height has, but more which irregular wave height parameter resembles the regular wave height best.

3.3.2 Structure Slope

In Figure 3.1 the influence of slope angle on the stability is shown for a selected set of stability equations.

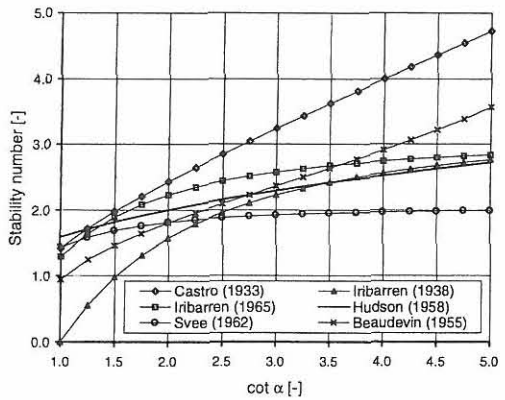

Figure 3.1: Influence of slope angle on stability. Redrawn from Bruun (1985)

The positive tendency of higher stability with flatter slopes is predicted by all of the plotted equations. However large deviations are observed despite the fact that all of the equations are based on regular waves. The large variations in Figure 3.1 might be explained by the two-fold influence of the slope angle:

- The proportion of the stone weight that acts stabilizing is decreased as the slope steepen.
- The type of breaking that occurs for a given wave situation is different for different slope angles and thus the wave induced forces.

Generally only the effect on stability have been included in the derivation of the various Hudson-type formulae and only later the influence on the type of breaking have been recognized as will be discussed in the next paragraph. The Hudson formula gives $D_{n50} \propto \cot^{-\frac{1}{3}} \alpha$ while the Van der Meer formulae give $D_{n50} \propto \cot^{-0.5} \alpha$ for plunging waves and $D_{n50} \propto \cot^{P-0.5} \alpha$ for surging waves. Comparing the two set of formulae, an almost similar positive trend is predicted by the Hudson formula and the Van der Meer formula for plunging waves.

3.3.3 Wave Period – Surf Similarity Parameter

The influence of the wave period was notified by the earlier Hudson–type formulae, see Mathews (1948), Hickson and Rodolf (1951), SN–92–60 (1960) and Rybtchevsky (1964). These design formulae suggest an increasing armour stone size with increasing period, see Table 3.2.

Researcher(s)	$D_{n50} \propto$
Mathews (1948)	$T^{\frac{1}{3}}$
Larras (1952)	$\frac{H}{L}\left(\sinh(\frac{4\pi z}{L})\right)^{-1}$
SN–92–60 (1960)	$L^{\frac{1}{3}}$
Van der Meer (1988)	$\begin{cases} \text{Plunging waves} & : T_m^{0.5} \\ \text{Surging waves} & : T_m^{-P} \end{cases}$

Table 3.2: Influence of wave period from selected stability formulae.

The second type of influence is presented by Larras (1952) suggesting the period to be included in the wave steepness. For a high wave steepness a high stone weight is required. With increasing period and decreasing steepness the effect diminishes.

Later Ahrens (1975) and Gunbak (1976) identified the surf similarity parameter as having significant influence on the stability. Minimum stability was observed for collapsing breakers (i.e. ξ = 3–4). For plunging breakers the armour stone size increases with increasing period whereas the size is reduced with period for surging breakers. However no quantification of the influence was given before Losada and Giménez–Curto (1979) and van der Meer (1988) derived equations including the surf similarity parameter using regular and irregular waves, respectively. The influence of surf similarity parameter predicted by the two set of design formulae is given in Figure 3.2.

Though different, the two formulae show similar tendencies. The differences are contributed to the use of regular waves and irregular waves in each case. The point of minimum stability is shifted to the right and the wave heights do not resemble as previously discussed.

3.3.4 Duration of Wave Attack

Most of the stability formulae were derived using regular waves causing a rather constant impact to the structure and an equilibrium in damage was reached in a short time. However, using irregular waves an equilibrium is not reached since

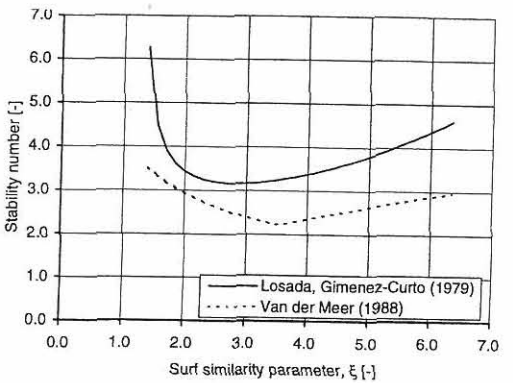

Figure 3.2: Influence of surf similarity parameter period on stability. $\cot\alpha, P = 0.5, N_z = 1000, S = 8.$

the maximum wave height increases with increasing duration according to the probability distribution. Thus, when a longer duration result in an increased maximum wave height the influence of the duration of wave attack cannot be neglected. Medina and McDougal (1988) included the effect of longer a duration by substituting the wave height in the Hudson formulae with the most probable maximum wave height likely to occur in N_z waves according to the Rayleigh distribution. Hereby, the influence becomes $D_{n50} \propto \sqrt{\frac{\ln N_z}{2}}$.

The effect of a continuing irregular wave attack was measured by Thompson and Shuttler (1975) for durations up to 15000 waves. About 100 tests were performed and latter reanalyzed by van der Meer (1988) concluding that the influence of number of waves on the diameter was $D_{n50} \propto N_z^{0.1}$.

For a wave attack of 500 – 5000 waves the two suggestions on the influence of wave attack are almost identical. However, the approach is only usable in deep water for which the influence relationships were developed.

3.3.5 Wave Grouping

No stability formulae have included the effect of wave grouping on the stability since no clear indication of the effects have been presented. Johnson et al. (1978) indicated that wave trains with long wave runs (groups) and high GF are most damaging. However, Burcharth (1979) concluded that wave trains containing wave jumps, i.e. changes in wave heights where a small wave is followed by a higher wave, are most damaging. Finally, van der Meer (1987) found no signifi-

cant differences between wave trains with high GF and narrow banded spectrum vs. low GF and broad banded spectrum.

Medina et al. (1990) tried to solve some of these apparent contradictions with respect to the influence of wave grouping and conducted a series of rubble mound stability tests. Two fundamentally different wave grouping characteristics were considered: 1) the average run length related to the spectral shape and 2) the energy flux exceedance pattern and the groupiness factor related to the phase distribution. Medina et al. (1990) concluded that the spectral shape was not relevant for armour stability. On the contrary, the stability was highly influenced by the groupiness factor GF defined on basis of the Hilbert Transform technique (described in Enclosure 1). Unfortunately the limited number of tests did not permit a precise description but as much as 50% of the variability of the average damage could be resolved by using the groupiness factor.

However, Vidal et al. (1995) showed that there is a correlation between the groupiness factor and the statistics of large wave heights. This correlation is expected since the groupiness factor is defined on basis of the deviation of the instantaneous wave energy, i.e $\sigma[H^2(t)]$. Since the wave height has major influence on the stability it seems still uncertain which effect the degree of groupiness has.

3.3.6 Water Depth

The effect of the water depth is not quantified in any stability formulae and has only been included in the formulae by changing a constant in order to differentiate between broken waves, waves breaking in front of the structure and non-breaking waves.

For non–Rayleigh distributed wave heights Van der Meer (1988) found that in more shallow water the stability is higher than in deeper water since the highest waves broke before reaching the structure. Based upon this Van der Meer suggested to use $H_{2\%}$, i.e. the wave height exceeded by 2% of the waves, to take into account deviations from the Rayleigh distribution. Accordingly the coefficients in the stability formulae were changed using the ratio $H_{2\%}/H_s = 1.40$ derived from the Rayleigh distribution. Although $H_{2\%}$ was found to be a good parameter other wave height parameters solely based upon the highest waves will give similar results.

In breaking waves in shallow water the wave height is determined solely by the water depth making it reasonable to include the water depth in the stability formulae as done by Hedar (1960, 1986). Hedar used the fraction h_b/H_b and the influence on the diameter therefore becomes $D_{n50} \propto f(\cdot)(h_b + 0.7H_b)$. However, since the fraction h_b/H_b at the point of breaking is almost constant the influence

vanishes and the Hedar formulae resembles the Hudson–type formulae despite the inclusion of permeability.

3.3.7 Permeability

The discussion about forces in chapter 2 argued for the importance of permeability/porosity, though no clear importance seemed valid. Regarding stability the influence of more permeable structures seems clear.

Bruun and Johannesson (1974) showed the importance of permeability but the influence was not included in any stability formulae before 1986. Hedar (1960, 1986) considered two types of structures, an impermeable and a permeable and concluded that the permeable structure has the highest stability.

Later van der Meer (1988) included the permeability by use of a socalled notional permeability coefficient P describing the construction of four typical cross sections. Generally, the same trend as that found by Hedar (1986) was identified; The stability increases with more permeable structures. The quantification of the influence of the permeability in terms of the notional permeability coefficient is somewhat arbitrary since the choice of the P–parameter is a matter of subjective judgement.

Structure config.		Stability number, $\frac{H_s}{\Delta D_{n50}}$		Percentage
Type	P	Van der Meer	SPM (1984)	difference
Impermeable	0.1	1.25	1.59	-21.4
Permeable	0.4	1.56	1.59	-1.9
Permeable	0.5	1.67	1.59	5.0
Homogeneous	0.6	1.79	1.59	12.6
Comparison based on: Collapsing breaker, $\cot\alpha = 2$, $N_z = 1000$, $S = 2$, $K_D = 2$				

Table 3.3: Influence of permeability in relation to the SPM (1984) formula.

In Table 3.3 the influence of permeability on stability given by Van der Meer (1988) is compared with the stability given by the Hudson–type formula. The configuration of the considered permeable structure compares very well with the structure of Hudson and the stability numbers are of similar size. If an impermeable structure is considered the armour stone diameter should be increased by 27% in order to obtain the same degree of stability. When considering the homogeneous structure, i.e. the most permeable, the necessary diameter can be decreased by approximately 11%.

3.4 Summary on Hydraulic Stability

The wave height and the structure slope have always been considered the two most dominating parameters influencing the stability. Later the influence of the wave period was recognized due to its strong relation to the level of up– and downrush reached in one wave. To separate between plunging and surging waves the wave period was combined with the structure slope in the surf similarity parameter. However, including the wave period in the stability formulae changed the believed effect of the wave height. Other parameters describing the influence of duration of wave attack, wave grouping, relative water depth and permeability have later been recognized to have some effect on the stability.

In conclusion, the influence of each of the parameters on the stability is well documented in qualitative terms. However, when trying to quantify the influence of each parameter the numerous involved structural and hydraulic parameters make it difficult to separate to influence from each single parameter considered.

CHAPTER 4

Investigation of Stability and Forces

The discussion in chapter 3 described the state of the art within the common approach of relating the stone weight directly to the wave characteristics. The more immediate approach of relating the stone weight to the forces exerted on the individual stones was discussed in chapter 2 and revealed the problems using this approach.

In the present chapter the character of the wave induced loading and the correlation with the hydraulic stability is investigated based on physical model tests. During the winter/spring 1997 a series of physical model tests have been conducted at SINTEF with focus on the hydraulic performance of the single layer rubble mound breakwater armour layer. For full reference see Hald and Tørum (1997).

The single layer was chosen because this armour layer type is the most frequently used breakwater in Norway. Furthermore, despite the fact that there have been several site specific investigations of the single layer breakwaters, e.g. for Søvær Fishing Port, Bratteland and Tørum (1971) and for Berlevaag Harbour, Kjelstrup (1977), only a few systematic investigations have been conducted until now.

4.1 The Single Layer Breakwater

Along the Norwegian coastline more than 600 breakwaters have been build since 1866. Some of these breakwaters are located on severely exposed locations with significant wave heights up to 6.5 m. The present value of these breakwaters is estimated to approximately 4.000 mill. NKr. The far most build breakwater type is the socalled single layer rubble mound breakwater utilizing only one layer of rock in the armour layer. This type of breakwater has developed from the time when heavy equipment was not easily available and the armour layer was constructed by dumping the stones from the breakwater crest.

Many of the older breakwaters in Norway were designed and built before any good knowledge of wave climate and on breakwater hydraulics was available, i.e. before the sixties. Thus experience and subsequent trial–and–error procedures were used.

Traditionally, the armour layer was constructed by dumping the armour stones from the breakwater crest from rail wagons or trucks. This dumping of the stones has to some extent been an art and the result depended also on the skills of the foreman. If an armour stone did not come into its right position it was necessary to use dynamite to blow it away before any new stones were placed. During the construction it was aimed at placing the stones orderly with the longest side almost perpendicular to the filter layer and the smallest area facing the waves, but often the result was a random placement. In order to make the stones roll in position the slope needed to be fairly steep and typical breakwaters were constructed with a slope of 1:1.25 to 1:1.5.

The period of construction was frequently over several years with longer breaks during winter and autumn due to hard weather. The winter storms have settled the unfinished breakwater and incurred small damages to it. Possible damages were subsequently repaired during the following construction period and the net result was an improved stability of the finished breakwater.

In some cases today backhoes have been used to place the stones orderly in the armour layer. This method can only be applied from a level of approximately 2 m below LWL because of the limited range of the backhoe. Below this level the armour stones are placed traditionally by dumping from crest. This calls for special attention paid to the lower part in order to secure a safe foundation for the orderly placed upper part. Recently some of the newer build breakwaters built this way have suffered heavy damage.

4.2 Model Test Setup

Based on investigations of cross sectional parameters and armour stone characteristics of the Svartnes, Årviksand and Sørvær (Tørum (1993)) breakwaters a 3D scale model of 1:30 – 1:40 has been designed. Characteristics of the armour stones are given in Table 4.1.

Armour layer	W_{50}	ρ_m [g/cm^3]	$\frac{W_{85}}{W_{15}}$ [-]	l_{50} [mm]	b_{50} [mm]	t_{50} [mm]	$\frac{W_{50}}{\rho_m (tbl)_{50}}$ [-]
Årviksand	11.7 t	2.8	2.5	-	-	-	0.40
Sørvær	22.0 t	-	1.7	-	-	-	-
Svartnes	18.0 t	-	1.6	-	-	-	-
Stone type A	152 g	2.7	1.8	80.5	54.1	33.3	0.40
Stone type B	306 g	2.7	1.9	96.2	67.5	42.0	0.41

Table 4.1: Armour stone characteristics.

The breakwater scale model was composed of a core with stones of 4–8 mm, a toe of 118 g stones, a filter layer of 6.4 g stones and a superstructure. The filter layer stone size has been designed according CIRIA–CUR (1991) and with a thickness of 50 mm corresponding to 3–4 stone diameters. On the filter layer the armour layer was constructed with a constant slope of 1:1.5. Two types of armour stones with different mass but similar grading and shape characteristics were used, see Table 4.1, type A and B. The toe has been designed to withstand the most severe waves in order to avoid reconstruction after every test. In Figure 4.1 the model cross section is shown.

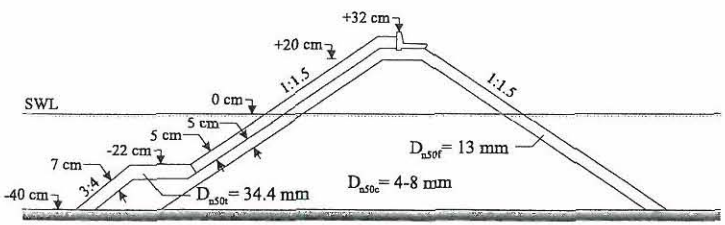

Figure 4.1: Model test cross section.

The model was installed on a slope of 1:30 in a 54 m long and 5 m wide basin approximately 25 m from the wave generator, see Figure 4.2. The breakwater head was constructed by rotating the cross section for the trunk 180° around a vertical axis through the centerline of the model. Opposite the wave generator

waves were absorbed on a parabolic shaped beach. To damp eventual cross modes perforated steel boxes were installed along both basin walls behind the breakwater model and in the gap between the model and the wall.

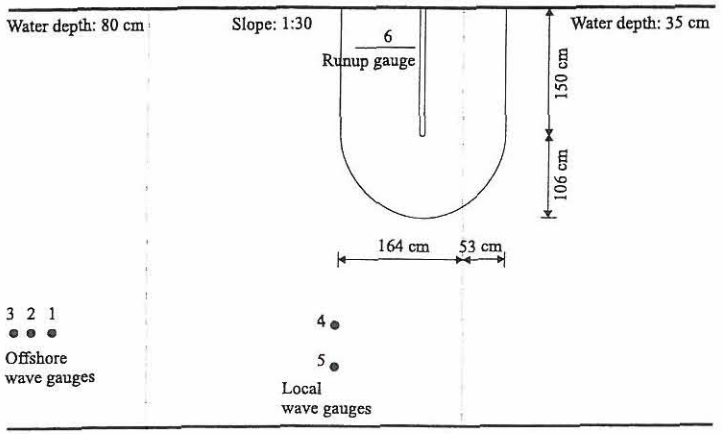

Figure 4.2: Model test layout.

Five resistance type wave gauges were used to measure the incident wave, see Figure 4.2. Three gauges were placed offshore on a constant water depth of 0.8 m and two gauges were placed in the gap between the breakwater model and the basin wall on a water depth of 0.4 m corresponding to the water depth at the toe. To measure the up- and downrush a resistance type gauge was placed on the slope. The sampling frequency was kept constant at 20.0 Hz. Elevation time series were analyzed by zerocrossing and spectral analyses and relevant wave parameters retrieved.

4.3 Stability of Armour Layer

4.3.1 Test Programme

Five different cross sections with five different types of armour stone placements were investigated. The tests were performed according to the test programme in Table 4.2.

Test identifier	Test runs	s_m	Armour layer characteristics	Cross section
A	3	3%	1–layer orderly, stone type A	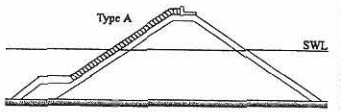
	3	5%		
B	3	3%	1–layer randomly, stone type B	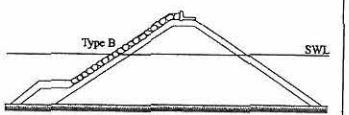
	3	5%		
Ca	1	5%	1–layer orderly above level –7 cm stone type A 2–layer randomly below level –7 cm stone type A	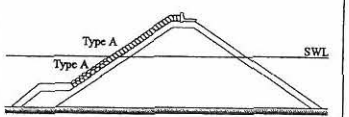
Cb	3	5%	1–layer orderly above SWL stone type A 2–layer randomly below SWL stone type B	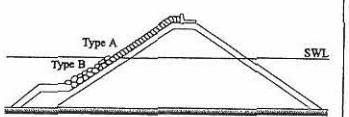
D	3	3%	1–layer orderly above level –7 cm stone type A 1–layer randomly below level –7 cm stone type B	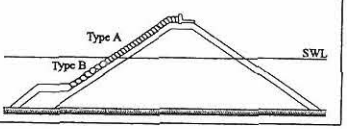

Table 4.2: Test programme for stability investigations.

In each test the steepness s_m was kept constant and the wave height was increased by 1.5 cm until failure was reached. The waves were generated according to a

JONSWAP spectrum with $\gamma = 3.0$. Each sea state was run for approximately 2000 waves without any repetitions of the signal. The armour stone placements and the sea states correspond to typical Norwegian breakwaters and typical prevailing storm situations in the Norwegian Sea.

Due to the stochastic nature of the waves and the constructed model all tests were repeated up to 3 times in order to provide some statistical sound data.

4.3.2 Damage Development

On the trunk profiles were measured by laser for every 10 cm over the width of the breakwater. Average profiles $\overline{z}_i(x)$ were obtained from 10 profiles, corresponding to a measurable width of 0.9 m. The difference profile $\Delta\overline{z}(x)$ between two individual profiles was calculated so erosion becomes negative, i.e.

$$\Delta\overline{z}(x) = \overline{z}_{i+1}(x) - \overline{z}_i(x) \tag{4.1}$$

Examples of representative damage profiles are shown in Figure 4.3– 4.5.

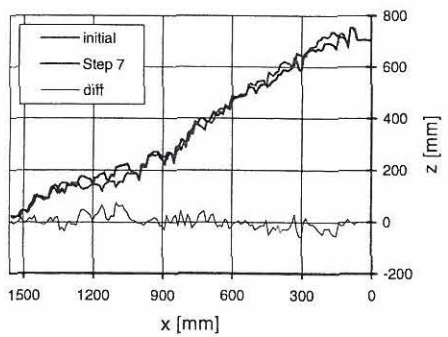

Figure 4.3: Damage profile for orderly placed stones on trunk, s_m = 3%.

The damage in Figure 4.3 begins above SWL by displacement of single stones from the armour layer followed by down–slope rolling of the stones. When the wave height increases the damage develops by displacement of more and more stones from the armour layer. As the stones are moved from the armour layer the remaining stones in the armour layer begin to turn downwards. In some cases the armour stones are hindered from turning by a high degree of interlocking and support from neighbouring stones. When sufficient stones have been displaced or turned downwards the high degree of support decreases and failure is inevitable.

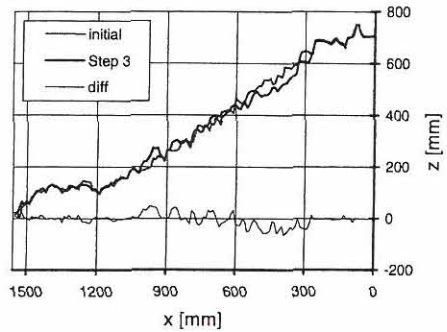

Figure 4.4: Damage profile for randomly placed stones on trunk, s_m = 3%.

For the randomly placed armour layer in Figure 4.4 the damage begins around SWL as a result of large settlements of the armour layer below water level. In single tests a long transverse fissure just above SWL with a width of 2–4 cm was observed. An increase in wave height resulted in displacement of more and more stones in the area around SWL. When armour stones were displaced, the stones above subsequently rolled or slide down to fill up the gab. This is a result of the relative steep slope and the little degree of interlocking present when placing the stones randomly in a single layer.

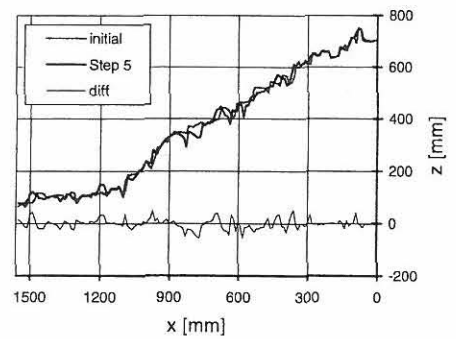

Figure 4.5: Damage profile for combined placement method, type Cb, s_m = 5%.

For the combined placement method, type Cb, in Figure 4.5 the damage initiate in the transition between the upper orderly and the lower randomly placed part.

From this level and below stones are displaced from the randomly placed part up till a certain damage level. After reaching this damage level the orderly part starts to slide. This overall behaviour is representative for all of the combined methods. However more a specific discussion is left to paragraph 4.3.6.

4.3.3 Damage Registration

The damage was registered by counting the accumulated number of moved stones N_m and by calculating the average eroded area A_e after each sea state run. The stones included in N_m were defined as the stones moved more than one D_{n50} from their original position and the stones that does not have a stabilizing effect.

The average eroded area was calculated by integration of negative values of $\Delta\overline{z}(x)$ between the toe and the breakwater crest.

$$A_e = \int_{x_{toe}}^{x_{crest}} (\overline{z}_{i+1}(x) - \overline{z}_i(x))\, dx \tag{4.2}$$

The damage level S was then calculated by

$$S = \frac{A_e}{D_{n50}^2} \tag{4.3}$$

Physically S can be interpreted as the number of squares with the length D_{n50} that fits into the average eroded area.

As a comparison between the two damage measures, i.e. the counting and the profiling method, the equivalent number of stones moved N_{mS} corresponding to the measured damage level S was calculated.

$$N_{mS} = \frac{Sl(1-n)}{D_{n50}} \tag{4.4}$$

where

l : Length of measurable part of trunk section, i.e. 0.9 m
n : Porosity of armour layer, $n = 0.4$

For small degrees of damage the counting method is considered the most reliable since the profiling also includes settling while profiling is considered better for larger degrees of damage when counting is more difficult.

Corresponding to the accumulated number of moved stones after each sea state the percentage damage $N_{\%D}$ and $N_d = \frac{N_m}{l/D_{n50}}$ that represents the number of stones moved in a down-slope row with the diameter D_{n50} were calculated.

The reason for using two damage measures is that the total number of stones in the armour layer is different for tested cross sections. E.g. when comparing the orderly and the randomly placed armour layers the same percentage damage corresponds to the same amount of erosion, but a different number of displaced stones. Same N_d gives same number of displaced stones but different eroded area.

4.3.4 Stability of Orderly Placed Stones

In Figure 4.6 the damage development for orderly placed stones on the trunk is shown for the wave steepness of 3% and the wave steepness of 5%, respectively.

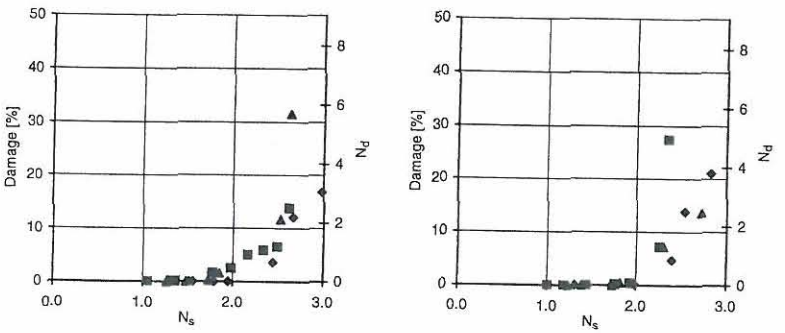

Figure 4.6: Damage development for orderly placed stones on trunk, s_m = 3% (left) and s_m = 5% (right).

From Figure 4.6 only little spreading between repeated tests and no or only little influence of wave steepness is observed. Generally the damage develops slowly. Considering a damage level of 5% the stability number is approximately 2.3 which corresponds to a stability coefficient K_D in the Hudson formula of 8.1.

4.3.5 Stability of Randomly Placed Stones

In Figure 4.7 the damage development for randomly placed stones on the trunk is shown for the wave steepness of 3% and the wave steepness of 5%, respectively.

From Figure 4.7 only little spreading between repeated tests and only little influence of wave steepness is observed. Opposite the orderly placed armour layer the damage development for the randomly placed armour layer is very rapid. Considering a damage level of 5% the stability number is approximately

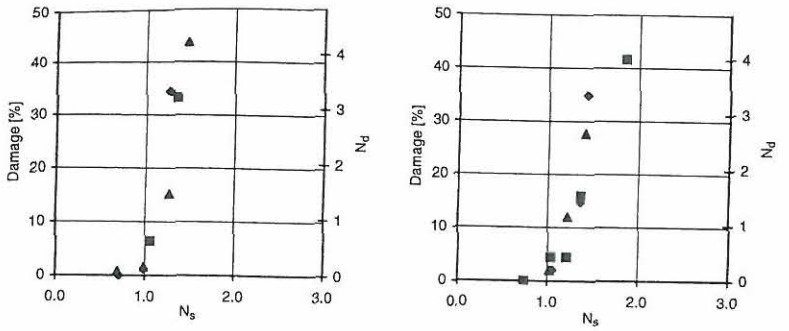

Figure 4.7: Damage development for randomly placed stones on trunk, s_m = 3% (left) and s_m = 5% (right).

1.05 for a steepness of 3% and 1.1 for a steepness of 5% which corresponds to a stability coefficient K_D in the Hudson formula of 0.8 and 0.9, respectively.

4.3.6 Stability of Armour with Combined Placement Methods

Figure 4.8–4.9 depicts the damage development for the tests with orderly placed armour stones on top of an armour layer constructed by randomly placed stones. For a more complete description of the combined placement methods it is referred to Table 4.2.

In Figure 4.8 the damage development for the construction type Ca (left) and Cb (right) is shown for a wave steepness of 5%.

For the construction type Ca the stone type A have been used in both the orderly and in the randomly placed armour layer. In Figure 4.8 (left) a slow damage development is seen. However, this is not a true picture of the behaviour since sliding of the orderly placed part starts at a certain damage level as previously described. At a damage level of 5% the stability number is 1.6 corresponding to a stability coefficient of 2.7.

For the construction type Cb the stone type B have replaced stones type A in the randomly placed lower part of the armour layer in type Ca. The damage development for type Cb is shown in Figure 4.8 (right). Compared to the Ca–type the behaviour of the armour layer is similar: Almost same slow damage development of the lower randomly placed armour layer followed by a rapid damage development of the upper orderly placed armour layer. At a damage

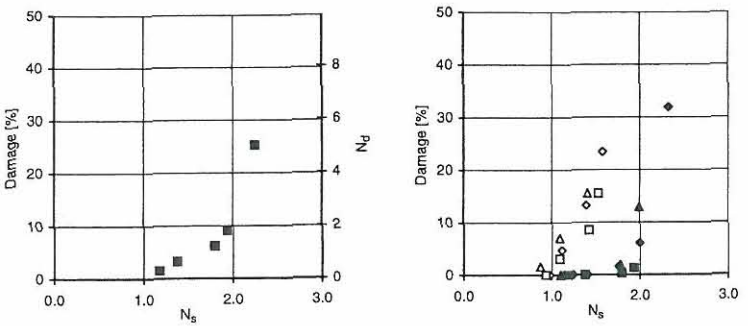

Figure 4.8: Damage development for combined placement methods, type Ca (left) and Cb (right), closed = stone type A, open = stone type B.

level of 5% the stability number is 1.2 corresponding to a stability coefficient of 1.2. This level is significantly lower than for type Ca since the transition between the two methods of placement is at a higher level, see Table 4.2.

In Figure 4.9 the damage development for the construction method D is shown for a wave steepness of 3%.

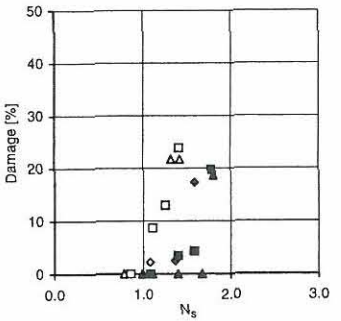

Figure 4.9: Damage development for combined placement method, type D, closed = stone type A, open = stone type B.

The construction method D differs from the C–types by the use of only one layer of stones in the randomly placed lower part of the armour layer and when comparing the way damage develops a more rapid damage development for the randomly placed part and a more slowly developed damage for the orderly placed part is observed. This is due to the larger settlements related to the single layer randomly placed armour layer. Corresponding to 5% damage the stability number is more or less similar with the Cb–type.

4.3.7 Overall Stability Performance

The stability performance of the placement methods A–D is summarized in Table 4.3 in terms of stability number and coefficient corresponding to 5% damage and $N_d = 1$. For comparison the K_D–coefficient for a conventional two–layer rubble mound breakwater is in the order of 2–4 following the recommendations in SPM (1984).

Method	$N_{\%D} = 5\%$		$N_d = 1$	
	N_s	K_D	N_s	K_D
A	2.3	8.1	2.3	8.1
B	1.1	0.9	1.3	1.5
Ca	1.6	2.7	1.6	2.7
Cb	1.2	1.2	–	–
D	1.1	0.9	–	–

Table 4.3: Stability performance of placement methods A–D.

The low stability obtained when placing the stones randomly as in method B is a result of the settlements of the armour layer causing stones to be isolated from neighbouring stones. Once isolated gravity is the only remaining stabilizing force. The settlements are not so severe when placing two layers of stones randomly since stones seldom become isolated and there will always exist some support from the neighbouring stones. The large increase in stability when using the placement method A in relation to the conventional two–layer rubble mound breakwater is a result of the very high degree of friction and support between the individual stones. In this case the settlements are not severe since the method of placing the stones does not allow the stones to rearrange.

4.4 Wave Induced Loading

4.4.1 Wave Force Registration

For measuring forces a single stone was selected and a reprint was made in coated plastic foam and succeedingly mounted on a force transducer able to measure two force directions. The force transducer was designed and manufactured by MARINTEK A/S, SINTEF, see Figure 5.4. The principle of the transducer is measuring shear strain in different cross sections enabling measurements of the force both parallel and normal to the slope. To avoid any contact with neighbouring stones a chicken wire was wrapped around the mounted stone with a distance of approximately 1 cm. The reprint was made in order to increase the natural frequency of the loading system enough to be able to measure possible impact forces. After mounting the stone a natural frequency in water of approximately 150 Hz was obtained.

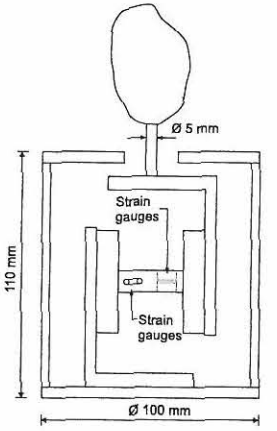

Figure 4.10: SINTEF force transducer with model stone mounted.

The force transducer with mounted stone was placed in four positions over the slope as shown in Figure 4.11. Also the definition of force directions is shown. Before positioning, the force transducer was calibrated in dry conditions up to 500 g.

Both tests with regular waves and irregular waves were conducted with the transducer positioned in all four positions. For regular waves a wave steepness of 3% and of 5% was tested by increasing the wave height in three steps: 9.0 cm, 12.0 cm and 15.0 cm. For irregular waves the wave height was kept constant at 13.5 cm

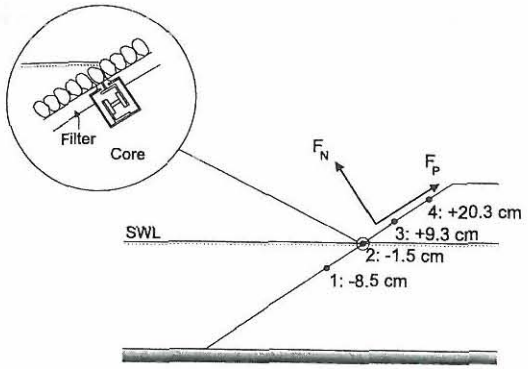

Figure 4.11: Position of force transducer and positive direction of forces.

for both steepnesses. Forces were sampled at 500.0 Hz and subsequently lowpass filtered with a cutoff frequency of 250.0 Hz for regular waves, and at sampled 40.0 Hz and subsequently lowpass filtered with a cutoff frequency of 20.0 Hz for irregular waves.

In the measured force time series maxima and minima peaks have been determined by zerocrossing analyses of the time derivative of the measured force time series. In order to determine only independent peaks, registered peaks within a desired filter width are sorted out leaving only one peak within one wave period.

4.4.2 Wave Force Characteristics

Measured force characteristics are shown in Figure 4.12–13. Generally, force characteristics are invariant with varying wave height within the tested range why only results from tests with $H = 15.0$ cm are presented.

Comparing Figure 4.12 and 4.13 somewhat larger forces are observed for a steepness of 3%. Also notice that the largest forces occur 10 cm below and 10 cm above SWL (in position 1 and 3) despite that the waves break directly upon the stone positioned in SWL (in position 2).

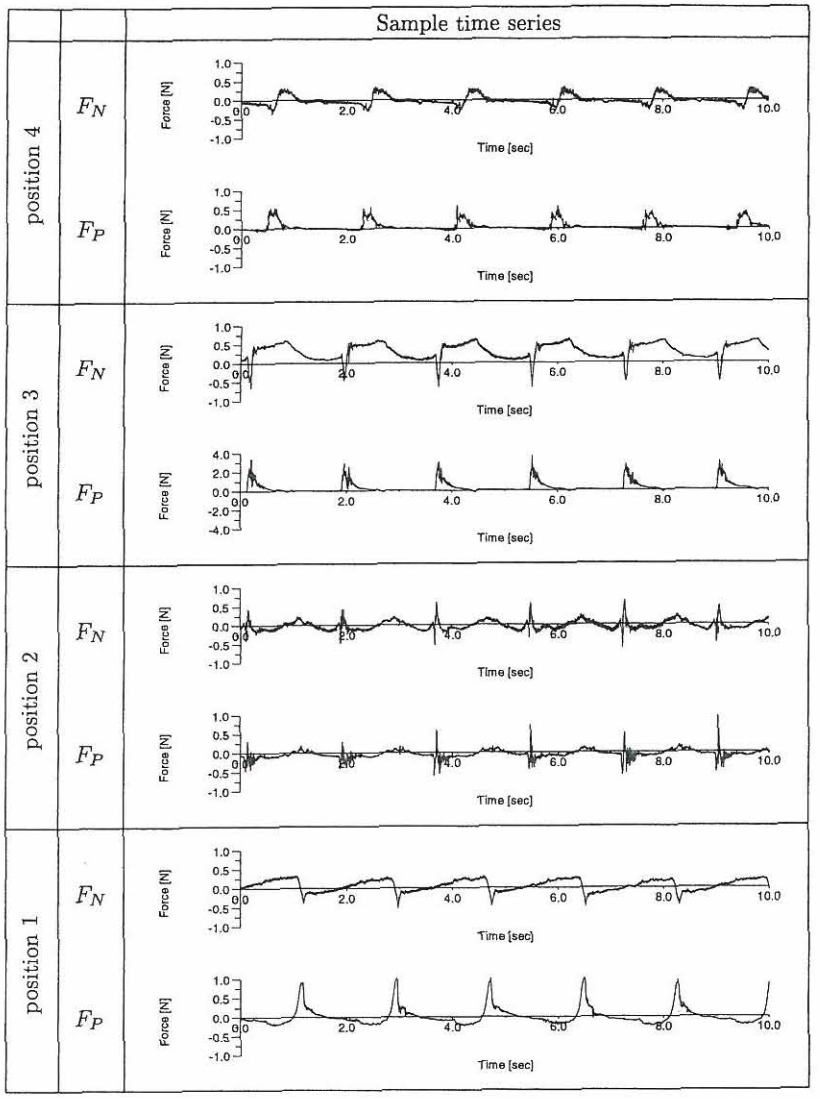

Figure 4.12: Sample normal and parallel force time series for $s_m = 3\%$, $H = 15$ cm.

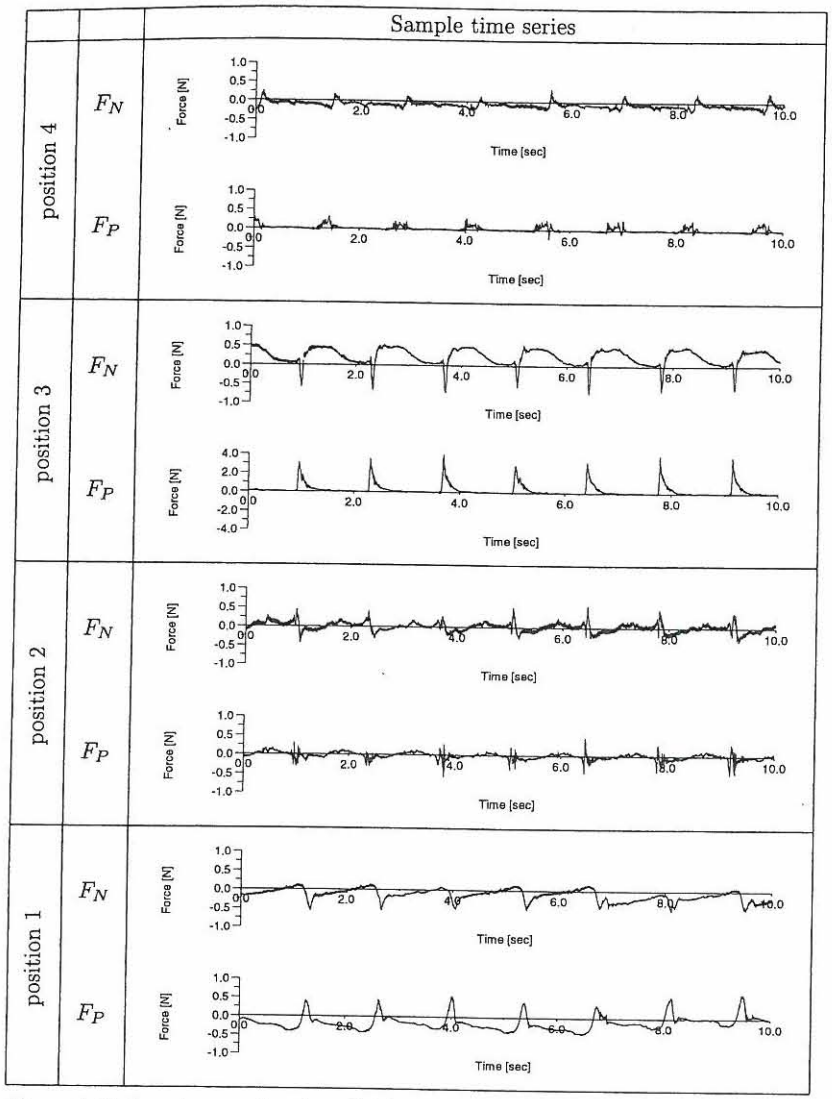

Figure 4.13: Sample normal and parallel force time series for $s_m = 5\%$, $H = 15\,cm$.

4.4.3 Regular Wave Induced Loading

To illustrate how the total force and corresponding direction varies down the slope all combinations of normal and parallel force at different time steps within one test are plotted in a (x,y)–coordinate system – a socalled hodograph. As the total force varies in each direction, the average force within intervals of 5° was calculated. In Figure 4.14 hodographs for each position and each combination of wave height and period are shown.

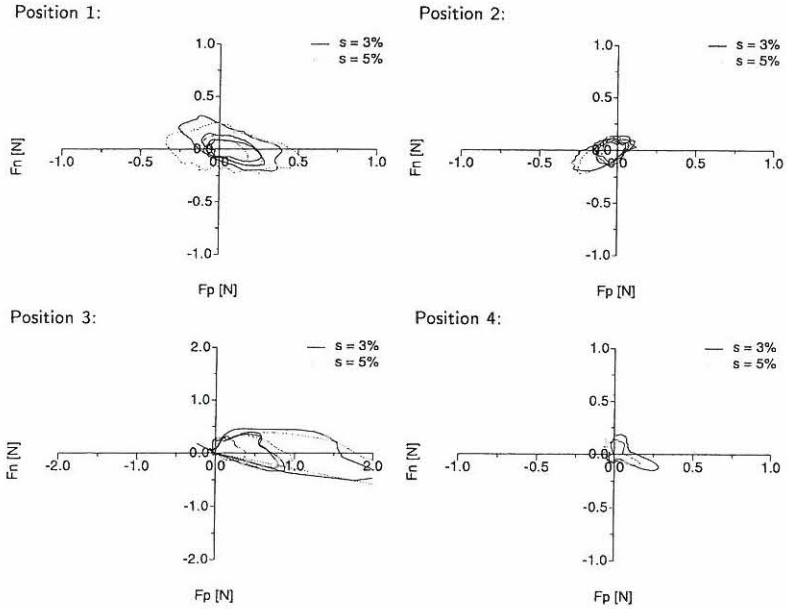

Figure 4.14: Hodographs based on F_m at position 1–4 for regular waves.

Generally, the shape of each hodograph for all combinations of wave height and period within each position is very similar, c.f. Figure 4.14. The largest forces occur below and above SWL in position 1 and 3. In position 1 the dominating forces are either directed outwards and down–slope or inwards and up–slope. In position 2 the forces are smaller and of more or less the same magnitude in all directions. Further up–slope in position 3 the largest forces occur in up slope direction and mainly parallel to the slope. In position 4 the force is of the same character as in position 3 but only smaller.

The most interesting forces are the destabilizing forces in outward directions and in order to get an impression of the vertical distribution along the slope three outward directions are selected: 45° down–slope, 90° slope normal and 45° up–slope, see Figure 4.15.

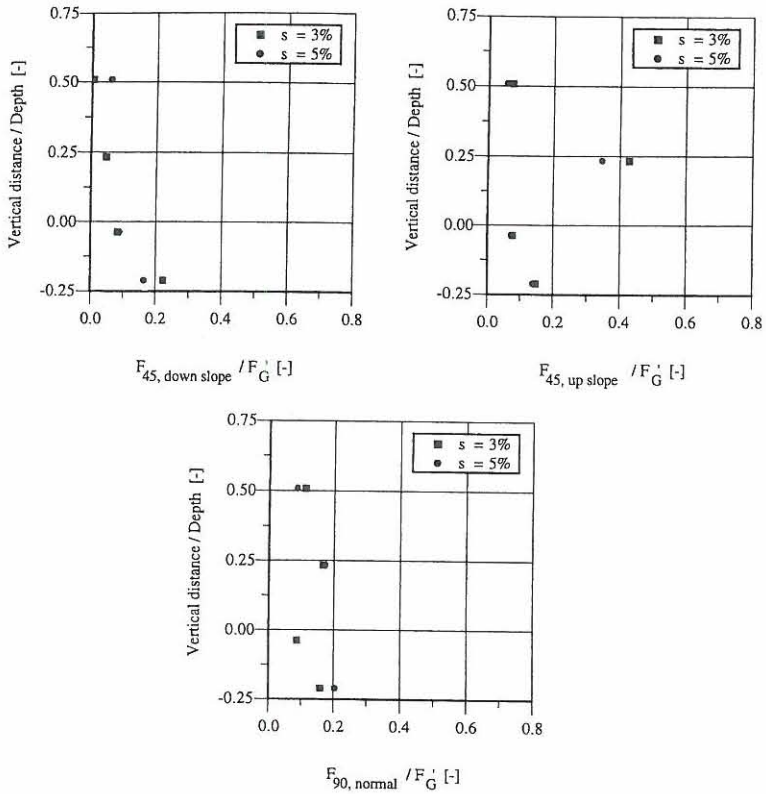

Figure 4.15: Vertical distribution of outward directed mean force F_m based on regular wave tests, $H = 15$ cm.

Considering Figure 4.15 it is observed that each position except 0.25 times the water depth above SWL, i.e. position 3, the force magnitude is of the same order of magnitude for all directions. In position 3 the force increases as the direction becomes more upward directed.

4.4.4 Irregular Wave Induced Loading

Regarding irregular wave induced forces the same characteristics as for regular waves are observed within each individual wave cycle. As for the regular wave tests force hodographs are plotted for the four positions, but opposite the regular wave tests the average force is no longer of interest since only a fraction of the waves are large enough to induce forces able to remove stones from the armour layer. Therefore the average of the highest 1/250 of the force peaks is used as a representative parameter. This parameter is termed $F_{1/250}$. Of course it could be argued that another fraction such as 1/50 should be used but the same conclusions are reached with this parameter as with $F_{1/250}$. In Figure 4.16 the force hodographs in all four positions are depicted.

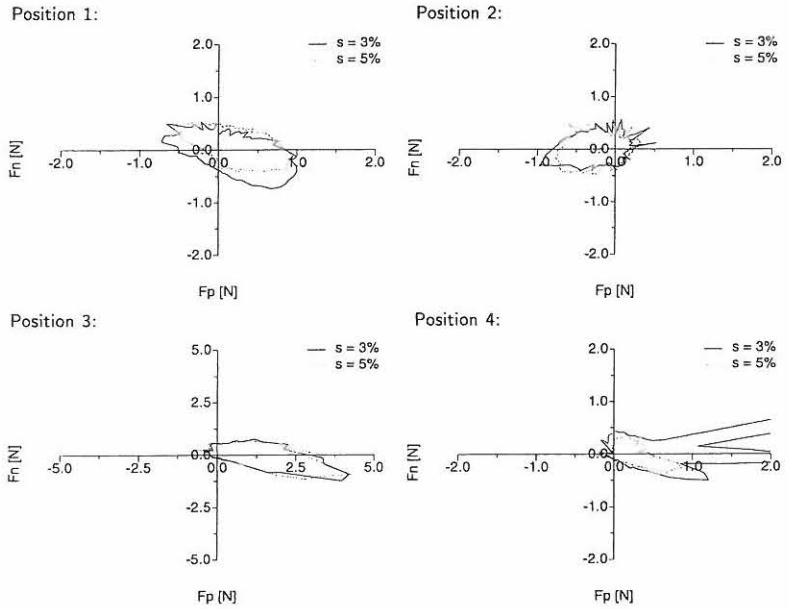

Figure 4.16: Hodographs based on $F_{\frac{1}{250}}$ at position 1–4 for irregular waves.

The shape of the hodographs presented in Figure 4.16 corresponds very well with the hodographs obtained with regular waves and the same conclusions apply. Regarding the vertical distribution of the total force acting away from the slope the distributions are presented in Figure 4.17.

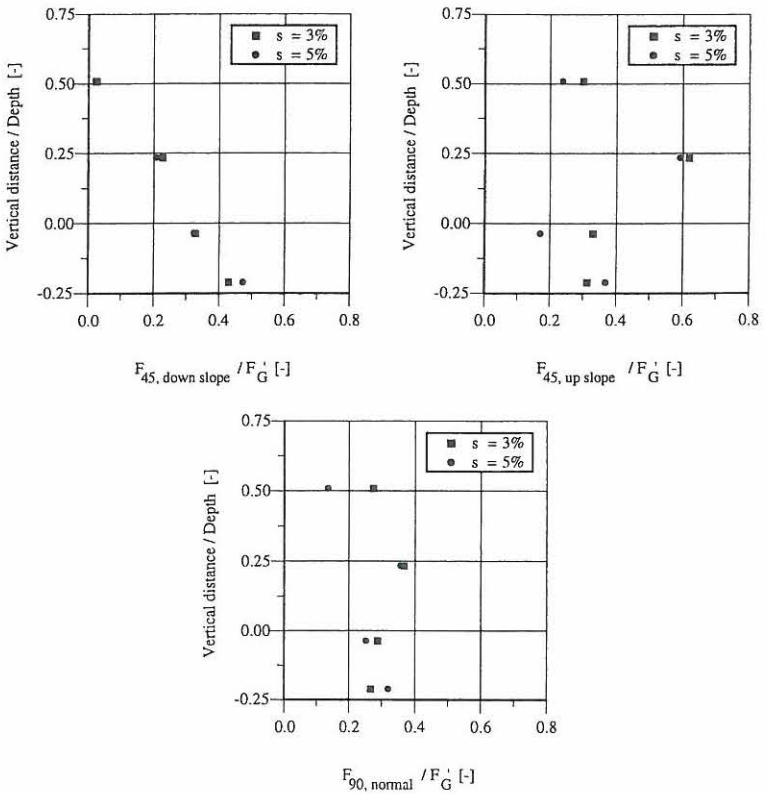

Figure 4.17: Vertical distribution of outward directed peak force $F_{\frac{1}{250}}$ based on irregular wave tests, H_s = 13.5 cm.

The displayed forces are somewhat higher than the regular wave induced forces but still it is observed that the largest forces occur approximately one fourth water depth above and one fourth water depth below SWL.

4.5 Comparison of Stability and Forces

Different methods of placing the armour stones in the armour layer have been investigated, see Table 4.2 and the stability performance is presented in Table 4.3. The highest degree of stability is obtained by placing the stones orderly. This placement method more than doubles the stability in terms of the Hudson–type stability coefficient compared to the conventional random placement method in two layers. Placing the stones randomly in one layer a very low stability of approximately one third of the stability obtained by the conventional method is found. Generally, no influence of steepness was observed.

Comparing video recordings and photos from the model tests it is observed that for the randomly placed stones, damage is initiated below SWL. However, for the orderly placed stones damage is initiated above SWL.

With respect to the wave induced forces on single armour stones the normal and the parallel force have been measured in 4 positions over the slope. Both tests with regular and irregular waves have been conducted with two wave steepnesses. In SWL large slamming forces of short duration were observed. Large outward directed forces were identified both above and below SWL. The influence of wave period was little as was the case for the stability tests whereas the influence of wave height was significant in some cases, especially in the positions above and below SWL.

Relating the stability observations to the force measurements it is interesting to see that only in the case of random placements, the downward directed force is able to remove the individual stones from their original position. This downward directed force is not sufficient to remove any stones when placed orderly because of the higher degree of interlocking and support from neighbouring stones. In this case high normal/upward forces are required to remove any stone. These forces are present above SWL in position 3, especially in the 45° upslope direction.

CHAPTER 5

Investigation of Waves and Forces

Following chapter 4 the present chapter is devoted to investigate the correlation between the loading and the characteristics of the waves inducing the loads in order to obtain a relationship between governing parameters.

The present chapter describes the details of a parametric study of the wave induced loading to various wave conditions. To investigate the influence of the different parameters describing the waves, a series of model tests have been designed and conducted at AAU. The influence on the wave forces is shown and finally models describing the wave force in three directions are presented.

5.1 Model Tests

A typical breakwater model was designed enabling the wave forces on a single armour stone to be measured as waves act on the slope. The model was constructed with the additional aim of being able to reproduce the same internal structural characteristics when rebuild, i.e. make the tests reproducible so only the character of the waves influence the wave forces. In light of this the crest height was chosen to prevent overtopping.

5.1.1 Model Setup

All tests were conducted in a 1.6 m wide and 26 m long wave flume. The breakwater model test section of 0.6 m width was installed with a sloping foreshore of 1:100 in front in one side of the flume and a wave guidance walls limited the breakwater model to the other side leaving a gap of 1.0 m width. Behind the breakwater model a spending beach with a slope of approximately 1:5 was constructed of gravel, see Figure 5.1.

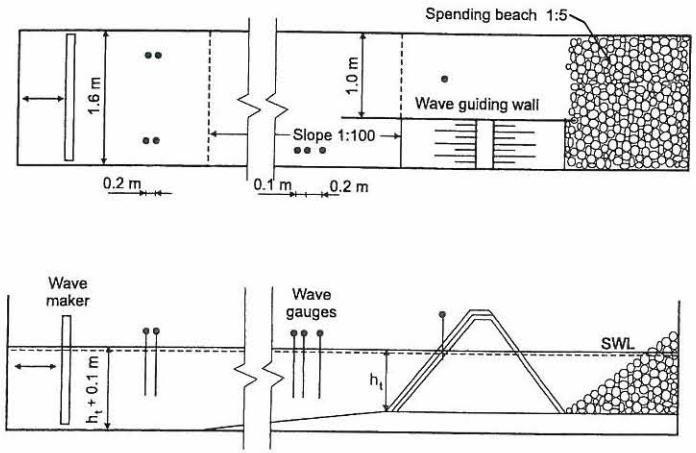

Figure 5.1: Outline of breakwater model setup in flume.

Eight resistance type wave gauges were installed; Two pair offshore close to the paddle, three locally in front of the breakwater model, and one in the gap beside the model. The two pair of offshore gauges were used for both active wave absorption and data acquisition. For active absorption elevation time series were sampled at 40.0 Hz and for data acquisition elevation time series were sampled at 20.0 Hz.

The breakwater model was constructed with a core material having an average stone diameter of approximately 6 mm, a filter layer with stones of diameters varying between 15–20 mm with a width of 50 mm, and an armour layer placed in two layers with an average stone mass $W_{50} = 352$ g corresponding to a equivalent cube length of 51 mm. Armour stone characteristics are shown in Figure 5.2.

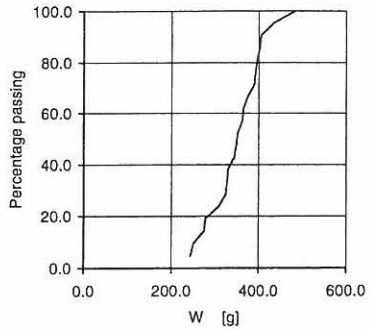

Figure 5.2: Armour stone mass distribution.

5.1.2 Force Transducer and Mounting Frame

From the armour stones a single stone of average size was picked and a reprint was made in coated plastic foam. The mass of the reprint was 92.2 g compared to the average mass of 352 g. Following the model stone was attached to one end of a 8 mm diameter steel rod and mounted to a force transducer designed and manufactured by AAU, see Figure 5.3. The force transducer is measuring normal strain in two cross sections making it possible to calculate the slope normal and slope parallel force acting on the stone when placed in the breakwater model. Eight strain gauges were mounted in each cross section, two on each side, and connected to form two wheatstone bridges. This configuration secure that the influence of bending in the plane and torsion on the measured strain is eliminated

The transducer and stone was mounted in an U–shaped metal beam fixed to the side walls and bottom in a metal frame. To avoid wave action directly on the transducer an aluminum box enclose the transducer. The mounting frame was placed directly on the core and succeedingly the filter material was placed with in the frame. Onto the mounting frame (including the U–beam and filter layer) perforated metal sheets were attached and armour stones were placed directly on the sheets. To avoid any contact between the model stone and neighbouring armour stones, the neighbouring stones were glued together onto the perforated metal sheet. The measuring system was designed for this specific study and in Figure 5.4 the model stone and force transducer mounted in the frame is shown. A more detailed illustration of each step in the sampling procedure of the measuring system is found in Appendix A.

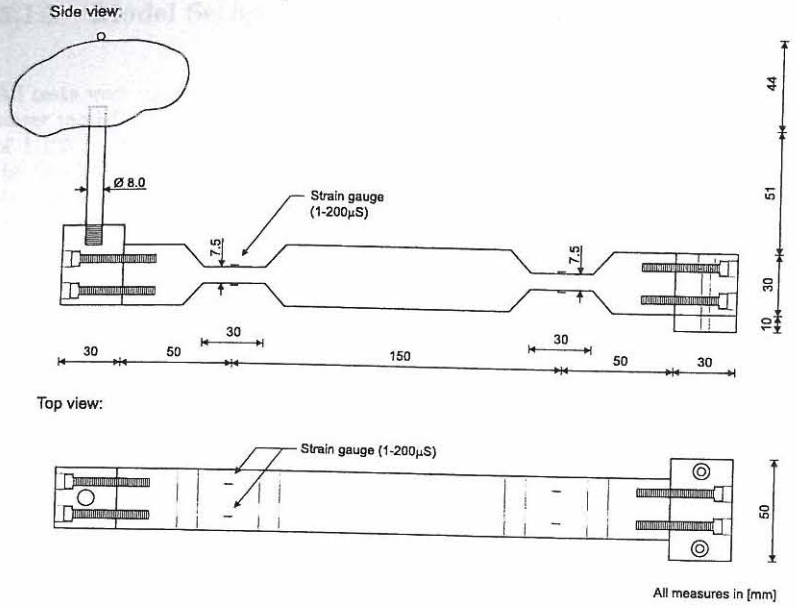

Figure 5.3: Force transducer with model stone mounted.

The force transducer with mounted stone was calibrated in both dry and wet conditions under static conditions with loads up to 500 g. Calibration was frequently checked and found to remain stable, see Appendix A. After mounting the stone and transducer a natural frequency in water of approximately 6.2 Hz with a damping ratio of 0.4 was obtained, see Appendix A.

These characteristics seems sufficient for measuring the loading below and above SWL since impact–like forces occurring around SWL were unable to cause stone motion. Tests in chapter 4 with a much higher natural frequency showed that only when the waves broke directly on the stone impact–like forces were present.

Force time series were sampled at 20.0 Hz and subsequently lowpass filtered with a cutoff frequency of 10.0 Hz. An exploratory test repeating the control signal to the wave generator and varying the sample frequency showed very little variation in the measured force time series.

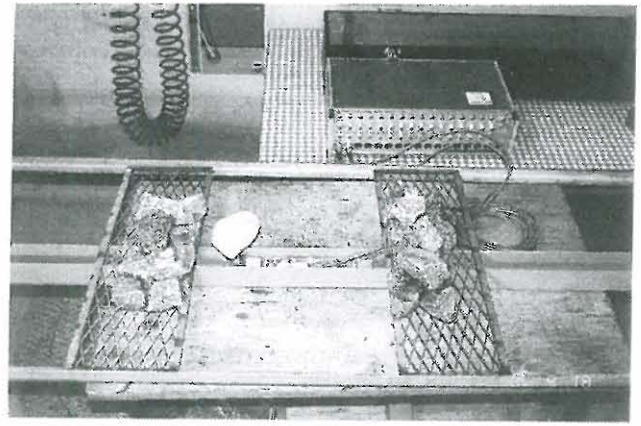

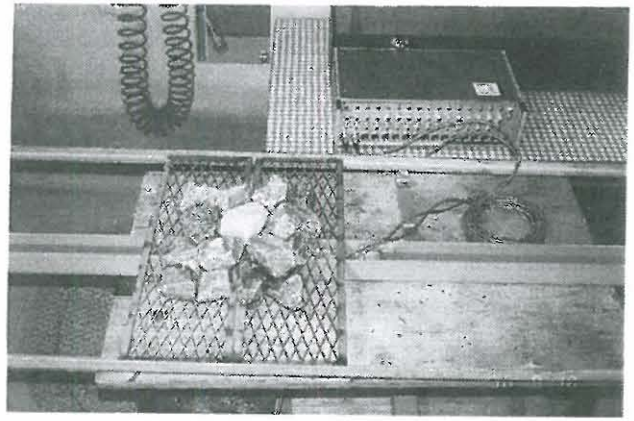

Figure 5.4: Model stone and force transducer mounted in frame.

5.1.3 Wave Generation

The waves were generated according to the JONSWAP spectrum. The applied version, specified in the Danish Code of Practice (DS–449 (1983)), is a three–parameter spectrum defined by the significant wave height H_s, the peak frequency f_p and the peak enhancement factor γ.

$$S(f) = \frac{1.4}{\gamma}\frac{5}{16}H_s^2 f_p^4 f^{-5}\gamma^{\alpha}\exp\left[-\frac{5}{4}\left(\frac{f_p}{f}\right)^4\right] \tag{5.1}$$

where

$$\alpha = \exp\left[-\frac{(f-f_p)^2}{2\sigma_f^2 f_p^2}\right]$$

$$\sigma_f = \begin{cases} 0.10 & \text{if } f \le f_p \\ 0.50 & \text{if } f > f_p \end{cases}$$

Since eq. (5.1) only gives the correct target wave height when $\gamma = 3.3$, the spectrum was modified for other values of γ by adding/subtracting energy uniformly distributed over the entire frequency range.

Control signals were generated by the software package PROFWACO (Frigaard et al. (1993)). The control signals were calculated by convolution of a white noise signal through a digital filter with characteristics of eq. (5.1). White noise signal were generated by a build–in random number generator, and different elevation time series with identical spectral wave parameters were generated by applying different seed numbers. By filtering of white noise very long time series can be generated without any repetition of the signal.

As rather non–linear waves are foreseen, control signals correct to second order were calculated in order to avoid generation of spurious sub– and superharmonic waves (see Schäffer (1996) for a comprehensive historical summary). For on–line generation of the non–linear waves the second order control signals were calculated by non–linear filters, see Høgedal et al. (1994), implemented in the software package PROFWACO, see Frigaard et al. (1993).

To avoid the incident wave trains from being infiltrated by re–reflected waves from the wave paddle an active wave absorption system was applied in combination with the wave generation. This system was controlled by the software package AWASYS (Frigaard (1993)). The system is based on real time separation of the wave field in incident and reflected waves and is operated by on–line signals from a pair of wave gauges in front of the paddle. An evaluation of the performance is given in Hald and Frigaard (1997).

5.1.4 Test Programme

Three different slope angles with the stone mounted in two positions, one 10 cm below SWL and one 10 cm above SWL, were investigated. The tests were performed according to the conditions in Table 5.1.

Slope			Stone pos.		h_t			γ				s_{p0}			H_s				
1:1.5	1:2	1:3	-10.0 cm	10.0 cm	30.0 cm	40.0 cm	50.0 cm	1.0	3.3	10.0	empty	1.0%	3.0%	5.0%	5.0 cm	7.5 cm	10.0 cm	12.5 cm	15.0 cm
A			1		A		C		B		A	A	B	C	1	2	3	4	5
	B		1		A	B	C		B		A	A	B	C	1	2	3	4	5
	B		1		A		C	A		C	A	A	B	C			3	4	
	B			3	A		C		B		A	A	B	C	1	2	3	4	5
		C	1		A		C		B		A	A	B	C	1	2	3	4	5

Table 5.1: Test programme and identifier for investigation of forces.

Each test was composed of the conditions in the header of Table 5.1. E.g. the test b1abab4 was performed on a 1:2 slope with the stone positioned -10.0 cm below SWL and $h_t = 30.0$ cm, $\gamma = 3.3$, $s_{p0} = 3.0\%$, $H = 12.5$ cm.

In total 133 tests were conducted and all tests were run for a duration of 2000 waves. The wave height was increased from 5.0 cm is steps of 2.5 cm up till 15.0 cm and the corresponding peak period was calculated from the wave steepness s_{p0}.

5.2 Data Reduction and Analysis

Offshore and local elevation time series were used to separate incident and reflected waves. A time domain reflection analysis procedure given by Frigaard and Brorsen (1995) was implemented in the software package used for analyzing the elevation time series. In short, two elevation signals are phase shifted in such a way that the incident parts are in phase while the reflected parts of the signals are in mutual opposite phase. Hereby the sum of the two manipulated signals is proportional to and in phase with the incident wave. By amplifying the summation signal the actual incident wave is found. The implementation of the principle is done in the time domain using digital filters.

From the 4 gauges offshore two estimates of the incident wave were calculated whereas two estimates were calculated from the 3 local gauges. The local elevation time series were phase shifted an additional phase, corresponding to the distance from wave gauges to the the model stone, in order to achieve a time series at the position of the model stone. Both offshore and locally one elevation time series was obtained for further analysis by averaging the relevant estimated incident elevation time series.

Each incident elevation time series were subsequently analyzed by spectral and zerocrossing analysis to achieve the energy and the wave height distributions. Spectral estimates were based on FFT of subseries with a window length of 1024 data points and 10% overlap. Zerocrossing estimates were based on the average value of the zerodown– and the zeroup–crossing estimates. Also the groupiness factor GF, the groupiness factor function $GF(t)$ and the wave envelope $E(t)$ were calculated based on the Hilbert transform technique described in enclosure 1. The groupiness factor function is calculated as the groupiness factor in a moving data window of a length corresponding to one average period of the respective time series.

Force time series were analyzed solely in the time domain. Maxima peaks within each wave cycle were determined by zerocrossing of the time derivative of the measured force time series. To determine only independent peaks, registered peaks within a desired filter width have been sorted out leaving only one peak within one wave period. From the peak distribution characteristic parameters were retrieved. Furthermore, the varying magnitude and direction of the force was analyzed by plotting combinations of the normal and the parallel force in a hodograph. The hodographs were constructed by dividing the entire angular space in intervals of 10° leaving only 36 directions. In each direction the distribution of the resulting force was calculated and 3 force estimates retrieved; $F_{1/25}$, $F_{1/250}$ and F_{max}. The parallel force is being defined as positive when acting upslope and the normal force is being positive when acting outwards as in Figure 4.10.

Both wave and force analyses were implemented in a software package tailor–made for this specific investigation. Examples of analyses from test b1abab4 are shown in Figure 5.5–5.6. From the analyses different characteristic wave and force parameters have been retrieved and listed in Appendix B.

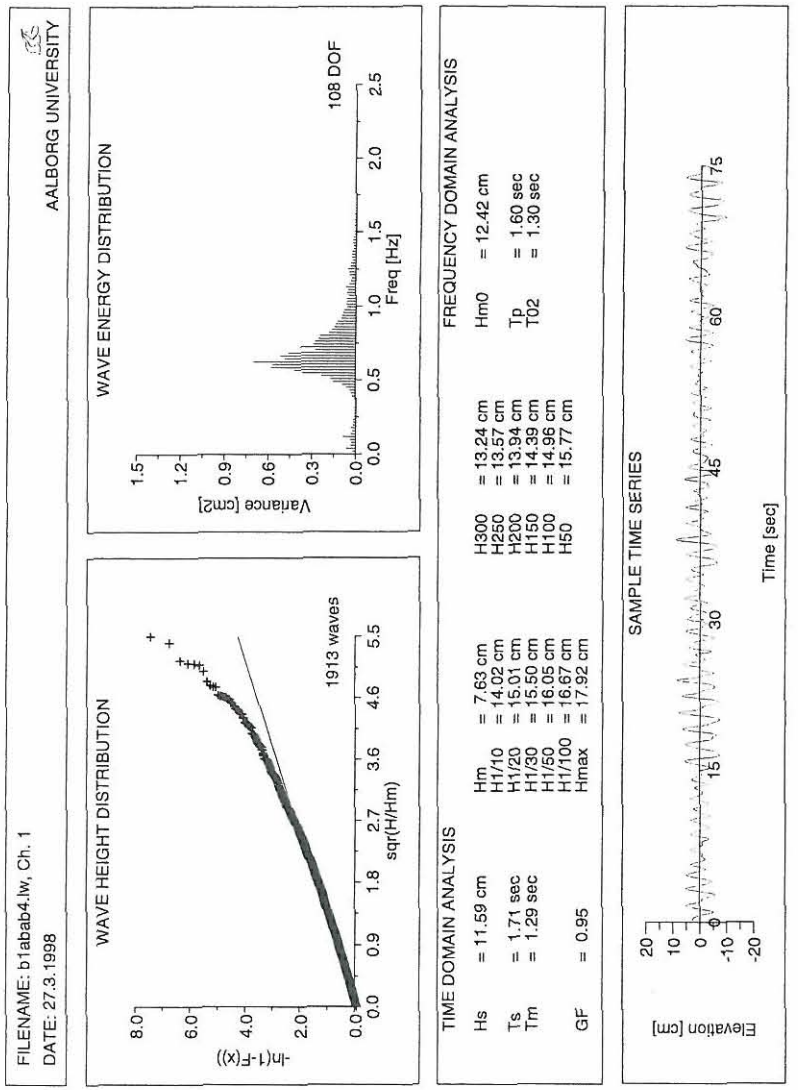

Figure 5.5: Example of wave analysis of test b1abab4.lw.

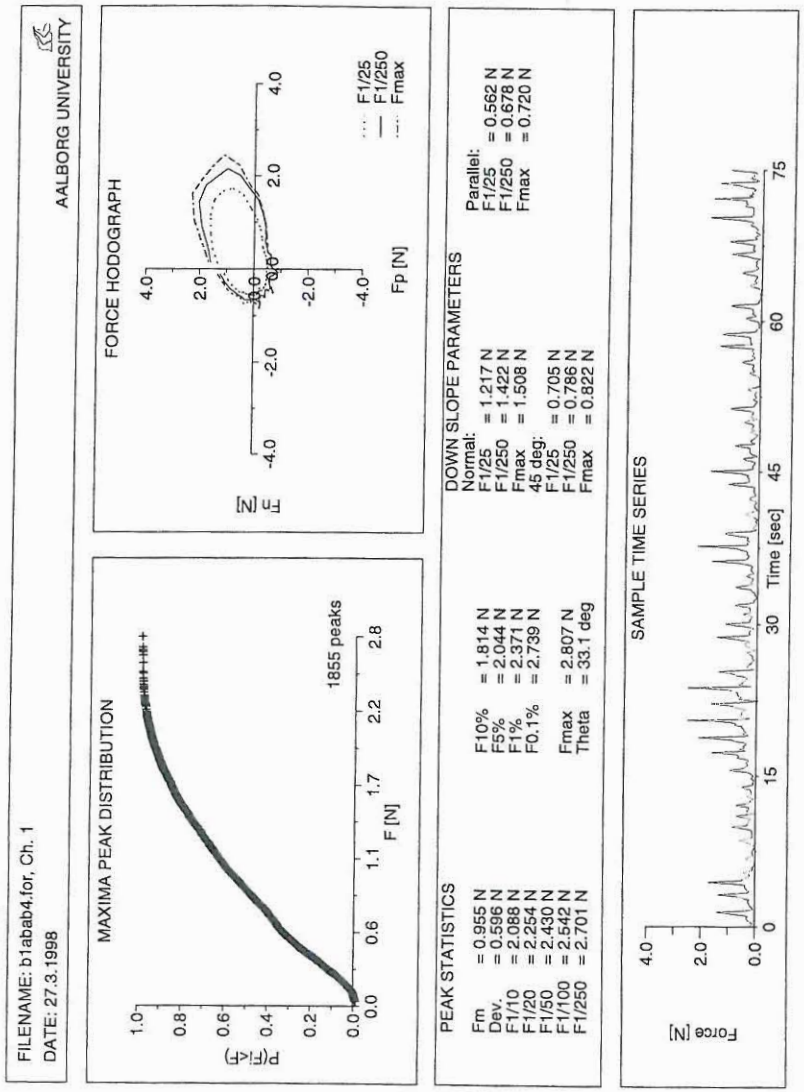

Figure 5.6: Example of force analysis of test b1abab4.for.

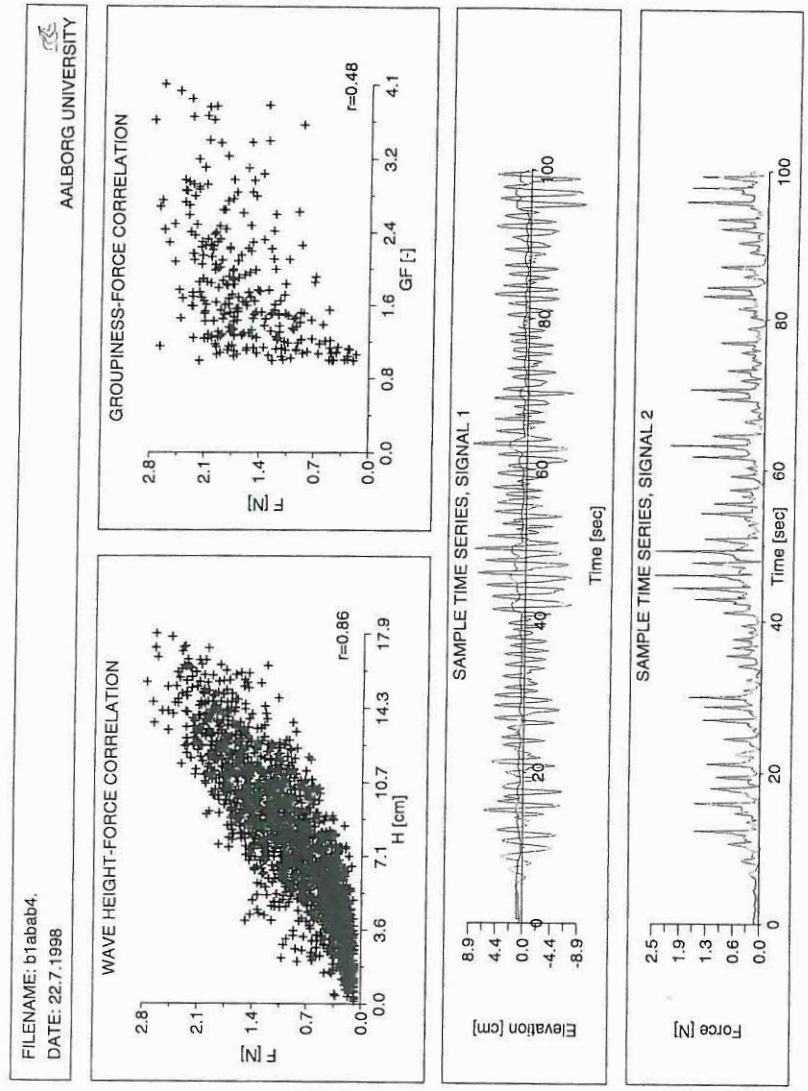

Figure 5.7: Example of correlation analysis of test b1abab4.

5.3 Character of Waves

The effect of shoaling and breaking on the wave parameters is described by the correlation between local and offshore wave steepness as shown in Figure 5.8. Both the average period and the peak period are depicted showing the same trends. Generally, both the local and the offshore steepnesses agree well for low values indicating that the change in water depth does not change both the wave height and the period. This complies well with the simple shoaling theory when no breaking takes place. For high values the local steepness is somewhat lower than the offshore steepness due to breaking of the highest waves during shoaling. With the data points based on the peak period being more scattered the average period will be used for further comparison.

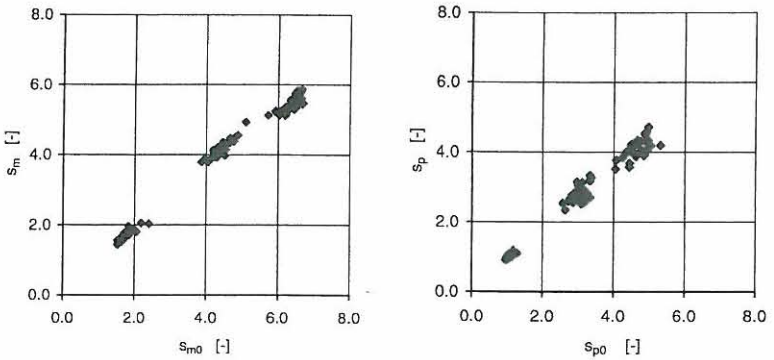

Figure 5.8: Correlation between local steepness and offshore steepness based on average and peak period.

Characteristics of the local waves in line with model stone are shown in Figure 5.9 and 5.10 in terms of the rate of dispersion and the rate of non–linearity.

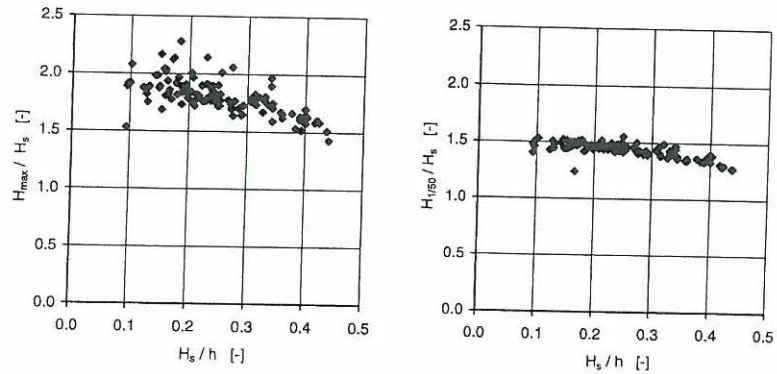

Figure 5.9: Influence of rate of dispersion H_s/h on H_{max} and $H_{1/50}$.

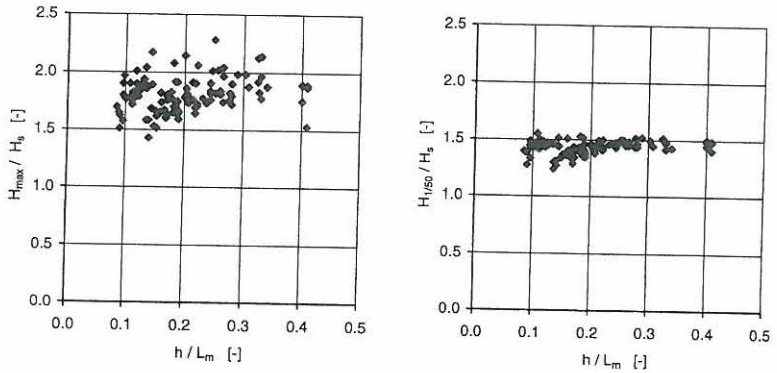

Figure 5.10: Influence of rate of non-linearity h/L_m on H_{max} and $H_{1/50}$.

Generally, the largest waves break making the wave height estimates decrease as the ratio H_s/h increases toward the breaking limit. The effect of the ratio of non–linearity h/L_m is that the maximum wave heights tend to decrease as the wave length increases. However, due to the strong correlation between wave height and wave period, this is not only an effect of wave length but more an effect wave breaking.

In Figure 5.11 the correlation between two characteristic wave height parameters and the groupiness factor is depicted for all tests. Generally, the height of the highest waves seems to be independent of the groupiness factor.

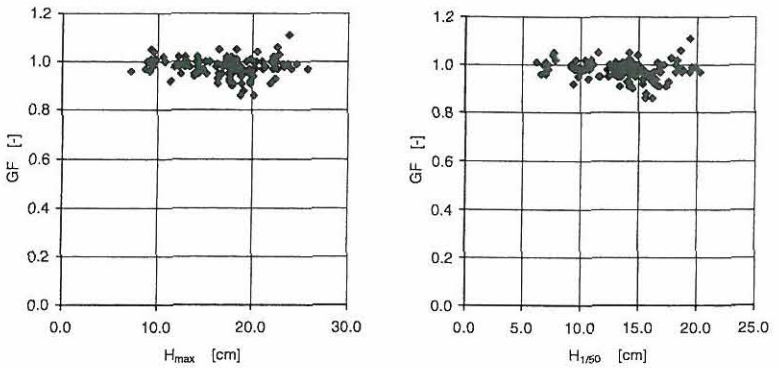

Figure 5.11: Correlation between groupiness factor GF and wave height H_{max} and $H_{1/50}$.

5.4 Wave Forces below SWL

5.4.1 Character of Forces

A study of the individual probability distributions of the individual force peaks in each force record indicate that a Gumbel distribution is suitable for describing the peak force.

$$P\left(\frac{F_i}{F_m} > \frac{F}{F_m}\right) = \exp\left[-\exp\left(-\frac{F_i/F_m - \gamma}{\beta}\right)\right] \tag{5.2}$$

An example of a probability distribution curve for test b1abaa4 is given in Figure 5.12. Also maximum likelihood estimates of the coefficients in the Gumbel distribution β and γ are given in terms of average values μ and standard deviations σ and the correlation coefficient R^2.

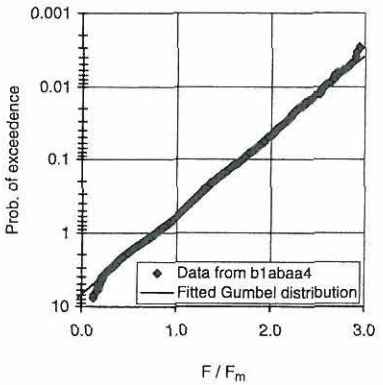

Estimated Gumbel parameters:

	μ	σ
β	0.45	0.05
γ	0.73	0.04
ρ	0.99	0.01

Figure 5.12: Example of probability distribution of test b1abaa4 and estimated Gumbel parameters.

Generally, a good fit is obtained with a correlation coefficient of 0.99 ± 0.01 except for low values of the force where a threshold value γ of 0.73 ± 0.04 is estimated. Largest variations are observed for the scaling factor β, but no significant pattern in the variations was found. Another promising candidate distribution is the Weibull distribution. However this distribution was unable to fit all the conducted tests and it tended to underpredict the highest waves.

In excess of the magnitude of the peak force also information concerning force components in other directions are of interest. Representative force hodographs are shown in Figure 5.13–5.18 for selected tests.

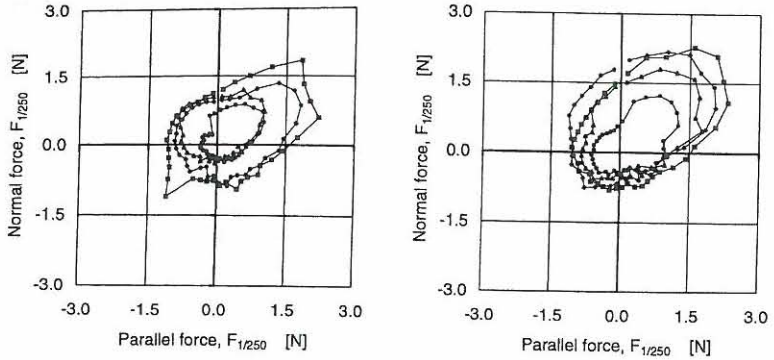

(a) $s_{p0} = 1\%$ (b) $s_{p0} = 5\%$

Figure 5.13: Force hodographs for tests with varying wave height and steepness. Constant slope=1:1.5, $h = 0.3\ m$, $\gamma = 3.3$.

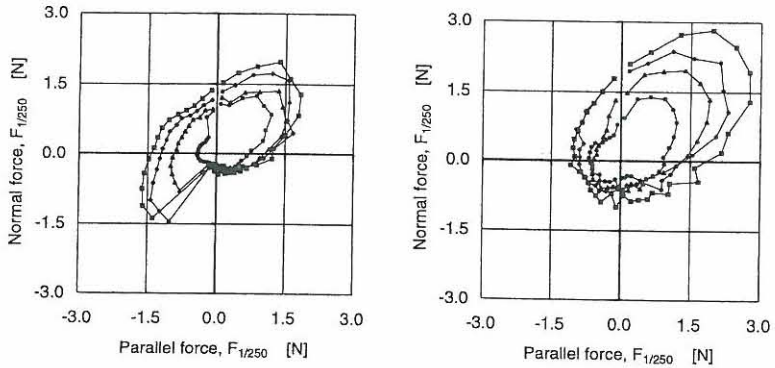

(a) $s_{p0} = 1\%$ (b) $s_{p0} = 5\%$

Figure 5.14: Force hodographs for tests with varying wave height and steepness. Constant slope=1:1.5, $h = 0.5\ m$, $\gamma = 3.3$.

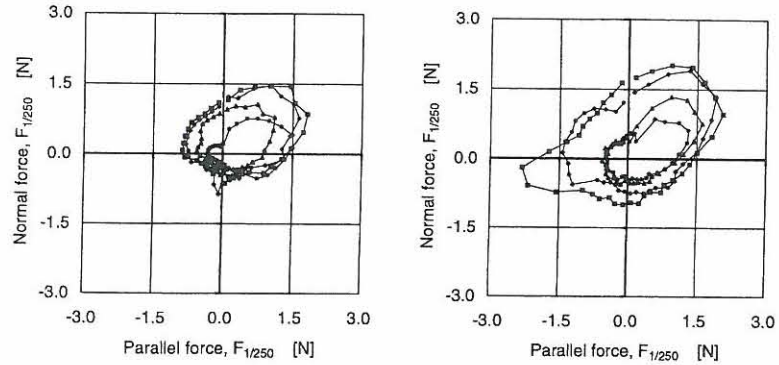

(a) $s_{p0} = 1\%$ (b) $s_{p0} = 5\%$

Figure 5.15: Force hodographs for tests with varying wave height and steepness. Constant slope=1:2, $h = 0.3\ m$, $\gamma = 3.3$.

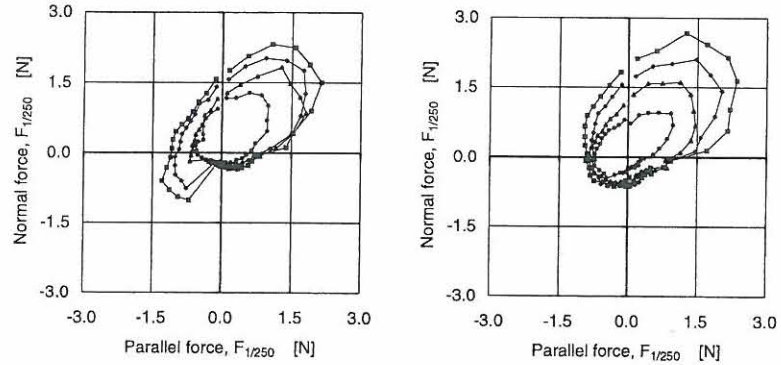

(a) $s_{p0} = 1\%$ (b) $s_{p0} = 5\%$

Figure 5.16: Force hodographs for tests with varying wave height and steepness. Constant slope=1:2, $h = 0.5\ m$, $\gamma = 3.3$.

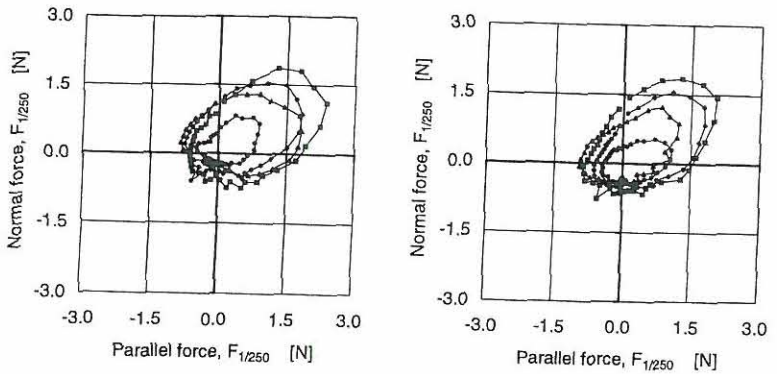

(a) $s_{p0} = 1\%$ (b) $s_{p0} = 5\%$

Figure 5.17: Force hodographs for tests with varying wave height and steepness. Constant slope=1:3, $h = 0.3\,m$, $\gamma = 3.3$.

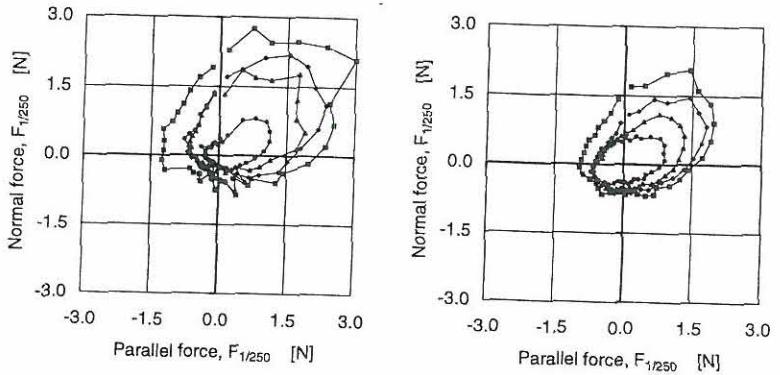

(a) $s_{p0} = 1\%$ (b) $s_{p0} = 5\%$

Figure 5.18: Force hodographs for tests with varying wave height and steepness. Constant slope=1:3, $h = 0.5\,m$, $\gamma = 3.3$.

Typically, a large force is directed upward. This force reduced in magnitude as the direction turns from the maximum direction over the slope normal direction and down to the slope parallel direction. All inward directed force directions are of relatively small magnitude except for the tests with longer waves on steeper slopes. A more detailed discussion regarding variations for the different conditions is left to the succeeding paragraphs.

A matter that is not depicted in Figure 5.13–5.18 is that the shape of each individual hodograph only varies a little depending on which forces estimate that is considered. E.g. similar shape is obtain when considering $F_{1/250}$ and $F_{1/25}$.

For further analyses the force estimate $F_{1/250}$ is extracted from the measurements and three force components are selected:

- The peak force: Magnitude in peak direction.
- The 90° force: Magnitude in 90° slope normal and outward direction.
- The 45° force: Magnitude in 45° down slope and outward direction.

Above directions are chosen to be representative of a destabilizing force necessary to initiate motion of an armour stone. The three components are all outward directed and covers both lifting as well as up– and downslope motion of the stones.

The characteristic directions of the peak force are shown in Figure 5.19 whereas the correlation between the peak force and the 90° force as well as the 45° force is shown in Figure 5.20.

From Figure 5.19 the direction is seen to vary mainly between 115° and 165° . Depending on the slope angle of the structure the peak force acts almost vertically upwards with a small tendency to act upslope.

From Figure 5.20 a strong correlation between the peak and the 90° force is observed. This correlation probably occur because the mechanism causing both forces is the same. When the downrush meets the next wave a strong reversal of the flow occur changing the force direction from being downward and slope parallel to being upward and slope parallel. The correlation between the peak and the 45° force is more scattered which probably is because the 45° force is more influenced by the downrush than the two other components.

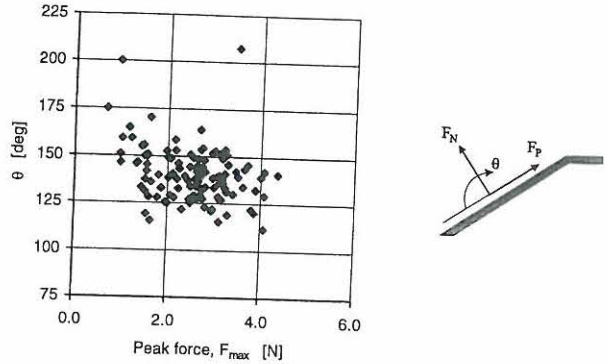

Figure 5.19: Correlation between direction θ and magnitude F_{max} of peak force.

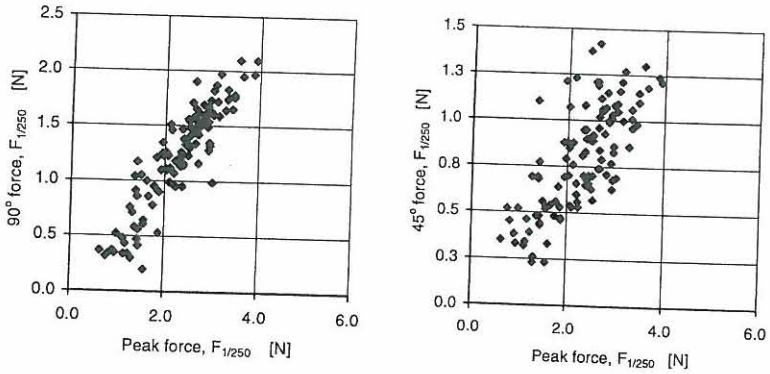

(a) *90° slope normal force $F_{1/250}$ and peak force $F_{1/250}$.*

(b) *45° down slope force $F_{1/250}$ and peak force $F_{1/250}$.*

Figure 5.20: Correlation between the peak force and the 90° and 45° force.

5.4.2 Influence of Wave Height

In Figure 5.21–5.23 the influence of wave height on the three force component is depicted. Both the influence of H_s and $H_{1/20}$ is given to illustrate the influence of wave height when considering different wave height estimates.

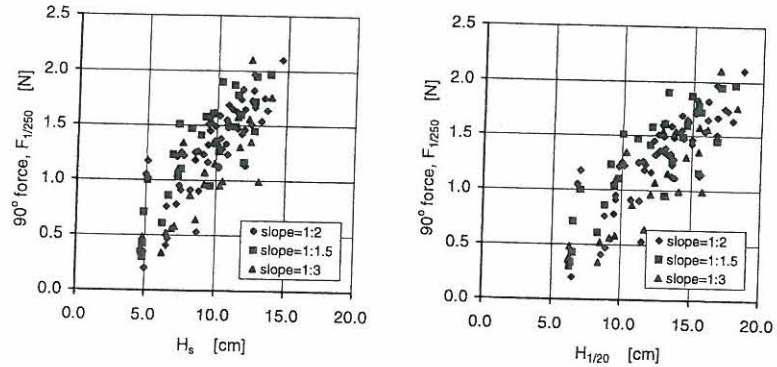

Figure 5.21: Influence of wave height on 90° force.

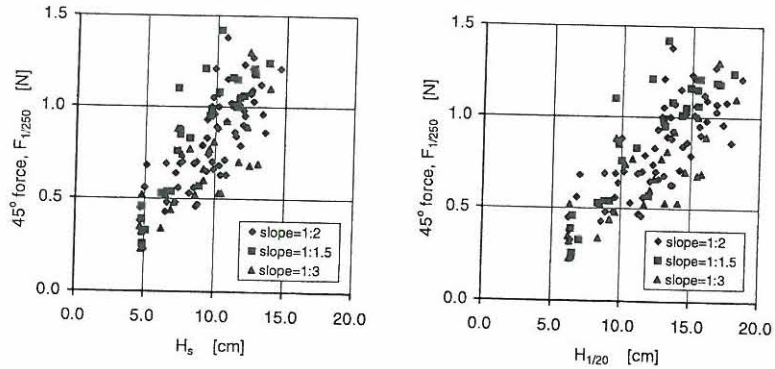

Figure 5.22: Influence of wave height on 45° force.

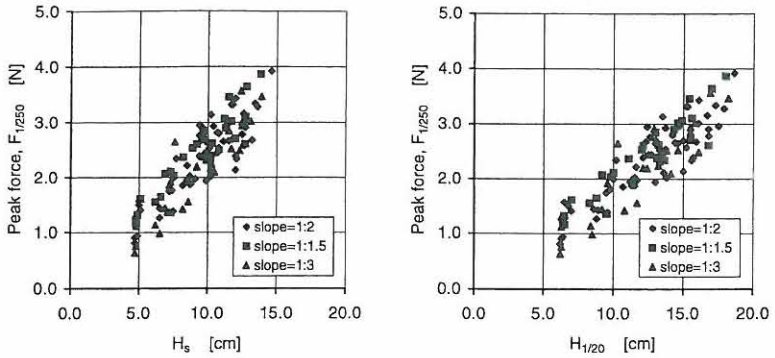

Figure 5.23: Influence of wave height on peak force.

All plots show some scatter as the considered forces not only depend on the height of the waves. However, the overall trend is almost linear, i.e. an increase in wave height will cause a similar increase in wave force. The linear trend does not change when using $H_{1/20}$ instead of H_s. This conclusion also holds for the estimates $H_{1/10}$, $H_{1/50}$, H_{250} and H_{150}.

5.4.3 Influence of Slope

From Figure 5.21–5.23 no clear influence of the slope angle can be observed when considering the overall set of data. However a more close inspection of the plots in Figure 5.21–5.23 indicate that on the steepest slope the largest forces always occur whereas the smallest forces occur on the flatter slopes. A more distinct influence of the slope angle can be observed when separating between surging and plunging waves, see Figure 5.24. Below the influence is summarized for the three force components:

- The 90° force is almost constant with varying slope angle for surging waves and decreases as the slope flattens for plunging waves.
- The 45° force decreases regressively as the slope becomes more flat. Almost no differences between surging and plunging waves is observed.
- The peak force is almost independent of breaker type on the steepest slope. From here the surging waves produce larger forces and the plunging waves produce smaller forces as the slope flatten.

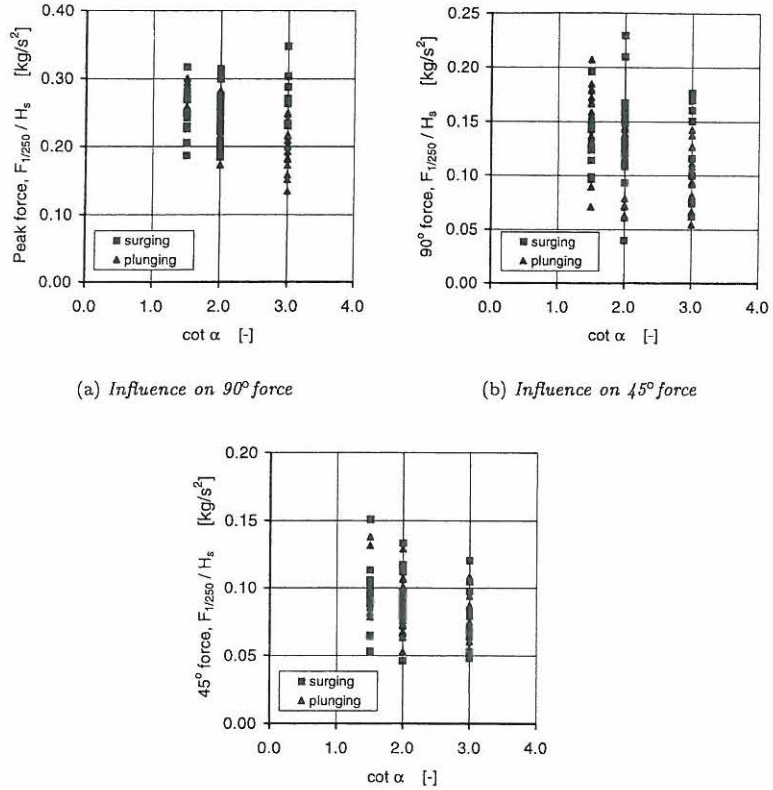

(a) *Influence on 90° force*

(b) *Influence on 45° force*

(c) *Influence on peak force*

Figure 5.24: Influence of slope angle on wave induced force.

5.4.4 Influence of Wave Period – Surf Similarity Parameter

In Figure 5.25–5.27 the influence of wave period and surf similarity parameter on the three force component is depicted. The influence is illustrated by normalizing the measured force with H_s.

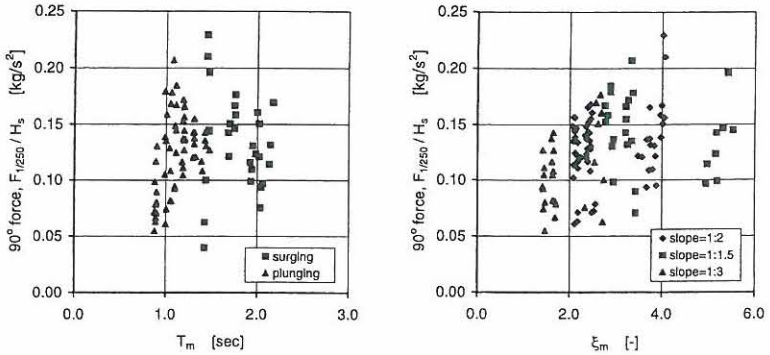

Figure 5.25: Influence of wave period and surf similarity parameter on 90° force.

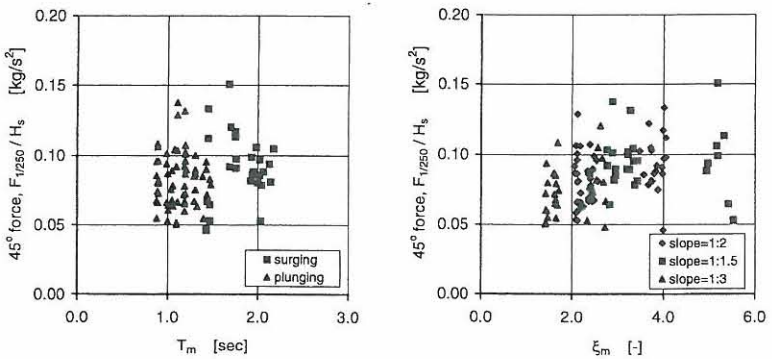

Figure 5.26: Influence of wave period and surf similarity parameter on 45° force.

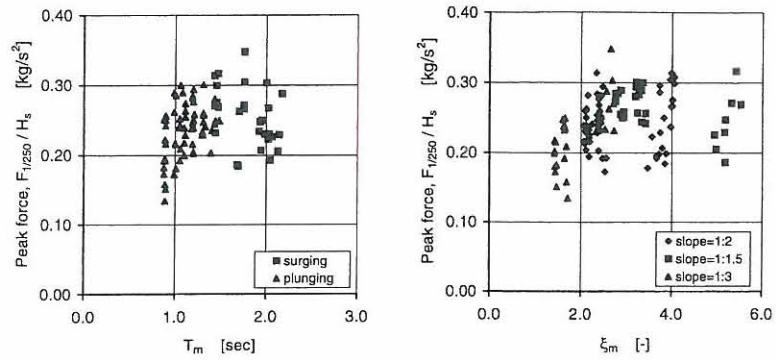

Figure 5.27: Influence of wave period and surf similarity parameter on peak force.

After normalizing some scatter still prevail and generally all three force components seems to be independent of both wave period and surf similarity parameter. However some average tendencies can still be derived when separating between surging and plunging waves:

- The 90° force is almost independent of wave period especially for surging waves. In plunging waves a slight increase with period is seen. Generally, the characteristics are similar to those of the peak force.
- The 45° force is independent of wave period. The only dependency of the surf similarity parameter is due to the varying slope angle.
- The peak force shown some increase with period in plunging waves and is almost independent of period in surging waves. The influence of period in plunging waves is more pronounced than for the 90° force.

With respect to the force dependency on the surf similarity parameter, the considered force components tend to maximize in the region $\xi_m = 3 - 4$. It is also within this region minimum stability occur as discussed in chapter 3.

5.4.5 Influence of Water Depth

The water depth in itself is not a good parameter and has therefore been included in the rate of dispersion H_s/h_t and rate of non–linearity h_t/L_m as discussed in paragraph 2.1.2. In Figure 5.28–5.30 the influence on the three force components is given.

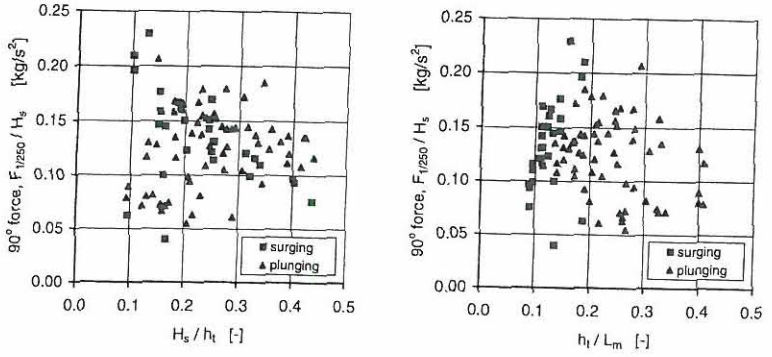

Figure 5.28: Influence of rate of dispersion and non–linearity on 90° force.

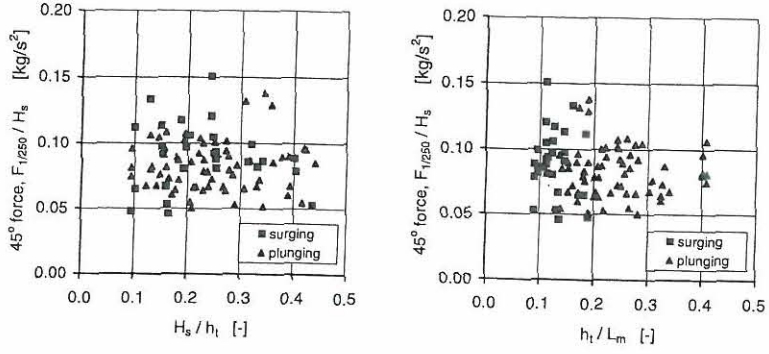

Figure 5.29: Influence of rate of dispersion and non–linearity on 45° force.

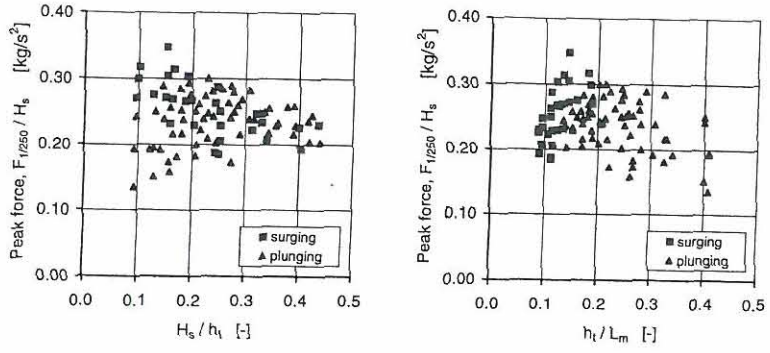

Figure 5.30: Influence of rate of dispersion and non–linearity on peak force.

Generally, with respect to plunging waves all plots show no or only poor influence of the two considered parameters and thus also of the water depth. On the other hand the influence is somewhat different in surging waves: Both the 90° and the peak force decrease with decreasing water depth whereas the 45° force is not influence by the water depth. With the 90° and the peak forces being produced by the reversal of the flow when downrush meets the succeeding wave, the decreasing effect on these two forces might be caused by the deaccelerating effect the limited water depth has on the downrushing water. Due to the poor influence of H_s/h_t and h_t/L_m the influence of the Ursell number will also be poor.

Please note that the discussed influence is only valid with the range of non–breaking to breaking waves close to the breaking criterion. The influence above $H_s/h > 0.5$, i.e. in broken waves, might be significantly different.

5.4.6 Influence of Peak Enhancement Factor

In Figure 5.31 the influence of peak enhancement factor in the JONSWAP spectrum on the three force component is depicted. Generally, the three components appear to be almost independent of the peak enhancement factor although both the 90° and the peak force tend to minimize at the value 3.3.

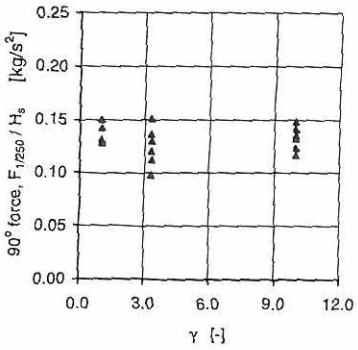

(a) *Influence on 90° force*

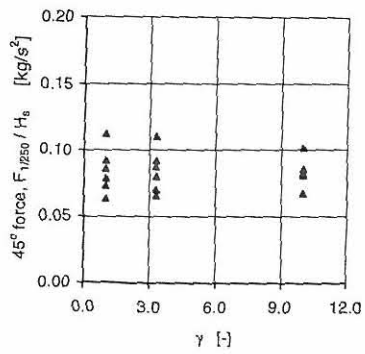

(b) *Influence on 45° force*

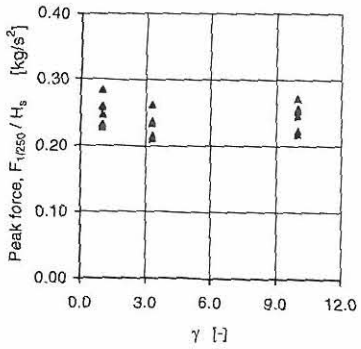

(c) *Influence on peak force*

Figure 5.31: Influence of peak enhancement on wave induced force.

5.4.7 Influence of Groupiness

In Figure 5.32 the influence of the groupiness factor on the three force component is depicted. Generally, the three force components occur almost independent of the groupiness factor although a slight increase with increasing groupiness factor is observed for the 90°force and the peak force. The 45°force appear independent of groupiness factor.

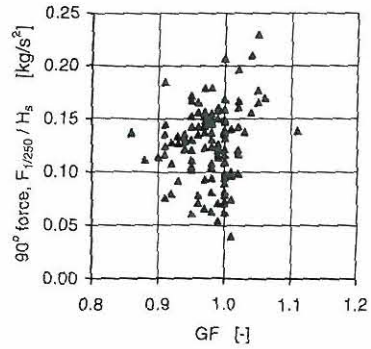

(a) *Influence on 90° force*

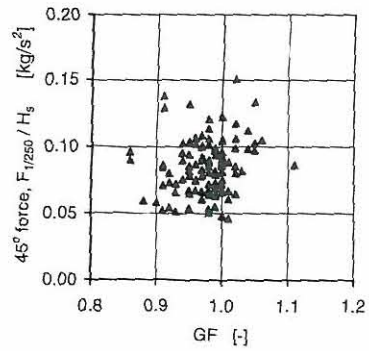

(b) *Influence on 45° force*

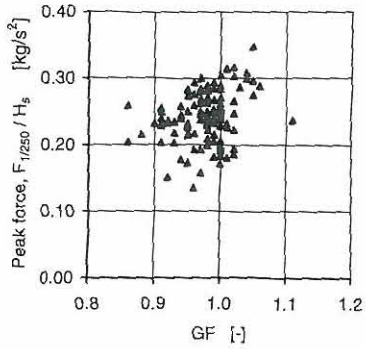

(c) *Influence on peak force*

Figure 5.32: Influence of groupiness factor on wave induced force.

A more thorough investigation of the influence of groupiness have been conducted by considering each individual test to be composed of single waves or sequences of waves of various size and shape. The elevation and force time series have been decomposed into smaller pieces and simultaneous wave and force parameters have been calculated. Basically four different correlation analyses have been conducted as described below:

- Peak force – Wave height ($F-H$): The height of each single wave identified by zerocrossing and the peak force within the simultaneous cycle have been found. The zerodown-crossing wave height H_{zdc} proved to give a significantly better correlation than the zeroup–crossing. This indicate that the depth of the trough before maximum elevation is important. However, further analyses showed that maximum peak force occurred when $\eta_{max} \approx \eta_{min}$.
- Peak force – Maximum elevation ($F - \eta_{max}$): Within each single wave identified by zerocrossing the maximum elevation and the peak force was found. The correlation between peak force and minimum elevation showed to be poor.
- Peak force – Groupiness factor ($F - GF$): The number of wave groups, defined when $GF(t) > 1$ have been identified by zerocrossing of the time series $GF(t) - 1$. Within each group the maximum groupiness factor and the maximum peak force have been found. Attempts to correlate maximum groupiness factor with simultaneous peak force and opposite did not show any good correlation.
- Peak force – Wave envelope ($F - E$): The envelope can be considered as an instantaneous wave height function. Within each single wave identified by zerodown–crossing the maximum value of the envelope function E_{max} and the peak force have been found. Similar attempts identifying the wave groups showed little correlation.

In Table 5.2 average value and standard deviation of the coefficient of correlation between the above selected wave parameters and the peak forces for all tests are given. Best correlation is observed for the peak force – wave height relation and least correlation is connected with the groupiness factor. Generally the two wave grouping related parameters show large scatter signifying that their influence is not above the more direct influence from the elevation time series.

R^2	$F-H$	$F-\eta$	$F-GF$	$F-E$
μ	0.82	0.65	0.62	0.75
σ	0.12	0.17	0.12	0.12

Table 5.2: Correlation between peak force and selected wave parameters.

In Figure 5.33 examples of scatter plots between individual peak forces and the selected wave parameters calculated from test b1abab4.

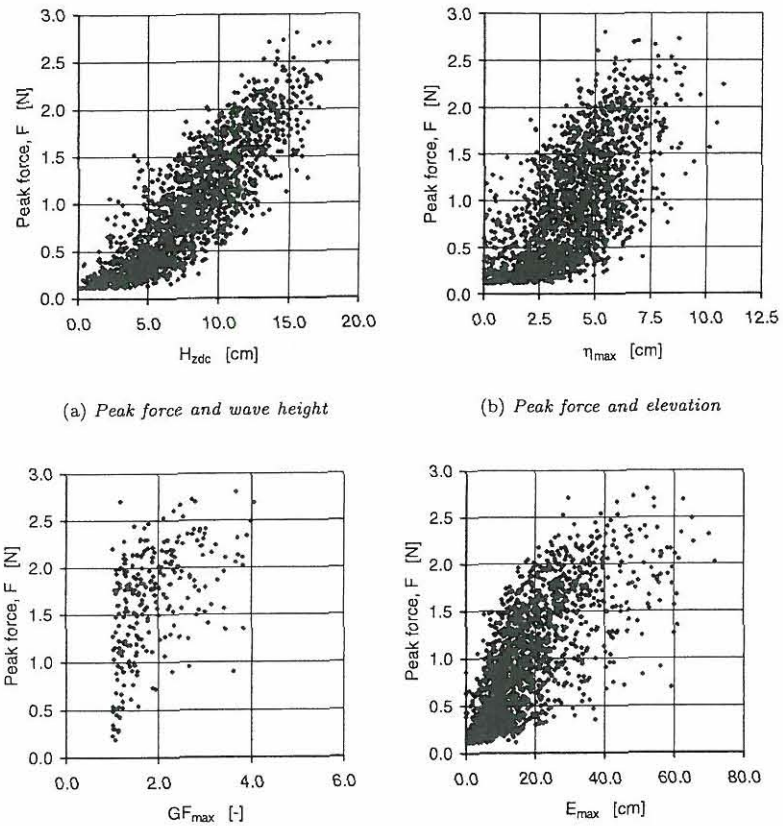

(a) *Peak force and wave height*

(b) *Peak force and elevation*

(c) *Peak force and groupiness factor*

(d) *Peak force and wave envelope*

Figure 5.33: Examples of correlation between individual peak forces and selected wave parameters from test b1abab4.

5.4.8 Wave–Force Models

In order to summarize the influence of each parameter three different wave–force models have been derived enabling calculation of $F_{1/250}$ for each of the three force components. To each force components two set of models have been established: One fitting all data and one fitting to plunging and surging waves separately.

$$\frac{F}{F'_G} = c_0 N_s^{c_4} \xi_m^{c_1} N_z^{c_3} \tan^{c_2}(\alpha) \frac{h_t}{H_s}^{c_5} GF \tag{5.3}$$

$$\frac{F}{F'_G} = c_0 N_{\frac{1}{50}}^{c_4} T_{om}^{c_1} N_z^{c_3} \tan^{c_2}(\alpha) \frac{h_t}{H_s}^{c_5} GF \tag{5.4}$$

where:

$F_{1/250}$	:	Average force of the highest 1/250 of the forces.
F'_G	:	Submerged weight of armour stone.
$N_s, N_{1/50}$	:	Stability number based on significant wave height H_s and average of highest 1/50 of the wave heights $H_{1/50}$.
ξ_m	:	Surf similarity parameter.
T_{om}	:	Dimensionless wave height, $T_{om} = T_m \sqrt{\frac{g}{D_{n50}}}$.
N_z	:	Number of waves.
α	:	Slope angle.
h_t	:	Water depth at the toe of the slope.
GF	:	Groupiness factor.
$c_0, c_1, c_2, c_3, c_4, c_5$	:	Fitting coefficients.

The coefficients in each model have been calculated by a Gauss–Newton iteration scheme minimizing the squared error function. See Christensen (1996) for reference.

Fitted models correlated to the measured data are given in Figure 5.34–5.36 as well as the best fit force model.

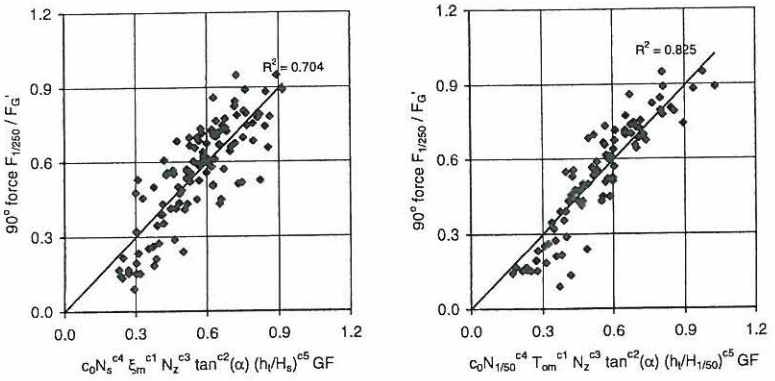

Figure 5.34: Fitted models for 90° force versus measured values of $F_{1/250}$.

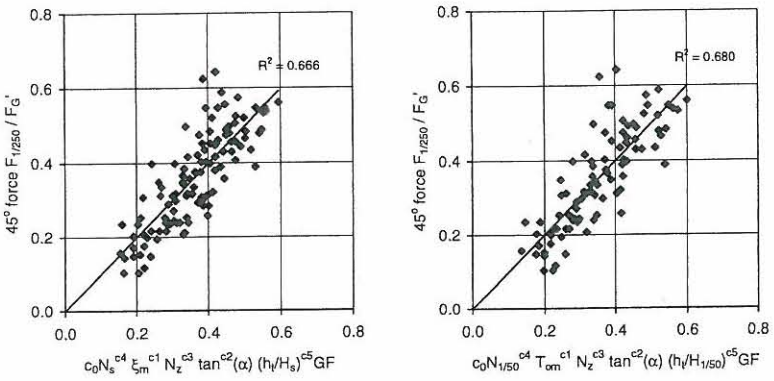

Figure 5.35: Fitted models for 45° force versus measured values of $F_{1/250}$.

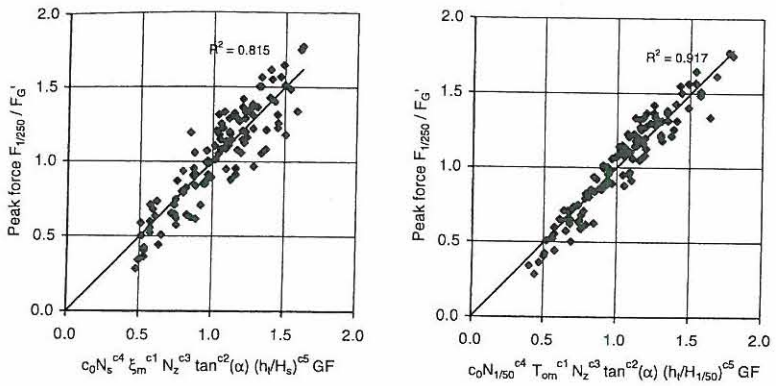

Figure 5.36: Fitted models for peak force versus measured values of $F_{1/250}$.

Models fitting all data are based on the significant wave height H_s whereas the models separating between plunging and surging waves are based on $H_{1/50}$. However when using H_s with the same coefficients instead of $H_{1/50}$ a little more scatter is observed. With respect to the influence of number of waves the best fit were obtained when omitting this term. This however might be due to the limited variation of the number of waves. The linear influence of the groupiness factor in the formulae improved the coefficient of correlation compared to no influence despite the more scattered behaviour observed in Figure 5.32. Largest improvements were observed for the 90°force and the peak force whereas only small improvements occur for the 45°force. Regarding estimated coefficients for surging waves, only a limited number of tests are available making the estimated coefficients less accurate. This is especially true for the coefficients on period and water depth. All estimated coefficients comply with the influence described in the previous paragraphs.

Generally, the best fit is obtained for the peak force. As a result of the correlation between the peak and the 90° force, the 90° force models also show good correlation. With respect to the 45° force a large scatter is present resulting in a somewhat lower correlation.

In Table 5.3 and Table 5.4 the fitted coefficients and their influence on selected wave parameters are summarized.

		c_0	c_1	c_2	c_3	c_4	c_5
90°force	All data	0.65	0.0	0.31	0.0	1.08	0.0
	Plunging	0.31	0.13	0.46	0.0	1.30	0.0
	Surging	0.40	-0.1	-0.11	0.0	0.85	0.2
45°force	All data	0.46	0.0	0.42	0.0	0.96	1.0
	Plunging	0.30	0.03	0.48	0.0	1.04	1.0
	Surging	0.31	0.0	0.22	0.0	0.94	1.0
Peak force	All data	1.11	0.0	0.17	0.0	1.01	0.0
	Plunging	0.21	0.52	0.33	0.0	0.95	0.0
	Surging	0.65	-0.1	-0.25	0.0	1.0	0.2

Table 5.3: Fitted parameters in models for 90°, 45° and peak force.

Wave–force model: $\frac{F}{F_G'} = af(D_{n50}, \Delta, g) H_n^b T_m^c \tan^d \alpha h_i^e G F^f$

Parameters:		a	b	c	d	e	f
90°force	All data	0.65	1.08	0.0	0.31	0.0	1.0
	Plunging	0.31	1.30	0.13	0.46	0.0	1.0
	Surging	0.40	0.65	-0.1	-0.11	0.2	1.0
45°force	All data	0.46	0.96	0.0	0.42	0.0	1.0
	Plunging	0.30	1.04	0.03	0.48	0.0	1.0
	Surging	0.31	0.94	0.0	0.22	0.0	1.0
Peak force	All data	1.11	1.01	0.0	0.17	0.0	1.0
	Plunging	0.21	0.95	0.52	0.33	0.0	1.0
	Surging	0.65	0.8	-0.1	-0.25	0.2	1.0

Table 5.4: Influence of various parameters on 90°, 45° and peak force.

5.5 Wave Forces above SWL

5.5.1 Character of Forces

Also the forces above SWL prove to be best described by the Gumbel distribution as illustrated in Figure 5.37 for test b3abac4. Also maximum likelihood estimates of the coefficients in the Gumbel distribution β and γ are given in terms of average values μ and standard deviations σ and the correlation coefficient R^2.

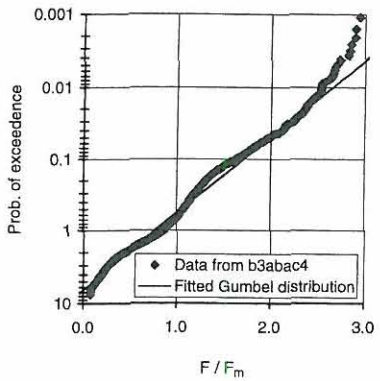

Estimated Gumbel parameters:

	μ	σ
β	0.46	0.04
γ	0.73	0.03
ρ	0.97	0.02

Figure 5.37: Example of probability distribution of test b3abac4 and estimated Gumbel parameters.

Compared to the forces below SWL a more poor fit is obtained with a correlation coefficient of 0.97 ± 0.02. The reason for the lower correlation appear from Figure 5.37 for low exceedence probabilities where the Gumbel distribution overpredict the actual present force. Furthermore, the force data are scattered along the fitted distribution. This is due to the fact that the runup wedge, causing the major part of the forces, at the position of the model stone is thin, and thus more easily effected by small changes in the structural and hydraulic conditions.

In Figure 5.13–5.18 representative force hodographs are shown for selected tests. Generally, a large normal force is observed and still the inward directed forces are small in magnitude. Regarding down–slope directed forces these seems to be independent of the wave height. Since the model stone is located above SWL a large contribution to the resulting force is due to a change in buoyancy when the water meets the stone. Hereby a large vertical upward directed force is produced.

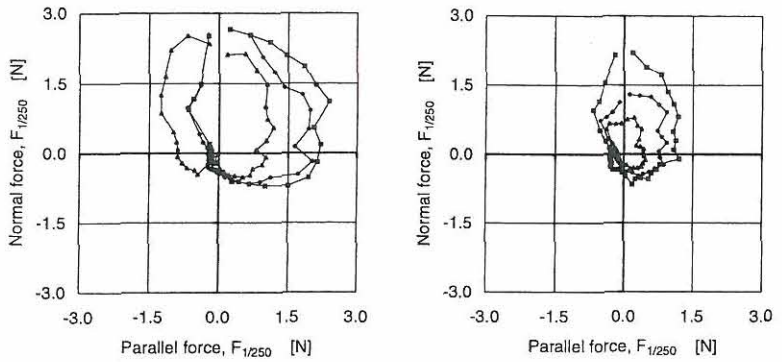

(a) $s_{p0} = 1\%$ (b) $s_{p0} = 5\%$

Figure 5.38: Force hodographs for tests with varying wave height and steepness. Constant slope=1:2, $h = 0.3\ m$, $\gamma = 3.3$.

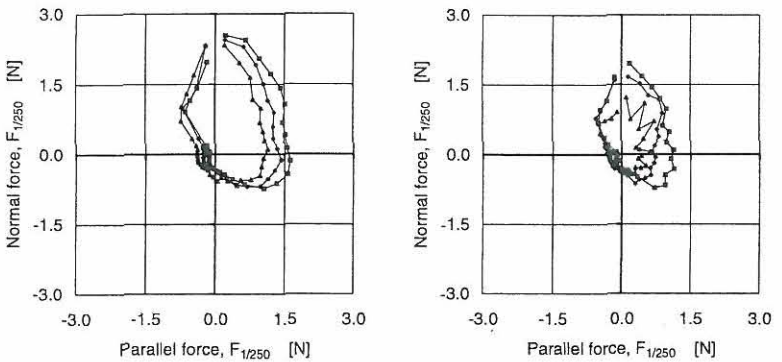

(a) $s_{p0} = 1\%$ (b) $s_{p0} = 5\%$

Figure 5.39: Force hodographs for tests with varying wave height and steepness. Constant slope=1:2, $h = 0.5\ m$, $\gamma = 3.3$.

Characteristic directions of the peak force given in Figure 5.40 show that the peak force is close to being slope normal as was indicated in the force hodographs.

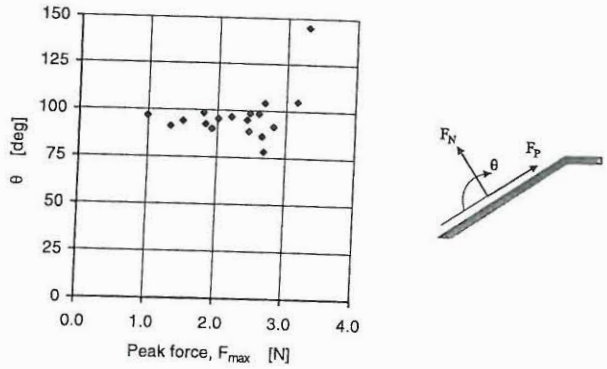

Figure 5.40: Correlation between direction θ and magnitude F_{max} of peak force.

The correlation between the peak force and the 90° and 45° force is depicted in Figure 5.41. As below SWL there is good correlation between peak force and 90° force but regarding the 45° force no correlation seems to be present.

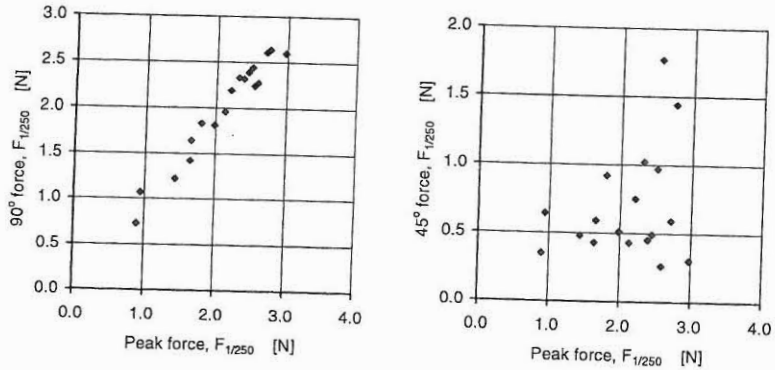

(a) *90° slope normal force $F_{1/250}$ and peak force $F_{1/250}$.*

(b) *45° down slope force $F_{1/250}$ and peak force $F_{1/250}$.*

Figure 5.41: Correlation between the peak force and the 90° and 45° force.

5.5.2 Influence of Wave Height

In Figure 5.42 the influence of wave height is depicted. All plots show significant scatter. The 90° and the peak force show almost the same pattern since the characteristic direction of the peak force is very close to the 90° force. These two force component show little increase with wave height. The 45° force show no influence of wave height at all.

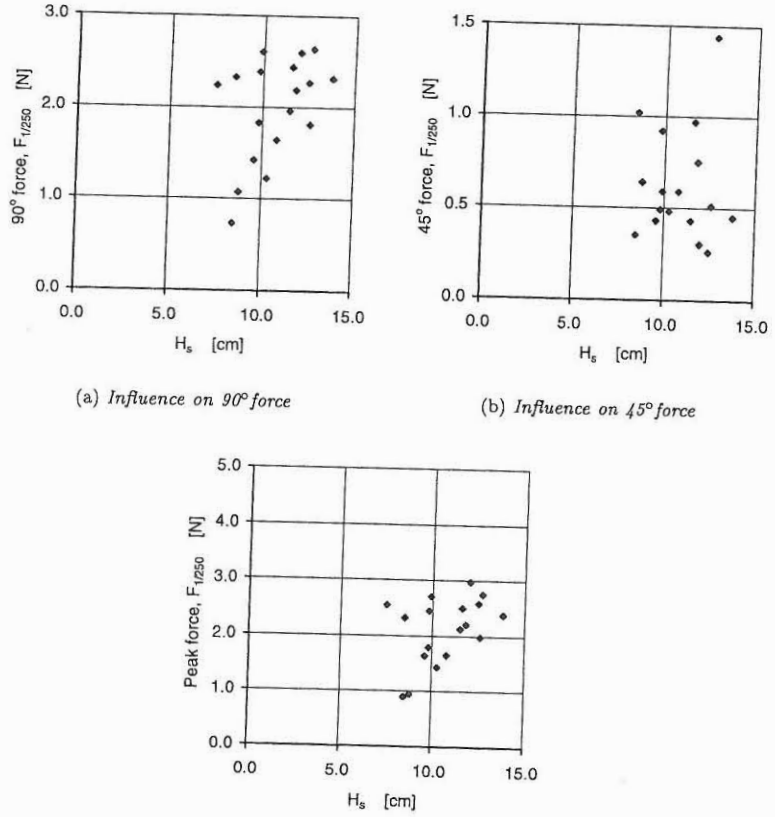

(a) *Influence on 90° force*

(b) *Influence on 45° force*

(c) *Influence on peak force*

Figure 5.42: Influence of significant wave height on wave induced force.

5.5.3 Influence of Wave Period – Surf Similarity Parameter

In Figure 5.43 the influence of surf similarity parameter (or period since only one slope angle is being tested) is depicted. Both the 90° and the peak force show an almost linear increase with increasing surf similarity parameter and thus also with increasing period. The 45° force show no clear influence of wave period. However, the limited data does not allow for any conclusions above $\xi_m = 4.0$ at which the force is expected to maximize.

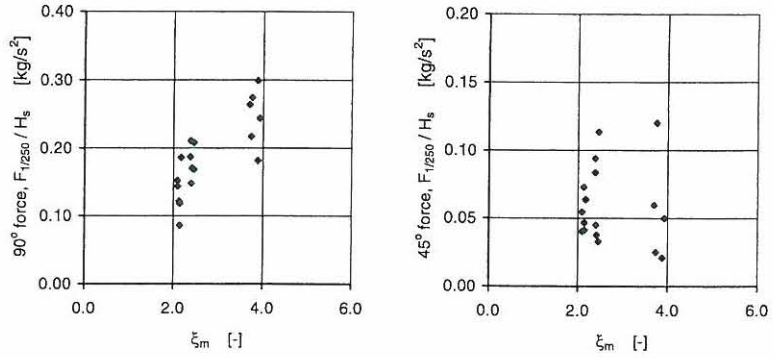

(a) *Influence on 90° force*

(b) *Influence on 45° force*

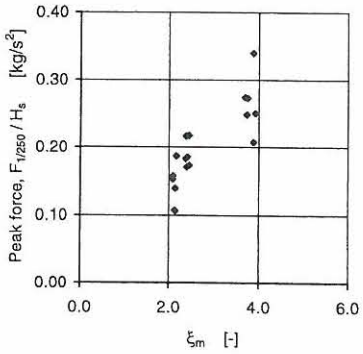

(c) *Influence on peak force*

Figure 5.43: Influence of surf similarity parameter on wave induced force.

5.5.4 Influence of Water Depth

In Figure 5.44–5.46 the influence of water depth on the three force components is depicted.

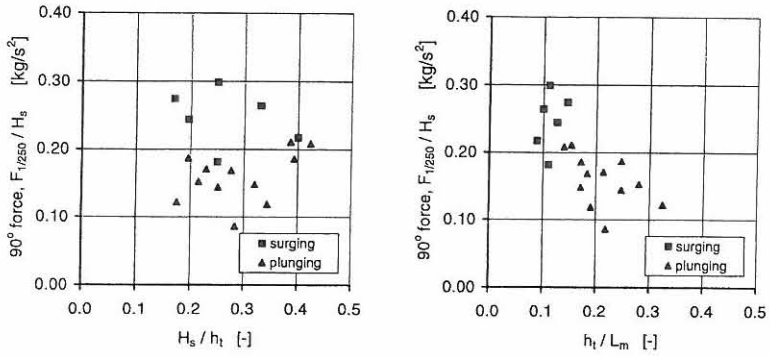

Figure 5.44: Influence of rate of dispersion and non-linearity on 90° force.

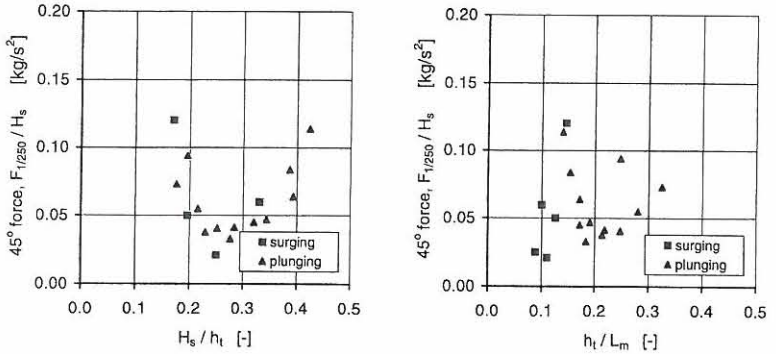

Figure 5.45: Influence of rate of dispersion and non-linearity on 45° force.

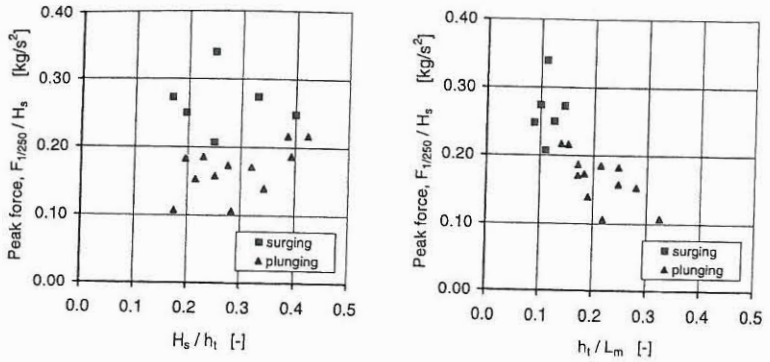

Figure 5.46: Influence of rate of dispersion and non–linearity on peak force.

Due to the limited number of tests it is not possible to conclude which influence the water depth has when separating between plunging and surging waves. However, considering all data the 90° and peak force seems to be highly dependent on the rate of non–linearity: Low values ($h_t/L_m < 0.2$) are connected with maximum forces. This seems to be a result of the surging waves always featuring the largest uprush. All three force components seems independent of the rate of dispersion and further, the 45° force is also independent of the rate of non–linearity.

5.5.5 Influence of Groupiness

In Figure 5.47 the influence of the groupiness factor is depicted. Similar to below SWL the 90° and the peak force show an almost linear increase with increasing groupiness factor. On the other hand no influence on the 45° force is observed. This is expected since the force component shows no influence with varying wave height.

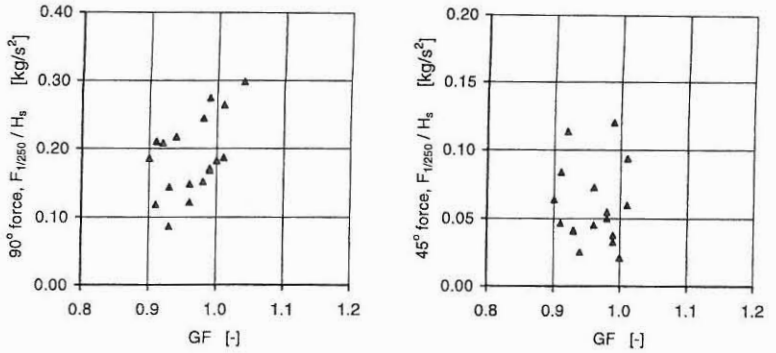

(a) *Influence on 90° force*

(b) *Influence on 45° force*

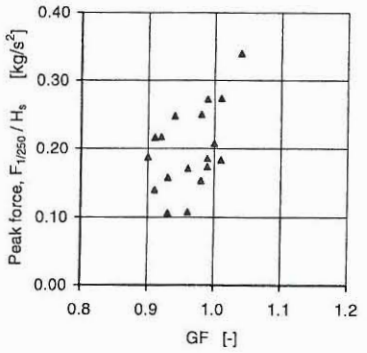

(c) *Influence on peak force*

Figure 5.47: Influence of groupiness factor on wave induced force.

5.6 Summary on Wave Induced Forces

Forces below SWL

The induced forces below SWL seems to be produced mainly by the downrush and the reversal of the flow when the downrush meets the uprush of the succeeding waves. The last situation is earlier identified as the resonance situation and from the conducted tests this situation also produce the largest forces, both in the upward and slope normal direction. Forces in other directions are smaller in magnitude but has a longer duration.

Three force components in outward directions were extracted from the force records: the peak force, the 90° force acting slope normal and the 45° force acting in the 45° downslope direction. The influence of different wave parameters on the forces was investigated and relevant models were fitted to the data, see Table 5.4 for a detailed influence of each wave parameter. Generally, a strong influence of wave height and groupiness factor was found whereas the influence of wave period and water depth is almost negligible. The effect of period is to some extend described when related to the slope angle in the surf similarity parameter. This parameter separate the behaviour of the forces between plunging and surging waves.

Forces above SWL

Above SWL the induced forces are produced mainly by the uprush. Both the large uprush velocities as well as the change in buoyancy when the water covers the stone contribute to the resulting forces. The magnitudes of the down–slope directed forces are small since only a small amount of the downrushing water act on the model stone. Instead of rushing down the slope a large amount of the water percolates into the breakwater.

The same three force components considered below SWL is also extracted for the forces above SWL and the influence of selected wave parameters was investigated qualitatively. No models were fitted to the data due to the limited amount of data.

CHAPTER 6

Evaluation of Wave–Force Models

Based on the correlation between waves and forces the purpose of the present chapter is to compare derived wave–force models in chapter 5 with the general approach when describing stability as discussed in chapter 3. The influence of selected wave parameters on stability is compared to existing stability formula using selected wave–force models to derive comparable stability equations.

6.1 Stability Assessment and Force Models

For comparison of the stability and the wave forces it is necessary to relate the wave forces to some kind of stability criterion on which the necessary stone size (or weight) can be calculated. Based upon several static pull–out tests Wang and Peene (1990) found that the resistance of quarry stone is mainly weight related. Simple stability formulae relating the wave induced force to the stabilizing gravity force can therefore be derived if assuming a certain mode of failure. Basically, three types of stone motions were considered:

- Hudson–type failure: $\dfrac{F}{F'_G} \geq 1.0$
- Lifting failure: $\dfrac{F}{F'_G \cos(\alpha + 90 + \theta)} \geq 1.0$
- Rolling/sliding failure: $\dfrac{|F_P - F'_G \sin\alpha|}{\tan\phi(F'_G \cos\alpha - F_N)} \geq 1.0$

The Hudson–type failure is simply the ratio of the amplitude of destabilizing and stabilizing force. The lifting failure is very similar in type as the Hudson–type failure. However, this type of failure takes into account the actual directions of the acting forces and is simply a projection of the forces onto the same direction. The rolling/sliding failure will give a stability criterion similar to that of Iribarren (1938,1965). If $F_P < F'_G \sin\alpha$ then the criterion for sliding becomes identical to that of rolling. On steeper slopes down–slope rolling occur over up–slope rolling, i.e. F_P is always less than 0.

In each of the three stability criterion the wave–force models derived in chapter 5 have been introduced as the driving force and the diameter have been isolated to obtain a stability formula, see Table 6.1–6.2 for the Hudson–type failure. This calculated diameter is a measure of the necessary D_{n50}.

In order to evaluate the efficiency of the derived stability formulae, the calculated diameter have been compared to the diameter necessary to remain in position found in model tests. The model test results used for comparison are from Thompson and Shuttler (1975) and Van der Meer (1988) and only wave conditions corresponding to the same level of damage have been used, i.e. from the model tests conducted with a fixed stone size and structure, the damage development was investigated and corresponding to a fixed damage of $S = 3$ or 5% damage the wave condition resulting in this degree of damage were retrieved. Hereby a combination of D_{n50}, Δ, h_t, H_s, T_m and $\cot\alpha$ was obtained. The retrieved wave conditions were used to calculate a diameter from the stability formulae in Table 6.1–6.2 or the Hudson–type and Van der Meer stability formulae. The diameter from the model tests was used for reference in the relation $(D^{calc}_{n50} - D^{test}_{n50})/D^{test}_{n50}$ in order to depicted the degree of scatter in each of the stability formulae with different wave parameters.

Since the tests from Thompson and Shuttler (1975) and Van der Meer (1988) were conducted with structures of different permeability/porosity, only data corresponding to a structure having a notional permeability coefficient P of 0.1 are used. Despite the fact that the structure in chapter 5 corresponds to a permeability coefficient of 0.3–0.4, a significantly better agreement with both the Hudson and the Van der Meer formula was obtained when using data from $P = 0.1$– structures instead of data from structures having $P = 0.5$ and $P = 0.6$.

In the following only comparisons based on the Hudson–type failure are shown. Using the lifting failure mode no improvements over the Hudson–type failure were achieved. However, using the 45° and peak force more scatter was introduced. Similar comparisons based on the rolling/sliding failure mode introduced more scatter in the relations and was unable to predict the influence of wave height, wave period and slope angle.

6.1.1 Comparison with Hudson–type

The 90°, 45° and the peak force model fitted to all data have been introduced into the stability criterion $F/F'_G \geq 1.0$ and the necessary diameter D_{n50} was extracted. In Table 6.1 the three stability formulae are given.

Stability formula: $D^g_{n50} = a\frac{\sqrt{g}^c}{\Delta^b} H_s^b T_m^c \tan^d\alpha \left(\frac{h_t}{H_s}\right)^e GF^f$

Parameters:	a	b	c	d	e	f	g
90° force	0.65	1.08	0.0	0.31	0.0	1.0	1.08
45° force	0.46	0.96	0.0	0.42	0.0	1.0	0.96
Peak force	1.11	1.01	0.0	0.17	0.0	1.0	1.01

Table 6.1: Stability formulae based on 90°, 45° and peak force.

As discussed in the previous paragraph the derived stability relations are compared to measured data using the relation $(D^{calc}_{n50} - D^{test}_{n50})/D^{test}_{n50}$. For reference a necessary diameter is calculated using the SPM (1977) formula with $K_D = 2$ and a comparison of the scatter is shown in Figure 6.1. Generally, the SPM (1977) formula capture the influence of wave height and slope angle well although the scatter increases as the slope flattens. On the other hand the influence of wave period is not described well as the formula tends to underpredict the diameter for large periods.

In Figure 6.2–6.4 the scatter obtained by using the stability formulae in Table 6.1 is depicted.

In Figure 6.1 the scatter obtained by using the SPM (1977) formula to measured data is shown.

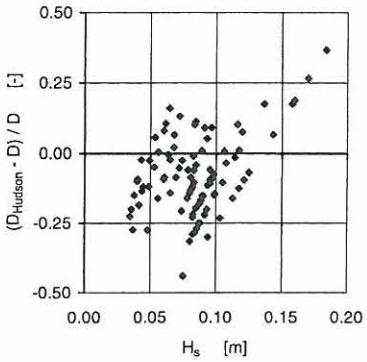

(a) *Scatter with wave height*

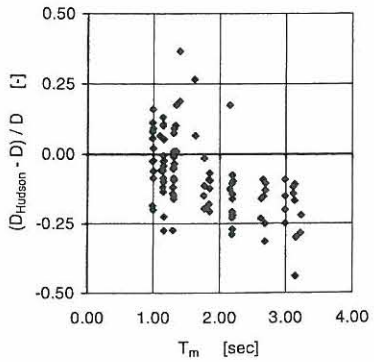

(b) *Scatter with wave period*

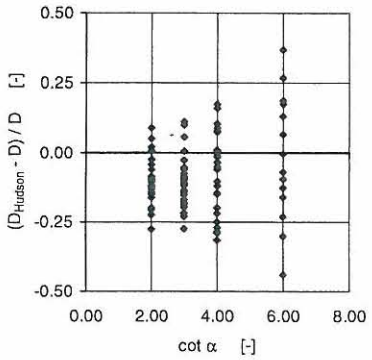

(c) *Scatter with slope angle*

Figure 6.1: Comparison of scatter obtained by using the SPM (1977) formula on measured data, $\mu = -0.08$, $\sigma = 0.14$.

In Figure 6.2 the scatter obtained by using the stability formula based on the 90° force to measured data is shown. The 90° force formula show tendencies very similar to those of the SPM (1977) formula.

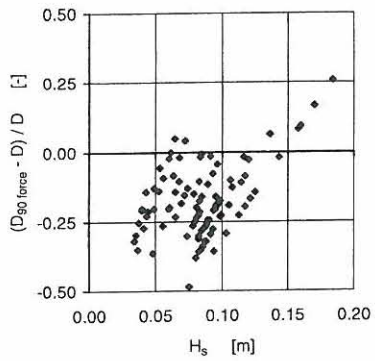

(a) *Scatter with wave height*

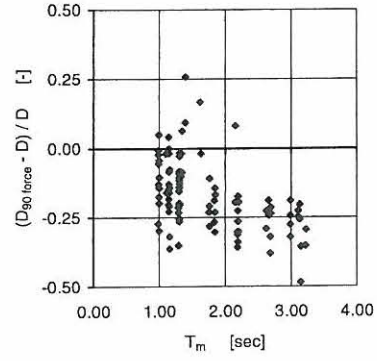

(b) *Scatter with wave period*

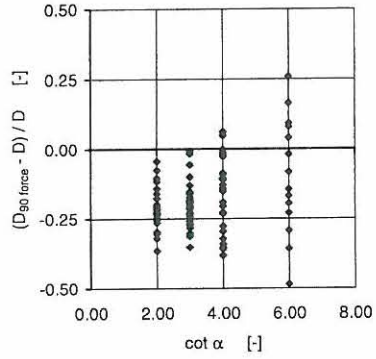

(c) *Scatter with slope angle*

Figure 6.2: Comparison of scatter obtained by using the 90° force formula on measured data, $\mu = -0.17$, $\sigma = 0.13$.

In Figure 6.3 the scatter obtained by using the stability formula based on the 45° force to measured data is shown. Using the 45° force formula similar tendencies as before are observed although the scatter is reduced significantly.

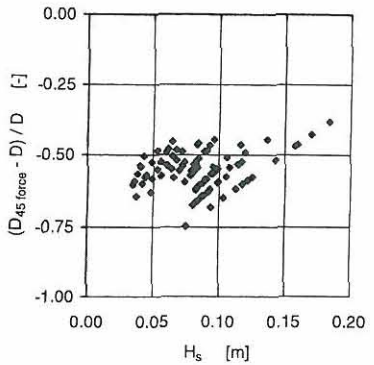

(a) *Scatter with wave height*

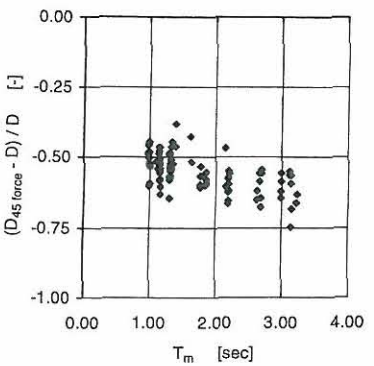

(b) *Scatter with wave period*

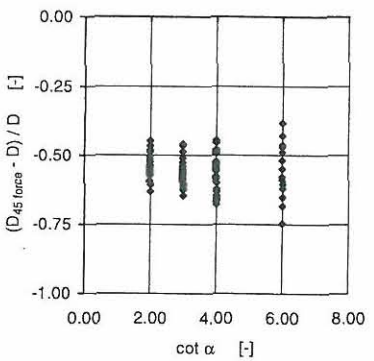

(c) *Scatter with slope angle*

Figure 6.3: Comparison of scatter obtained by using the 45° force formula on measured data, $\mu = -0.56$, $\sigma = 0.06$.

In Figure 6.4 the scatter obtained by using the stability formula based on the peak force to measured data is shown. No improvements using the peak force to describe the stability are gained since the scatter is increased considerably compared to the SPM (1977) formula.

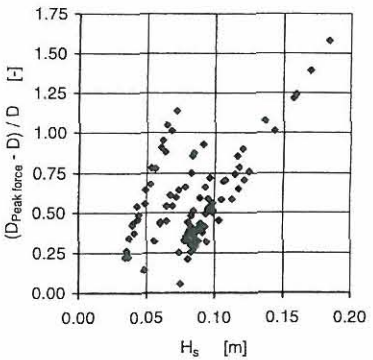

(a) *Scatter with wave height*

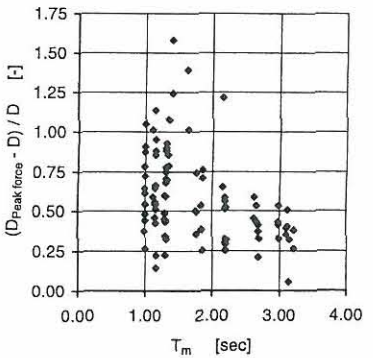

(b) *Scatter with wave period*

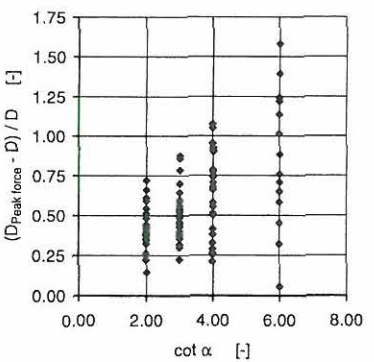

(c) *Scatter with slope angle*

Figure 6.4: Comparison of scatter obtained by using the peak force formula on measured data, $\mu = 0.58$, $\sigma = 0.28$.

6.1.2 Comparison with Van der Meer

Introducing the 90°, the 45°and the peak force models derived separately for plunging and surging waves in the stability criterion $F/F'_G \geq 1.0$ leads to the stability formula presented in Table 6.2.

Stability formula: $D^g_{n50} = a\frac{\sqrt{g}^c}{\Delta^b} H_s^b T_m^c \tan^d\alpha \left(\frac{h_t}{H_s}\right)^e GF^f$

Parameters:		a	b	c	d	e	f	g
90° force	Plunging	0.31	1.30	0.13	0.46	0.0	1.0	1.365
	Surging	0.40	0.85	-0.1	-0.11	0.2	1.0	0.800
45° force	Plunging	0.30	1.04	0.03	0.48	0.0	1.0	1.055
	Surging	0.31	0.94	0.0	0.22	0.0	1.0	0.940
Peak force	Plunging	0.21	0.95	0.52	0.33	0.0	1.0	1.21
	Surging	0.65	1.00	-0.1	-0.25	0.2	1.0	0.95

Table 6.2: Stability formulae based on 90°, 45° and peak force.

For reference the scatter obtained by using the Van der Meer formula is shown in Figure 6.5. When calculating the necessary diameter a constant damage level of $S = 3$ was used. The influence of the significant wave height is captured well by the Van der Meer formula whereas a little underprediction of the necessary diameter is observed for increasing period and flatter slopes.

The scatter obtained by using the stability formula in Table 6.2 is depicted in Figure 6.6 6.8. From Figure 6.6–6.8 the following conclusions can be retrieved:

- The 90° force formula depicts a scatter comparable with that obtained by the Van der Meer formula. The formula provides a good description of the influence of wave period and wave height when considering plunging waves. In surging waves the influence of wave height is not described well. With respect to the slope angle the force increases as the slope flattens.
- The 45° force formula provides a good description of the influence of wave height, period and slope angle. The depicted scatter is less than obtained by the Van der Meer formula.
- The peak force formula depicts the largest scatter. The behaviour of the formula is comparable with that of the 90° force.

In Figure 6.5 the scatter obtained by using the Van der Meer formula to measured data is shown.

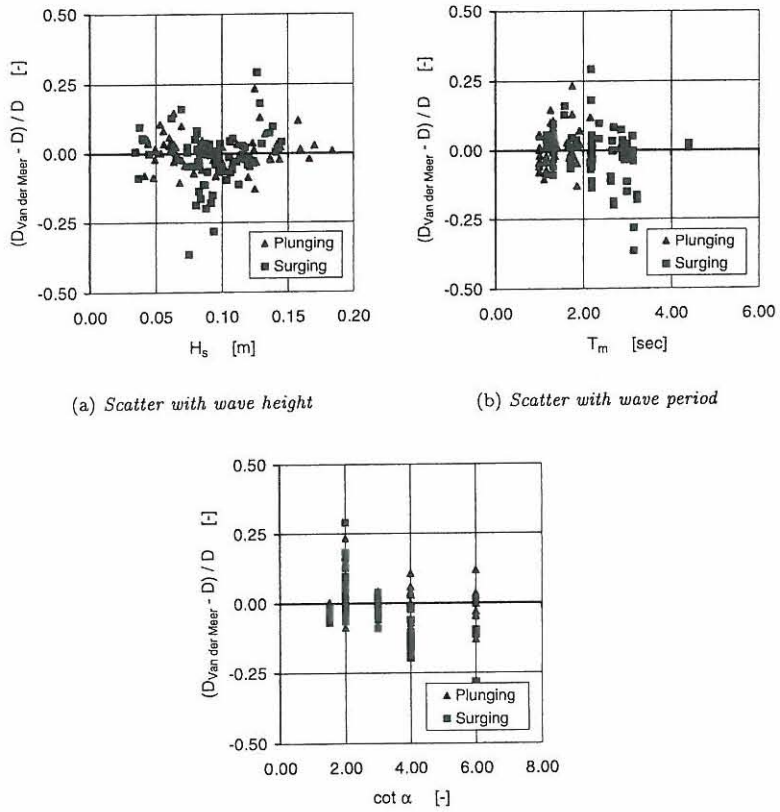

(a) *Scatter with wave height*

(b) *Scatter with wave period*

(c) *Scatter with slope angle*

Figure 6.5: Comparison of scatter obtained by using the Van der Meer formula on measured data, $\mu = -0.01$, $\sigma = 0.08$.

In Figure 6.6 the scatter obtained by using the stability formula based on the 90° force to measured data is shown.

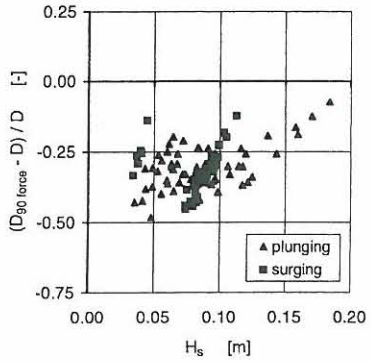

(a) *Scatter with wave height*

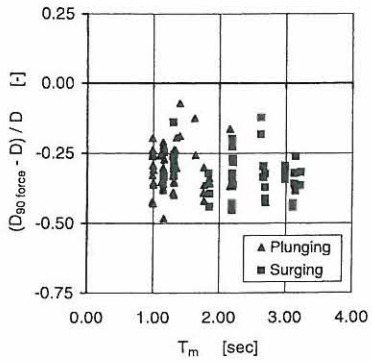

(b) *Scatter with wave period*

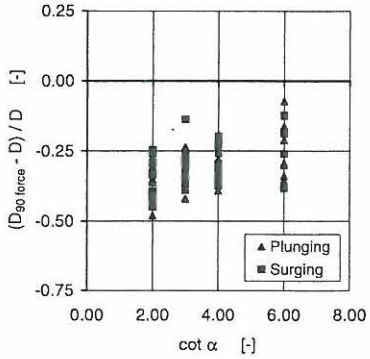

(c) *Scatter with slope angle*

Figure 6.6: Comparison of scatter obtained by using the 90° force formula on measured data, $\mu = -0.31$, $\sigma = 0.08$.

In Figure 6.7 the scatter obtained by using the stability formula based on the 45° force to measured data is shown.

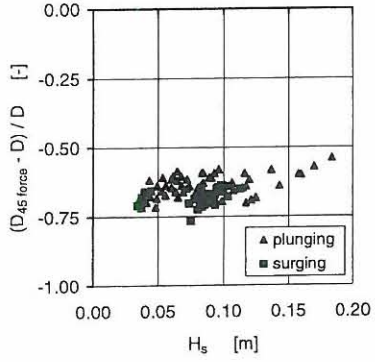

(a) *Scatter with wave height*

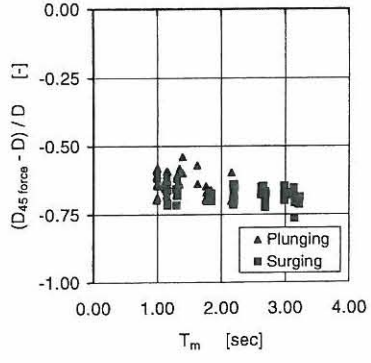

(b) *Scatter with wave period*

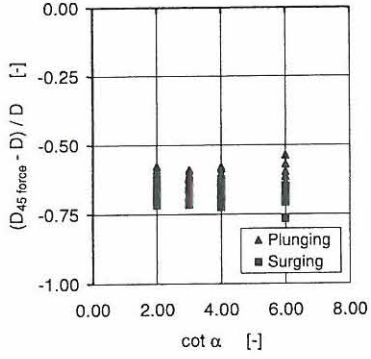

(c) *Scatter with slope angle*

Figure 6.7: Comparison of scatter obtained by using the 45° force formula on measured data, $\mu = -0.66$, $\sigma = 0.04$.

In Figure 6.8 the scatter obtained by using the stability formula based on the peak force to measured data is shown.

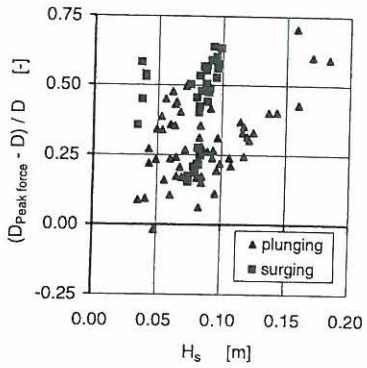

(a) *Scatter with wave height*

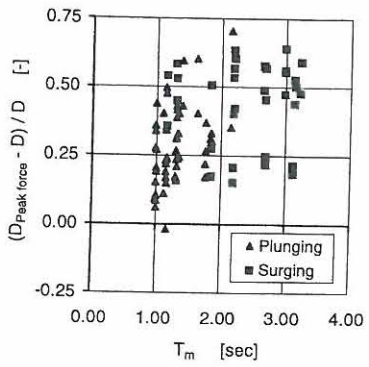

(b) *Scatter with wave period*

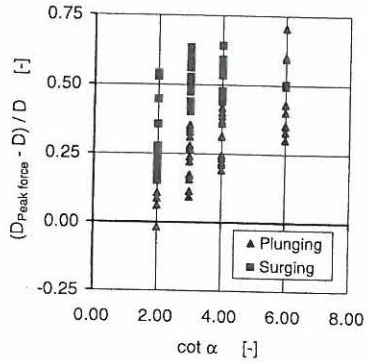

(c) *Scatter with slope angle*

Figure 6.8: Comparison of scatter obtained by using the peak force formula on measured data, $\mu = 0.38$, $\sigma = 0.21$.

6.1.3 Peak Enhancement and Groupiness Factor

The influence of wave grouping on the stability is determined by two factors: The spectral shape described by γ and the energy exceedence pattern described by GF.

In paragraph 5.4.7 the influence of γ on the wave forces was found to be insignificant. This is also in accordance with the conclusion reached by Medina et al. (1990) as described in paragraph 3.3.5. On the other hand the groupiness factor was found to cause a linear increase in the induced forces and thus also a decrease in stability. This influence is comparable with the influence of wave height. However, in should be kept in mind that the variations in GF are in the order of 0.9–1.1 whereas a much larger variation in wave height is expected. An increase of 10% in groupiness factor from 1.0 to 1.1 causes an increase of 23–43% in necessary stone mass (see Table 6.2 regarding influence of GF on each force component). Unfortunately the reference model test data did not allow for calculation of the groupiness factor making a direct comparison impossible. However, the influence of GF on the induced forces is the same independent of direction so the influence on the stability seems obvious.

6.2 Force Required for Armour Stone Motion

Due to the large scatter related to the peak force based stability formulae and the poor correlation with general accepted stability formulae this peak is considered not to be important for stability. A reason why the force is unable to lift any stones despite the magnitude might be the short duration compared to the 90° and the 45° force, c.f. Figure 5.6.

Considering the 45° force the amount of scatter is reduced significantly compared to all other considered stability formulae and the influence of slope angles compares to that of Van der Meer opposite the 90°and the peak force formulae. The stability ratio F/F'_G is much lower than one indicating that this force component is not decisive for stability.

Considering the 90° force, the stability formula fitted to all data gives a response similar to the SPM (1977) formula. Further considering the stability formula based on a separation between plunging and surging waves the same amount of scatter as obtained using the Van der Meer formula is achieved. This indicate that the 90° force gives a good description of the armour layer response. However, the influence of slope angle is significantly different from that of Van der Meer (c.f. paragraph 3.3.2). Comparing the influence of wave height and period in plunging waves described by the force formulae to that of Van der Meer, the

influence of wave height is stronger in the force based stability formulae whereas the influence of period is much weaker. The results obtained using the 90° force verify the simple approach using the Hudson–type formulae.

Implementing the influence of number of waves in the force based stability formulae in a similar way as Van der Meer neither decrease nor increase the amount of scatter present. A reason for this might be that for a sufficiently large number of waves the considered force estimate, i.e. the average of the highest 1/250 of the forces, only changes slightly when changing the number of waves (c.f. the distribution of forces in paragraph 5.4.1).

With respect to the influence of water depth on the stability, no influence is observed in plunging waves whereas some influence on the 90° force is observed in surging waves and no influence on the 45° force is seen. Thus, the influence of water depth on the stability in waves below the breaking criterion $H_s/h < 0.5$ is insignificant.

CHAPTER 7

Conclusion

Following an introduction of the principles and the use of rubble mound breakwaters and the related failure modes, the design methods applied when designing the most vital part of the rubble mound breakwater, namely the main armour layer, was discussed in more details. The discussion revealed that the design situation was, despite major research efforts to obtain reliable design tools and a vast amount of published on the breakwater response, characterized by a number of empirical formulae necessitating the use of model tests. Even then large variability in the actual and the predicted behaviour of the rubble mound breakwater is observed. This description gave rise to the question: *Why is it so difficult to design breakwaters?*

To enlighten the problem, the aspects of designing a breakwater was broke down into four individual involved physical processes:

- Wave propagation from deep to more shallow water where the structure is situated and the transformation of the wave characteristics.
- The wave induced flow up and down the slope and inside the breakwater produced when the waves break on the slope.
- The induced loading on individual stones produced by the velocity and acceleration of the flow.
- The response of the armour layer according to the forces acting on the stones.

In chapter 2 each of the four processes and the link between them were described to retrieve the state of physical understanding. The discussion revealed that the

stochastic characterization of the waves before reaching the structure is sufficient when dealing with non–breaking waves. The processes of breaking are poorly understood and beside influencing the waves before reaching the structure, the breaking process is also decisive for the character of the velocity and acceleration in the induced flow. In general, when dealing with breaking waves two types of breakers are identified each featuring different characteristics on the flow: The plunging and the surging breakers. Due to the complexity of the wave breaking and the complex construction of the breakwater no theory is at present available from which it is possible to calculate the relevant flow characteristics. This also effect the calculation of the induced loading. Furthermore, even if a good description of the forces acting on a single stone was available the effects of these forces on the stone motion are not clear. Whether a stone remains in position or not is extremely dependent on the ability of the neighbouring stones to create a good stabilizing support as well as high friction forces. If stones start to rock these conditions change.

Table 1.1 gave an overview of the different stability formulae presented up till today. The presented stability formulae all contain some similarities but also large differences among the different formulae exists. Based on two of the most used stability formulae the large prevailing scatter was exemplified in Figure 1.4 based on model test results. These prevailing problems were discussed in more detail in chapter 3. In chapter 3 a list of governing variables was compiled and the influence of the most significant parameters on the assessment on the hydraulic stability was discussed. The large amount of variables involved show the very complex character of especially the construction of the breakwater. It is only possible to describe the rubble mound breakwater in average terms and in practice hardly two breakwaters are alike making it very difficult to establish reliable design formulae. In general, the influence of each of the parameters on the stability is well documented in qualitative terms. However, when trying to quantify the influence of each parameter the numerous involved structural and hydraulic parameters make it impossible to separate to influence from the single parameter considered.

The correlation between the wave induced forces and the stability was discussed in chapter 4 based on physical model tests with scale models of different prototype breakwaters. Different methods of armour stone placements and the characteristics of the wave induced loading in four positions over the slope were investigated. Mainly different configurations of single layer slopes were considered.

With respect to the stability of the armour stones the tests with different methods of placing the stones showed that the lower part of the slope needs to be sufficiently stable allowing only small settlements in order to provide a secure foundation for the stones directly exposed to wave attack around SWL. Comparing a random placing of the individual stones with an orderly placing, where the

longest side of the stone is positioned almost perpendicular to the filter layer and the smallest area facing the waves, a very high stability can be obtained. Considering a damage level of 5% a stability coefficient K_D in the Hudson formula as high as $K_D = 8.1$ can be obtained when placing the stones orderly in a single layer compared to a stability of $K_D = 0.9$ when placing the stones randomly in a single layer. Combinations of two and single layers and of orderly and randomly placement only results in somewhat higher stability coefficients varying between 0.9 and 2.7. See paragraph 4.3.4 to 4.3.7 regarding a more detailed behaviour of each method of placement.

When relating stability and wave force observations it was found that an outward directed force of some duration was necessary to remove any stones. The large slamming forces of short duration present in SWL where waves break directly on the stones were not able to remove the stones.

A detailed parametric study of the wave induced forces was discussed in chapter 5 based on several model tests conducted with an idealized model of a typical rubble mound breakwater in order to investigate the direct relation between waves and forces.

The induced forces below SWL seems to be produced mainly by the downrush and the reversal of the flow when the downrush meets the uprush of the succeeding waves. The last situation also produces the largest forces, both in the upward and slope normal direction. Forces in other directions are smaller in magnitude but has a longer duration.

Three force components in outward directions were extracted from the force records: the peak force, the 90° force acting slope normal and the 45° force acting in the 45° downslope direction. The influence of different wave parameters on the forces was investigated and relevant models were fitted to the data. Generally, a strong influence of wave height and groupiness factor was found whereas the influence of wave period and water depth is almost negligible. The effect of period is to some extend described when related to the slope angle in the surf similarity parameter. This parameter separate the behaviour of the forces between plunging and surging waves.

Above SWL the induced forces are produced mainly by the uprush. Both the large uprush velocities as well as the change in buoyancy when the water covers the stone contribute to the resulting forces. The magnitudes of the down–slope directed forces are small since only a small amount of the downrushing water act on the model stone. Instead of rushing down the slope a large amount of the water percolates into the breakwater.

The same three force components considered below SWL is also extracted for the forces above SWL and the influence of selected wave parameters was investigated

qualitatively. No models were fitted to the data due to the limited amount of data.

To evaluate the efficiency of the derived force models to describe the stability of the armour layer a comparison with a Hudson–type and the Van der Meer formulae was performed based on the same set of model test data Van der Meer used. Considering the 90° force a good description of the armour layer response is obtained. A simple stability formula based on the 90° force compares extremely well with the well documented Hudson–type formula.

When separating between plunging and surging waves the 90° force based formula provides a scatter in the same order of magnitude as obtained using the Van der Meer formula. However, comparing the influence of wave height and period in plunging waves described by the force based formulae to that of Van der Meer, the influence of wave height is stronger in the force based stability formulae whereas the influence of period is much weaker.

Unfortunately, it was not possible to reduce the present scatter further by improving the simple stability considerations based on the force components by considering both lifting and rolling/sliding failure modes and by inclusion of an extra stabilizing friction force.

References

Ahrens, J.P., 1975
Large Wave Tank Tests of Riprap Stability, Technical Memorandum no. 51, Waterways Experiment Station, CERC.

Andersen, O.H., 1994
Flow in Porous Media with Special Reference to Breakwater Structures, Ph.D.–thesis, Series paper no. 7, Hydraulics and Coastal Engineering, Aalborg University.

Araki, S., Deguchi, I., 1998
Experimental Study on Profile Change of Rubble Mound Breakwater and Wave Forces on Rubble Stone, In: Proc. of the 8th Int. Offshore and Polar Engineering Conf., ISOPE, Montréal, Canada.

Barends, F.B.J., 1988
Discussion on paper 5, Proc. of the Conf.: Breakwater '88, In: Design of Breakwater, Proc. of the Conf.: Breakwater '88, Institution of Civil Engineers, Eastbourne.

Barends, F.B.J., Hölscher, P., 1988
Modelling Interior Process in a Breakwater, In: Design of Breakwater, Proc. of the Conf.: Breakwater '88, Institution of Civil Engineers, Eastbourne, pp. 49–80.

Bratteland, E., Tørum, A., 1971
Stability Tests on a Rubble Mound Breakwater Head in Regular and Irregular Waves. Sørvær Fishing Port, Norway, In: Proc. of the 1st Int. Conf. on Port and Ocean Engineering under Arctic Conditions, Trondheim, Norway, pp. 360–380.

Bruun, P. (ed.), 1985
Design and Construction of Mounds for Breakwaters and Coastal Protection, Developments in Geotechnical Engineering Vol. 37, Elsevier Science Publishing, Amsterdam.

Bruun, P., Johannesson, P., 1974
A Critical Review of the Hydraulics of Rubble Mound Structures, Report no. 3, Division of Port and Harbour Engineering, Norwegian Institute of Technology, Trondheim.

Burcharth, H.F., 1979
The Effects of Wave Grouping on On–Shore Structures, Coastal Engineering, Elsevier, Vol. 2, pp. 189–199.

Burcharth, H.F., 1993
The Design of Breakwaters, Internal report, Hydraulics and Coastal Engineering Laboratory, Aalborg University.

Burcharth, H.F., Andersen, O.H., 1995
On the One–Dimensional Steady and Unsteady Porous Flow Equations, Coastal Engineering, Elsevier, Vol. 24, pp. 233–257.

CERC, Waterways Experiment Station, 1977
Shore Protection Manual, 3rd. edition, Vol. 2, U.S. Government Printing Office, Washington D.C.

CERC, Waterways Experiment Station, 1984
Shore Protection Manual, 4th. edition, Vol. 2, U.S. Government Printing Office, Washington D.C.

Christensen, R., 1996
Analysis of Variance, Design and Regression, 1st edition, Chapman & Hall.

CIRIA/CUR, 1991
Manual on the use of Rock in Coastal and Shoreline Engineering, Published jointly by the Construction Industry Research and Information Association in the UK and the Centre for Civil Engineering Research, Codes and Specifications in the Netherlands.

Cornett, A., 1995
Wave–Induced Forcing and Damage of Rock Armour, Ph.D.–thesis, University of British Columbia, Vancouver.

DS–449, 1983
Code of Practice for the Design and Construction of Pile Supported Offshore Structures (In Danish), Teknisk Forlag.

Elgar, S., Guza, R.T., Seymor, R.J., 1985
Wave Group Statistics from Numerical Simulations of a Random Sea, Applied Ocean Research, Vol. 7, No. 2, pp. 93–96.

Frigaard, P., 1993
AWASYS – Users Guide, Hydraulics and Coastal Engineering Laboratory, Aalborg University.

Frigaard, P., Brorsen, M., 1995
A Time–Domain Method for Separating Incident and Reflected Irregular Waves, Coastal Engineering, Elsevier, Vol. 24, Nos. 3–4.

Frigaard, P., Høgedal, M., Christensen, M., 1993
PROFWACO – Users Manual, Hydraulics and Coastal Engineering Laboratory, Aalborg University.

Goda, Y., Suzuki, Y., 1976
Estimation of Incident and Reflected Waves in Random Wave Experiment, In: Proc. of the 15th Int. Conf. on Coastal Engineering, ASCE, Honolulu, USA, pp. 828–845.

Gu, Z., Wang, H., 1991
Gravity Waves over Porous Bottoms, Coastal Engineering, Elsevier, Vol. 15, Nos. 5–6, pp. 497–524.

Gunbak, A.R., 1976
The Stability of Rubble–Mound Breakwaters in Relation to Wave Breaking and Run–Down Characteristics and to the $\xi = \tan\alpha\, T/\sqrt{H}$ *Number*, Ph.D.-thesis, Division of Port and Harbour Engineering, Norwegian Institute of Technology, Trondheim.

Hald, T., Frigaard, P., 1997
Performance of Active Wave Absorption Systems – Comparison of Wave Gauge and Velocity Meter Based Systems, In: Proc. of the 7th Int. Offshore and Polar Engineering Conf., ISOPE, Honolulu, Canada.

Hald, T., Tørum, A., 1997
Stability Investigations of Single Layer Rubble Mound Breakwaters (in Danish), Report STF22 A97252, SINTEF Civil and Environmental Engineering, Dep. of Coastal and Ocean Engineering.

Hedar, P.A., 1960
Stability of Rock–Fill Breakwaters, Doctoral thesis, Chalmers Tekniska Högskola, No. 26.

Hedar, P.A., 1986
Armour Layer Stability of Rubble–Mound Breakwaters, Journal of Waterway, Port, Coastal, and Ocean Engineering, ASCE, Vol. 111, No. 5, pp. 800–816.

Hickson, R.E., Rodolf, F.W., 1951
Design and Construction of Jetties, In: Proc. of the 1st Int. Conf. on Coastal Engineering, ASCE, Long Beach, USA, pp. 227–245.

Hudson, R.Y., 1958
Design of Quarry–Stone Cover Layers for Rubble–Mound Breakwaters, Research report no. 2–2, Waterways Experiment Station, CERC, Vicksburg.

Hudson, R.Y., Jackson, R.A., 1953
Stability of Rubble–Mound Breakwaters, Technical Memorandum 2–365, Waterways Experiment Station, CERC, Vicksburg.

Høgedal, M., Frigaard, F., Christensen, M., 1994
Generation of Long Waves using Nonlinear Digital Filters, Proc. of Int. Symp.: Waves - Physical and Numerical Modelling, IAHR, Vancouver, Canada, pp. 128–137.

IAHR, 1987
List of Sea State Parameters, In: Wave Analysis and Generation in Laboratory Basins, Proc. of the 22nd IAHR Congress, Lausanne, Schweiz.

Iribarren, R.C., 1938
Una Formula para el Calcula de los Diques de Escollera (In Spanish), Revista de Obras Publicas, Madrid, Spain.

Iwata, K., Miyazaki, Y., Mizutani, N., 1985
Experimental Study of the Wave Force Acting on Armour Rubble of a Rubble–Mound Slope, Natural Disaster Science, Vol. 7, No. 2, pp. 29–41.

Jensen, T., Andersen, H., Grønbech, J., Mansard, E.P.D., Davies, M.H., 1996
Breakwater Stability under Regular and Irregular Wave Attack, In: Proc. of the 25th Int. Conf. on Coastal Engineering, ASCE, Orlando, USA, pp. 1679–1692.

Johnson, R.R., Mansard, E.P.D., Ploeg, J., 1978
Effects of Wave Grouping on Breakwater Stability, In: Proc. of the 16th Int. Conf. on Coastal Engineering, ASCE, Hamburg Germany, pp. 2228–2243.

Juhl, J., Jensen, O.J., 1989
Wave Slamming Forces on Armour Units, In: Proc. of Seminar on Stresses in Concrete Armour Units, ASCE, pp. 61–78.

Juhl, J., Jensen, O.J., 1990
Wave Forces on Breakwater Armour Units, In: Proc. of the 22nd Int. Conf. on Coastal Engineering, ASCE, Delft, The Netherlands, pp. 1538–1551.

Kjelstrup, Sv., 1977
Berlevaag Harbour on the Norwegian Arctic Coast, In: Proc. of the 4th Int. Conf. on Polar and Ocean Engineering under Arctic Conditions, Memorial University at St. Johns, New Foundland.

Klopman, G., Stive, M.J.F., 1989
Extreme Waves and Wave Loading in Shallow Water, E & P Forum, Report no. 3.12/156.

Kobayashi, N., Wurjanto, A., Cox, D., 1990a
Rock Slopes under Irregular Wave Attack, In: Proc. of the 22nd Int. Conf. on Coastal Engineering, ASCE, Delft, The Netherlands, pp. 1306–1319.

Kobayashi, N., Wurjanto, A., Cox, D., 1990b
Numerical Model for Waves on Rough Permeable Slopes, Journal of Coastal Research, Special Issue no. 7, pp. 149–166.

Kobayashi, N., Wurjanto, A., Cox, D., 1990c
Irregular Waves on Rough Permeable Slopes, Journal of Coastal Research, Special Issue no. 7, pp. 167–184.

List, J.H., 1991
Wave Groupiness Variations in the Nearshore, Coastal Engineering, Elsevier, Vol. 15, Nos. 5,6, pp. 475–496.

Losada, M.A., Giménez–Curto, L.A., 1979
The Joint Effect of the Wave Height and Period on the Stability of Rubble Mound Breakwaters using Iribarren's Number, Coastal Engineering, Elsevier, Vol. 3, No. 2, pp. 77–96.

Madsen, O.S., 1974
Wave Transmission through Porous Structures, Journal of the Waterways, Harbors, and Coastal Engineering Division, ASCE, Vol. 100, No. WW3.

Mase, H., Iwagaki, Y., 1984
An Analysis of Wave Data for Wave Grouping, Coastal Engineering in Japan, Vol. 27, pp. 83–96.

Mase, H., Kita, N., Iwagaki, Y., 1983
Random Wave Simulation Considering Wave Groups, Coastal Engineering in Japan, Vol. 26, pp. 61–75.

Medina, J.R., McDougal, W.G., 1988
Discussion of: Deterministic and Probabilistic Design of Breakwater Armour Layers, Journal of Waterway, Port, Coastal, and Ocean Engineering, ASCE, Vol. 116, No. 4, pp. 508–510.

Medina, J.R., Fassardi, C., Hudspeth, R.T., 1990
Effects of Group on the Stability of Rubble Mound Breakwaters, In: Proc. of the 22nd Int. Conf. on Coastal Engineering, ASCE, Delft, The Netherlands, pp. 1552–1563.

Melby, J.A., Kobayashi, N., 1996
Incipient Motion of Breakwater Armour Units, In: Proc. of the 25th Int. Conf. on Coastal Engineering, ASCE, Orlando, USA, pp. 1803–1815.

Minesterio de Obras Publicas y Urbanismo, 1988
Diques de Abrigo en España, Fachadas Norte y Galicia (In Spanish), Tomo 1, M.O.P.U.

Minesterio de Obras Publicas y Urbanismo, 1988
Diques de Abrigo en España, Fachadas Canarias, Suratlantica y Surmediterranea (In Spanish), Tomo 2, M.O.P.U.

Minesterio de Obras Publicas y Urbanismo, 1988
Diques de Abrigo en España, Fachadas Levante, Cataluña y Baleares (In Spanish), Tomo 3, M.O.P.U.

Polubarinova–Kochina, P.Y., 1952
Theory of Ground Water Movement, University Press, Princeton.

PIANC, 1976
Final Report of the International Commission for the Study of Waves, PIANC Bulletin no. 25, Vol. III.

PIANC, 1992
Analysis of Rubble Mound Breakwaters, Supplement to PIANC Bulletin no. 78/79.

Sandström, Å., 1974
Wave Forces on Blocks of Rubble–Mound Breakwaters (In Swedish), Bulletin no. 83, Hydraulics Laboratory, Royal Institute of Technology, Stockholm.

Sawaragi, T., Iwata, K., Kobayashi, M., 1982
Condition and Probability of Occurence of Resonance on Steep Slopes of Coastal Structures, Coastal Engineering in Japan, Vol. 25, pp. 75–90.

Sawaragi, T., Ryu, C., Iwata, K., 1983
Considerations of the Destruction Mechanism of Rubble Mound Breakwaters due to the Resonance Phenomenon, In: Proc. of the 8th Int. Harbour Congress, Antwerp, Belgium, pp. 3.197–3.208.

Schäffer, H., 1996
Second–Order Wavemaker Theory for Irregular Waves, Ocean Engineering, Elsevier, Vol. 23, No. 1, pp. 47–88.

Sigurdsson, G., 1962
Wave Forces on Breakwater Capstones, Journal of the Waterways and Harbors Division, ASCE, Vol. 88, No. WW3, pp. 27–60.

Svee, R., 1962
Formulas for Design of Rubble–Mound Breakwaters, Journal of the Waterways and Harbors Division, ASCE, Vol. 88, No. WW2, pp. 11–21.

Thompson, D.M., Shuttler, R.M., 1975
Riprap Design for Wind Wave Attack. A Laboratory Study in Random Waves, Report EX 707, Hydraulic Research Station, Wallingford.

Thornton, E.B., Guza, R.T., 1983
Transformation of Wave Height Distribution, Journal of Geophysical Research, American Geophysical Union, Vol. 88, No. C10, pp. 5925–5938.

Tørum, A., 1992
Wave Induced Water Particle Velocities and Forces on an Armour Unit on a Berm Breakwater, Report STF60 A92104, SINTEF Civil and Environmental Engineering, Dep. of Coastal and Ocean Engineering.

Tørum, A., 1993
Reliability of Norwegian Breakwaters (in Norwegian), Report STF60 F93057, SINTEF Civil and Environmental Engineering, Dep. of Coastal and Ocean Engineering.

Tørum, A., 1994
Wave–Induced Forces on Armour Unit on Berm Breakwaters, Journal of Waterway, Port, Coastal, and Ocean Engineering, ASCE, Vol. 120, No. 3, pp. 251–268.

Van der Meer, J.W., 1988
Rock Slopes and Gravel Beaches under Wave Attack, Ph.D.–thesis, Delft University of Technology, Published as Delft Hydraulics Communication No. 396.

Vidal, C., Losada, M.A., Mansard, E.P.D., 1995
Suitable Wave–Height Parameter for Characterizing Breakwater Stability, Journal of Waterway, Port, Coastal, and Ocean Engineering, ASCE, Vol. 121, No. 2, pp. 88–97.

Wang, H., Peene, S.J., 1990
A Probabilistic Model of Rubble Mound Armour Stability, Coastal Engineering, Elsevier, Vol. 14, pp. 307–331.

APPENDIX A

Characteristics of Breakwater Model

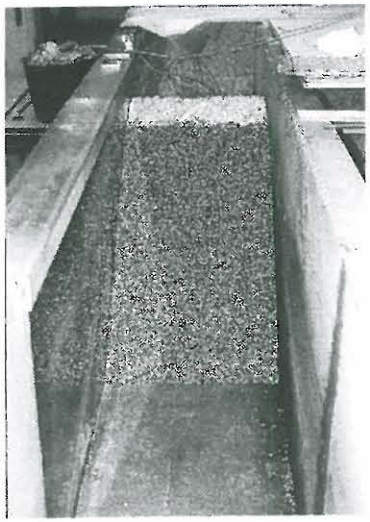

Breakwater core

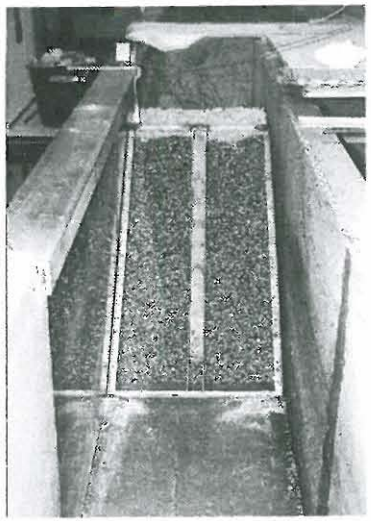

Frame mounted on core

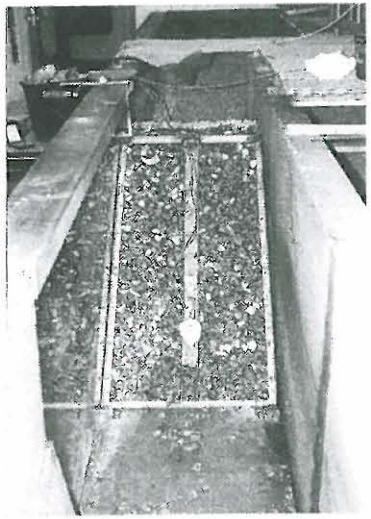

Model stone and transducer mounted

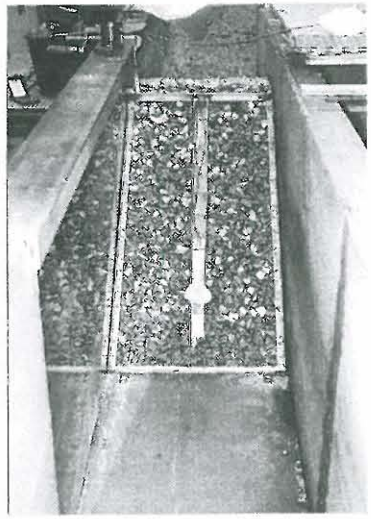

Aluminum box mounted

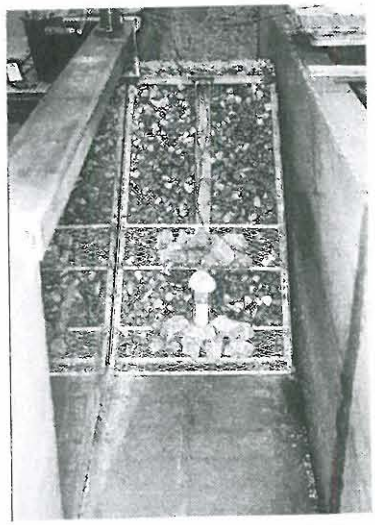

Neighbouring stones mounted

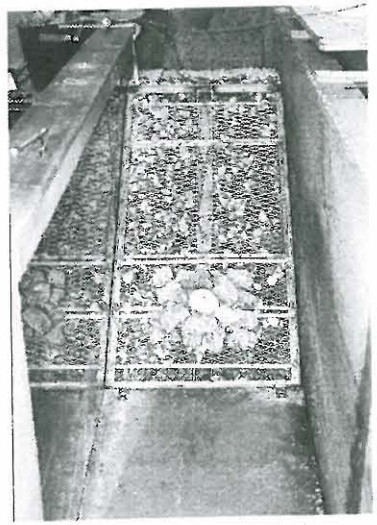

Metal sheets mounted

Calibration of force transducer

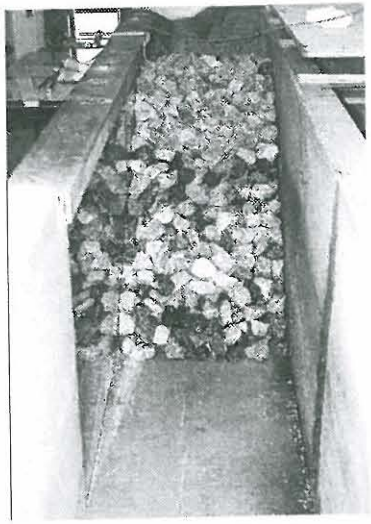

Armour layer placed

Calibration of force transducer

The force transducer with mounted model stone was calibrated against different known loads in different directions. The calibration was performed using different masses attached to one end of a wire and a newton meter attached to the other end. The newton meter was connected to the model stone and was used to check whether the actual subjected force on the stone corresponded to the load from the mass. By changing the angle between the slope and the wire the calibration in different directions and thus different combinations of the normal and the parallel force was obtained.

Within the tested range of loads the transducer behaved linearly in each direction. An example of a calibration curve for a load of 500 g is shown in Figure A.1.

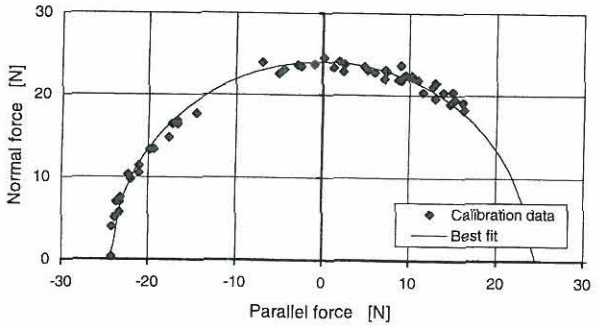

Figure A.1: Example of calibration of force transducer for 500 g load.

Dynamic characteristics of force transducer

The dynamic behaviour of the system composed of model stone and force transducer was investigated by imposing an impact force to the stone. Examples of obtained time series are shown below in Figure A.2 and A.3 for an impact force in both the normal and the parallel direction. From the time series the natural period was retrieved from zerocrossing analysis and the damping ratio was calculated from the logarithmic decrement. In the normal direction average natural period equals 0.16 s and average damping ratio equals 0.3. In the parallel direction average natural period equals 0.16 s and average damping ratio equals 0.4.

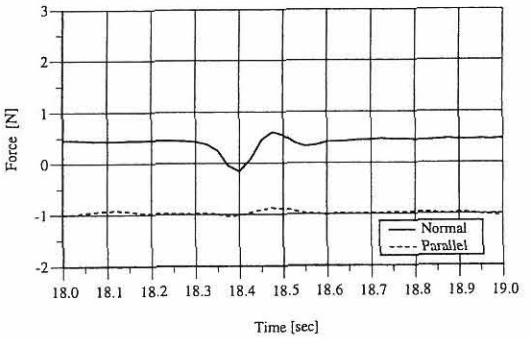

Figure A.2: Example of dynamic response to impulse force in normal direction.

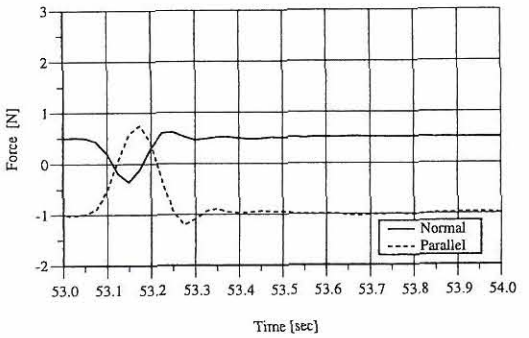

Figure A.3: Example of dynamic response to impulse force in parallel direction.

APPENDIX B

Results of Force Measurements

TEST PROGRAMME FOR POSITION 1

					OFFSHORE WAVES					LOCAL WAVES																	WAVE FORCES Normal:		45 deg down:		Peak:	
Test ID	cot a	h	gamma	N	Tm0	Tp0	Hs0	Hmax0	sp0	Tm	Tp	Hs	H1/10	H1/20	H1/30	H1/50	H250	H200	H150	H100	Hmax	GF	sm	sp	Im	Ip	F1/25	F1/250	F1/25	F1/250	F1/250	Theta
b1abaa1	2	0.3	3.3	1850	1.45	1.79	5.0	9.5	1.0	1.43	1.79	5.0	6.0	6.5	6.8	7.2	5.7	5.9	6.2	6.5	9.3	1.01	1.6	1.0	4.00	5.00	0.17	0.2	0.2	0.23	1.57	80.3
b1abaa2	2	0.3	3.3	1950	1.70	2.19	7.5	13.9	1.0	1.69	2.19	7.5	8.8	9.6	10.1	10.6	8.5	8.8	9.2	9.6	12.9	1.00	1.7	1.0	3.86	5.00	0.75	0.91	0.42	0.69	1.38	52.1
b1abaa3	2	0.3	3.3	2000	1.90	2.53	10.4	20.2	1.0	1.94	2.53	10.2	12.5	13.6	14.2	14.7	12.1	12.5	13.0	13.5	19.4	1.00	1.7	1.0	3.80	4.95	0.88	1.12	0.79	0.88	2.11	35.2
b1abaa4	2	0.3	3.3	2050	2.03	2.83	12.8	24.7	1.0	2.04	2.83	12.1	14.6	15.6	16.2	16.8	14.2	14.6	15.0	15.6	19.7	0.97	1.9	1.0	3.66	5.08	0.92	1.13	0.85	0.95	2.33	58.1
b1abab1	2	0.3	3.3	1800	0.88	1.04	4.8	9.5	2.8	0.88	1.04	4.7	5.6	6.2	6.5	6.8	5.3	5.5	5.8	6.1	9.6	1.00	3.9	2.8	2.54	3.00	0.26	0.34	0.36	0.45	0.81	56.6
b1abab2	2	0.3	3.3	1800	1.05	1.28	7.7	14.3	3.0	1.05	1.28	7.2	8.8	9.5	9.9	10.3	8.4	8.7	9.0	9.4	13.4	0.98	4.2	2.8	2.44	2.98	0.55	0.78	0.39	0.48	1.75	43.2
b1abab3	2	0.3	3.3	1800	1.18	1.50	10.4	18.2	3.0	1.19	1.48	9.9	11.7	12.7	13.2	13.8	11.2	11.6	12.0	12.6	17.9	0.97	4.5	2.9	2.36	2.94	1.11	1.36	0.52	0.66	2.44	52.1
b1abab4	2	0.3	3.3	1850	1.30	1.63	12.6	20.3	3.0	1.30	1.63	11.8	14.0	15.0	15.5	16.1	13.6	13.9	14.4	15.0	17.9	0.95	4.5	2.8	2.36	2.96	1.22	1.42	0.71	0.79	2.70	33.1
b1abab5	2	0.3	3.3	1900	1.38	1.71	14.2	22.4	3.1	1.39	1.79	13.2	15.0	15.9	16.3	16.8	14.6	14.9	15.3	15.8	18.9	0.91	4.4	2.8	2.39	3.08	1.31	1.54	0.9	1.12	2.68	43.6
b1abac2	2	0.3	3.3	1650	0.86	0.98	7.0	12.1	4.7	0.89	0.98	6.5	7.9	8.6	9.0	9.5	7.4	7.6	8.0	8.4	11.8	0.98	5.3	4.3	2.18	2.40	0.3	0.41	0.38	0.43	1.44	60.2
b1abac3	2	0.3	3.3	1700	0.97	1.16	9.7	16.7	4.6	1.00	1.20	8.7	10.6	11.5	12.0	12.4	10.0	10.3	10.7	11.3	14.3	0.95	5.8	3.9	2.12	2.54	0.38	0.53	0.36	0.46	1.88	62.7
b1abac4	2	0.3	3.3	1750	1.08	1.27	11.9	17.3	4.7	1.11	1.31	10.7	12.6	13.5	13.9	14.4	12.0	12.3	12.8	13.3	17.9	0.91	5.6	4.0	2.12	2.50	1.08	1.33	0.75	1.38	2.45	37.3
b1abac5	2	0.3	3.3	1600	1.16	1.40	13.6	19.7	4.4	1.20	1.48	12.6	14.2	15.2	15.7	16.2	13.5	13.9	14.3	14.9	20.2	0.86	5.6	3.7	2.11	2.60	1.47	1.71	0.98	1.21	2.57	261.9
b1bbaa1	2	0.4	3.3	1880	1.44	1.80	5.3	11.2	1.0	1.45	1.80	5.1	6.3	7.0	7.4	7.7	6.0	6.3	6.6	7.0	9.3	1.05	1.6	1.0	4.01	4.98	0.85	1.17	0.53	0.68	1.40	47.6
b1bbaa2	2	0.4	3.3	1900	1.72	2.23	7.7	14.6	1.0	1.75	2.23	7.5	9.1	10.0	10.4	10.9	8.7	9.0	9.4	9.9	14.2	1.02	1.6	1.0	3.99	5.09	1.03	1.25	0.8	0.88	2.00	48.0
b1bbaa3	2	0.4	3.3	1950	1.96	2.48	10.3	20.7	1.1	1.95	2.48	10.1	12.2	13.3	14.0	14.7	11.8	12.2	12.7	13.3	17.4	0.98	1.7	1.1	3.83	4.88	1.07	1.32	0.8	0.89	2.53	64.4
b1bbaa4	2	0.4	3.3	2000	2.12	2.65	12.9	24.5	1.2	2.02	2.60	12.5	15.4	16.8	17.5	18.3	15.0	15.5	16.1	16.9	22.2	1.02	2.0	1.2	3.57	4.59	1.17	1.51	0.95	1.07	2.78	52.2
b1bbab1	2	0.4	3.3	1750	0.88	1.04	5.1	11.2	3.0	0.88	1.02	4.9	5.9	6.4	6.7	7.0	5.6	5.8	6.0	6.3	9.2	0.96	4.1	3.0	2.48	2.88	0.28	0.35	0.29	0.33	0.94	89.4
b1bbab2	2	0.4	3.3	1820	1.05	1.27	7.6	14.1	3.0	1.05	1.27	7.2	8.9	9.8	10.2	10.8	8.4	8.7	9.2	9.7	13.1	1.00	4.2	2.9	2.44	2.96	0.77	1.21	0.52	0.64	1.82	38.1
b1bbab3	2	0.4	3.3	1800	1.19	1.45	9.9	18.6	3.0	1.19	1.45	9.5	11.3	12.3	12.9	13.5	10.8	11.2	11.6	12.2	16.8	0.95	4.3	2.9	2.41	2.94	1.21	1.45	0.52	0.74	2.67	63.7
b1bbab4	2	0.4	3.3	1900	1.30	1.55	12.0	20.8	3.2	1.31	1.62	11.4	13.7	14.7	15.3	15.9	13.2	13.6	14.1	14.7	19.4	0.96	4.3	2.8	2.42	3.00	1.45	1.63	0.77	0.86	2.96	61.4
b1bbab5	2	0.4	3.3	1900	1.42	1.70	14.3	23.0	3.2	1.44	1.83	13.4	16.1	17.3	18.0	18.8	15.5	16.0	16.5	17.2	23.3	0.98	4.1	2.6	2.46	3.12	1.52	1.75	0.88	0.98	3.34	30.3
b1bbac2	2	0.4	3.3	1650	0.86	0.99	7.1	12.4	4.6	0.90	1.00	6.6	8.1	8.9	8.4	9.9	7.5	7.8	8.2	8.7	12.1	0.99	5.2	4.2	2.19	2.43	0.39	0.47	0.4	0.48	1.43	60.2
b1bbac3	2	0.4	3.3	1700	0.97	1.06	9.3	16.3	5.3	0.99	1.14	8.5	10.5	11.6	12.2	12.9	9.8	10.2	10.7	11.3	15.5	1.00	5.6	4.2	2.12	2.44	0.81	1.18	0.47	0.56	2.22	61.0
b1bbac4	2	0.4	3.3	1750	1.07	1.22	11.7	19.0	5.0	1.11	1.28	10.7	13.0	14.2	14.8	15.6	12.3	12.7	13.2	13.9	19.0	0.97	5.6	4.2	2.12	2.44	1.29	1.55	0.81	0.71	2.82	49.4
b1bbac5	2	0.4	3.3	1600	1.16	1.40	13.9	21.3	4.5	1.20	1.42	12.6	14.9	16.1	16.7	17.4	14.1	14.5	15.0	15.7	21.9	0.91	5.8	4.0	2.11	2.50	1.6	1.82	0.95	1.09	3.02	38.5
b1cbaa1	2	0.5	3.3	1850	1.45	1.73	5.3	10.7	1.1	1.45	1.80	5.0	6.2	6.8	7.2	7.6	5.9	6.2	6.4	6.8	9.6	1.04	1.5	1.0	4.05	5.03	0.73	1.05	0.41	0.56	1.50	25.6
b1cbaa2	2	0.5	3.3	1900	1.74	2.05	7.9	14.7	1.2	1.76	2.05	7.7	9.4	10.2	10.6	11.1	9.0	9.3	9.7	10.1	13.0	1.00	1.6	1.2	3.96	4.62	0.97	1.22	0.65	0.7	2.34	37.1
b1cbaa3	2	0.5	3.3	1950	2.01	2.56	10.4	18.9	1.0	2.02	2.56	9.9	11.9	13.0	13.6	14.2	11.5	11.9	12.4	13.0	17.7	0.99	1.6	1.0	4.01	5.08	1.22	1.49	0.81	0.96	2.65	43.7
b1cbaa4	2	0.5	3.3	1950	2.17	2.80	12.6	24.9	1.0	2.14	2.80	12.7	15.5	16.8	17.4	18.2	15.0	15.5	16.1	16.8	22.5	1.00	1.8	1.0	3.75	4.91	1.35	1.67	0.91	1.03	2.91	46.1
b1cbab1	2	0.5	3.3	1800	0.87	1.05	4.8	10.2	2.8	0.89	1.06	4.7	5.7	6.3	6.6	7.0	5.4	5.6	5.8	6.2	8.9	1.00	3.8	2.7	2.56	3.05	0.3	0.37	0.32	0.38	0.90	61.2
b1cbab2	2	0.5	3.3	1850	1.03	1.29	7.8	13.9	3.0	1.04	1.28	7.4	8.8	9.6	10.1	10.7	8.4	8.7	9.1	9.5	13.9	0.94	4.4	2.9	2.39	2.94	0.66	0.85	0.5	0.58	1.77	48.8
b1cbab3	2	0.5	3.3	1800	1.21	1.46	10.2	17.3	3.1	1.20	1.48	9.8	11.8	13.0	13.6	14.2	11.3	11.7	12.2	12.8	18.0	0.86	4.4	2.9	2.39	2.95	1.36	1.62	0.88	1.05	2.71	31.9
b1cbab4	2	0.5	3.3	1850	1.34	1.85	14.3	24.0	3.4	1.33	1.63	13.6	16.4	17.9	18.7	19.6	15.8	16.3	16.9	17.8	23.7	0.99	4.9	3.3	2.25	2.76	1.37	1.64	0.8	0.86	3.26	40.0
b1cbab5	2	0.5	3.3	1850	1.45	1.80	15.2	24.3	3.0	1.47	1.80	14.6	17.1	18.6	19.3	20.3	18.3	16.9	17.6	18.4	24.1	0.97	4.3	2.9	2.40	2.84	1.71	2.1	1.02	1.21	3.82	39.3
b1cbac2	2	0.5	3.3	1700	0.87	0.95	7.0	11.6	5.0	0.89	0.98	6.5	8.0	8.8	8.2	9.6	7.5	7.8	8.1	8.6	12.2	1.02	5.3	4.3	2.18	2.40	0.58	0.76	0.57	0.69	1.27	41.1
b1cbac3	2	0.5	3.3	1700	0.97	1.15	9.6	17.0	4.6	1.00	1.17	9.1	10.7	11.7	12.2	12.9	10.1	10.5	10.9	11.5	17.9	0.96	5.8	4.3	2.07	2.42	0.96	1.23	0.67	0.79	1.97	39.2
b1cbac4	2	0.5	3.3	1750	1.07	1.25	11.9	19.3	4.9	1.10	1.25	11.1	13.3	14.6	15.4	16.3	12.6	13.0	13.6	14.4	21.1	0.97	5.9	4.6	2.08	2.34	1.42	1.65	0.78	1.02	2.65	37.4
b1cbac5	2	0.5	3.3	1800	1.15	1.42	13.7	21.4	4.4	1.20	1.42	12.6	15.3	16.7	17.3	18.2	14.5	15.0	15.6	16.4	22.2	0.87	5.8	4.0	2.11	2.50	1.69	1.97	1.11	1.27	3.18	55.9
b1aaaa3	2	0.3	1	2150	1.80	2.53	10.2	22.4	1.0	1.85	2.56	9.9	11.9	13.0	13.5	14.1	11.6	12.0	12.5	13.0	17.5	1.00	1.9	1.0	3.87	5.08	1.1	1.35	1.1	1.21	1.94	56.3
b1aaab3	2	0.3	1	1850	1.16	1.54	9.8	18.3	2.6	1.16	1.60	9.4	11.1	12.1	12.8	13.2	10.7	11.0	11.4	12.0	17.2	0.99	4.5	2.4	2.36	3.26	0.88	1.16	0.43	0.65	2.39	58.7
b1aaac3	2	0.3	1	1750	0.96	1.19	9.0	14.7	4.1	1.00	1.18	8.2	9.9	10.7	11.1	11.6	9.3	9.6	10.0	10.5	13.9	0.95	5.3	3.8	2.18	2.57	0.88	0.91	0.46	0.53	1.85	59.5
b1acaa3	2	0.3	10	2000	1.95	2.56	10.5	21.7	1.0	1.90	2.48	10.2	12.6	13.8	14.3	15.0	12.3	12.7	13.2	13.8	20.1	1.00	1.8	1.1	3.72	4.85	0.89	1.11	0.93	1.07	2.02	53.6
b1acab3	2	0.3	10	1750	1.24	1.46	10.4	18.3	3.1	1.22	1.46	9.8	11.6	12.5	12.9	13.4	11.1	11.4	11.8	12.3	18.4	0.91	4.2	2.9	2.43	2.91	1.13	1.33	0.5	0.7	2.44	46.9
b1acac3	2	0.3	10	1700	0.87	1.11	9.5	16.3	4.9	0.99	1.18	8.8	10.4	11.3	11.8	12.4	9.8	10.2	10.8	11.1	15.2	0.95	5.8	4.0	2.09	2.49	0.58	0.9	0.4	0.47	1.88	58.8
b1aaaa4	2	0.3	1	2200	1.92	2.70	12.8	23.3	1.1	1.93	2.70	12.0	14.1	15.0	15.5	16.0	13.8	14.2	14.5	15.0	18.9	0.94	2.1	1.1	3.48	4.87	1.2	1.46	0.0	1.23	2.14	42.4
b1aaab4	2	0.3	1	1950	1.26	1.70	11.6	18.5	2.6	1.28	1.65	10.8	12.8	13.7	14.2	14.7	12.4	12.8	13.2	13.7	17.9	0.98	4.4	2.5	2.40	3.14	1.3	1.48	0.85	0.92	2.54	117.5
b1aaac4	2	0.3	1	1850	1.07	1.30	11.2	17.4	4.2	1.12	1.31	10.3	12.2	13.1	13.5	14.0	11.7	12.0	12.4	13.0	17.6	0.93	5.3	3.8	2.18	2.55	1.14	1.38	0.55	0.68	2.40	48.0
b1acaa4	2	0.3	10	1850	2.15	2.84	12.8	25.7	1.0	2.15	2.84	12.0	14.7	15.7	16.2	16.8	14.2	14.6	15.1	15.6	20.4	1.00	1.7	1.0	3.88	5.12	0.9	1.14	0.81	0.9	2.39	49.5
b1acab4	2	0.3	10	1850	1.35	1.53	12.2	19.8	3.3	1.33	1.65	11.5	13.5	14.4	14.9	15.4	13.0	13.4	13.8	14.3	17.6	0.92	4.2	2.7	2.45	3.04	1.27	1.47	0.77	0.84	2.67	54.2
b1acac4	2	0.3	10	1750	1.09	1.31	12.0	18.0	4.5	1.10	1.31	10.8	12.8	13.6	14.0	14.5	12.2	12.6	13.0	13.4	17.9	0.90	5.7	4.0	2.09	2.49	1.08	1.23	0.48	0.63	2.50	55.1
b1caaa3	2	0.5	1	2100	1.86	2.47	10.1	20.4	1.1	1.86	2.47	9.7	11.7	12.9	13.5	14.2	11.4	11.8	12.3	13.0	18.3	1.05	1.8	1.0	3.73	4.95	1.27	1.8	0.87	1	2.87	51.0
b1caab3	2	0.5	1	1900	1.14	1.48	9.9	17.9	2.9	1.15	1.48	9.4	11.4	12.4	12.9	13.6	10.8	11.3	11.7	12.3	17.3	1.01	4.6	2.7	2.34	3.02	1.05	1.32	0.62	0.83	2.95	48.6
b1caac3	2	0.5	1	1700	0.97	1.14	9.3	16.6	4.6	1.00	1.14	8.5	10.3	11.2	11.8	12.5	9.6	10.0	10.4	11.0	15.1	1.00	5.4	4.2	2.14	2.44	0.95	1.25	0.58	0.69	1.95	35.0
b1ccaa3	2	0.5	10	1850	2.07	2.50	10.4	21.1	1.1	2.07	2.50	10.2	12.4	13.5	14.1	14.9	11.9	12.3	12.8	13.4	20.5	1.04	1.5	1.0	4.05	4.89	1.24	1.59	0.87	1	3.14	44.1
b1ccab3	2	0.5	10	1750	1.22	1.46	9.9	19.6	3.0	1.22	1.46	9.4	11.4	12.6	13.2	13.8	10.8	11.2	11.7	12.4	16.3	0.99	4.0	2.8	2.49	2.98	1.24	1.51	0.71	0.93	2.77	37.2

b1ccac3	2	0.5	10	1700	0.97	1.11	9.4	18.3	4.9	1.00	1.11	8.7	10.5	11.5	12.1	12.9	9.8	10.2	10.6	11.3	18.6	0.98	5.6	4.5	2.12	2.35	0.84	1.26	0.56	0.7	2.02	50.7
b1caaa4	2	0.5	1	2100	2.08	2.90	12.6	23.4	1.0	2.07	2.90	12.0	14.7	16.1	16.9	17.8	14.4	14.8	15.4	16.3	22.8	1.03	1.8	0.9	3.73	5.23	1.3	1.65	0.89	0.98	3.43	50.8
b1caab4	2	0.5	1	1900	1.27	1.65	12.1	21.7	2.8	1.29	1.65	11.7	13.8	15.2	15.9	16.9	13.3	13.7	14.3	15.1	22.3	1.00	4.5	2.8	2.36	3.01	1.45	1.74	0.91	1.01	3.32	42.5
b1caac4	2	0.5	1	1750	1.06	1.30	11.4	18.4	4.3	1.11	1.30	10.4	12.6	13.7	14.3	15.0	11.9	12.3	12.8	13.5	18.3	0.97	5.4	3.9	2.15	2.52	1.09	1.28	0.51	0.63	2.93	61.1
b1ccaa4	2	0.5	10	1850	2.28	2.84	12.9	27.3	1.0	2.25	2.84	12.5	15.8	17.5	18.3	19.4	15.2	15.7	16.4	17.4	23.8	1.11	1.6	1.0	3.98	5.02	1.35	1.73	0.93	1.08	2.96	46.1
b1ccab4	2	0.5	10	1820	1.35	1.62	12.2	22.9	3.0	1.35	1.55	11.8	14.1	15.3	16.0	16.7	13.4	13.9	14.4	15.2	21.4	0.98	4.1	3.1	2.46	2.82	1.51	1.83	0.93	1.06	3.32	53.6
b1ccac4	2	0.5	10	1750	1.08	1.27	11.9	20.5	4.7	1.10	1.27	10.8	13.0	14.2	14.8	15.5	12.4	12.8	13.3	14.0	19.4	0.96	5.7	4.3	2.09	2.41	1.46	1.69	0.9	1.15	2.81	61.9
a1abaa1	1.5	0.3	3.3	1850	1.46	1.77	5.1	10.3	1.0	1.47	1.83	4.9	5.9	6.5	6.8	7.2	5.7	5.9	6.1	6.4	9.5	0.98	1.5	0.9	5.53	6.89	0.57	0.71	0.21	0.26	1.32	55.6
a1abaa2	1.5	0.3	3.3	1950	1.68	2.05	7.4	13.5	1.1	1.68	2.05	7.3	8.7	9.5	9.9	10.4	8.4	8.7	9.1	9.5	12.9	1.02	1.7	1.1	5.18	6.32	0.85	1.04	0.9	1.1	1.36	29.2
a1abaa3	1.5	0.3	3.3	2000	1.90	2.50	9.9	22.7	1.0	1.93	2.56	9.6	11.9	13.1	13.7	14.3	11.5	11.9	12.4	13.1	17.3	1.02	1.7	0.9	5.19	6.88	0.81	0.95	0.86	0.95	2.38	59.4
a1abaa4	1.5	0.3	3.3	2050	2.02	2.75	13.1	28.3	1.1	2.06	2.75	12.0	14.4	15.5	16.1	16.6	14.0	14.4	14.9	15.5	19.8	1.01	1.8	1.0	4.95	8.61	0.88	1.16	0.98	1.06	2.71	48.5
a1abab1	1.5	0.3	3.3	1750	0.90	1.02	5.1	9.9	3.1	0.90	1.02	4.8	5.8	6.4	6.8	7.2	5.5	5.7	6.0	6.3	9.7	1.00	3.8	3.0	3.42	3.88	0.26	0.34	0.3	0.39	1.23	56.1
a1abab2	1.5	0.3	3.3	1820	1.05	1.20	7.3	14.0	3.2	1.06	1.25	6.9	8.4	9.2	9.6	10.0	8.0	8.3	8.6	9.1	14.8	0.97	3.9	2.8	3.36	3.96	1.01	1.23	0.41	0.54	2.07	49.5
a1abab3	1.5	0.3	3.3	1800	1.20	1.51	9.7	17.0	2.7	1.19	1.51	9.2	11.2	12.1	12.6	13.2	10.7	11.0	11.4	12.0	16.5	0.95	4.2	2.6	3.27	4.15	1.31	1.58	1.03	1.21	2.61	46.4
a1abab4	1.5	0.3	3.3	1850	1.32	1.60	12.0	19.0	3.0	1.31	1.60	11.3	13.4	14.3	14.9	15.4	12.9	13.3	13.7	14.3	18.8	0.94	4.2	2.8	3.25	3.96	1.27	1.49	0.94	1.01	2.91	59.1
a1abab5	1.5	0.3	3.3	1900	1.41	1.70	14.0	21.1	3.1	1.43	1.80	12.7	14.8	15.6	16.1	16.5	14.4	14.7	15.1	15.6	20.1	0.94	4.0	2.5	3.34	4.21	1.44	1.72	1.1	1.21	3.10	49.4
a1abac2	1.5	0.3	3.3	1650	0.86	0.97	6.6	11.5	4.5	0.88	0.97	6.2	7.6	8.3	8.7	9.2	7.1	7.4	7.7	8.1	10.8	1.00	5.1	4.2	2.84	3.25	0.43	0.61	0.46	0.53	1.56	46.4
a1abac3	1.5	0.3	3.3	1700	0.97	1.10	9.1	15.5	4.8	0.99	1.14	8.2	10.1	11.1	11.6	12.3	9.5	9.8	10.2	10.8	16.9	0.98	5.4	4.0	2.88	3.32	1.24	1.47	0.58	0.63	2.37	44.3
a1abac4	1.5	0.3	3.3	1750	1.07	1.25	11.6	17.6	4.8	1.11	1.28	10.3	12.2	13.2	13.7	14.2	11.7	12.0	12.4	13.0	18.0	0.91	5.4	4.0	2.88	3.32	1.69	1.9	1.34	1.42	2.62	51.8
a1abac5	1.5	0.3	3.3	1750	1.17	1.38	13.2	21.3	4.4	1.21	1.45	11.7	13.7	14.6	15.1	15.6	13.1	13.5	13.9	14.4	18.8	0.86	5.1	3.6	2.95	3.53	1.41	1.6	0.98	1.05	3.02	43.5
a1cbaa1	1.5	0.5	3.3	1850	1.46	1.77	5.3	10.7	1.1	1.47	1.77	5.1	6.4	7.0	7.4	7.8	6.0	6.3	6.6	6.9	10.8	1.02	1.5	1.0	5.42	6.53	0.69	1	0.27	0.33	1.62	35.7
a1cbaa2	1.5	0.5	3.3	1900	1.75	2.15	7.7	15.3	1.1	1.75	2.10	7.5	9.0	9.8	10.2	10.8	8.7	9.0	9.3	9.8	14.2	0.98	1.6	1.1	5.32	6.39	0.88	1.1	0.75	0.85	2.04	44.1
a1cbaa3	1.5	0.5	3.3	1950	1.99	2.56	10.4	20.0	1.0	1.98	2.56	10.2	12.4	13.6	14.2	15.0	12.0	12.4	12.9	13.5	18.8	0.98	1.7	1.0	5.16	6.68	1.03	1.26	0.92	1.08	2.34	39.1
a1cbaa4	1.5	0.5	3.3	2000	2.16	2.65	13.2	29.4	1.2	2.13	2.65	12.7	15.5	16.8	17.5	18.4	15.1	15.5	16.1	16.9	23.2	0.99	1.8	1.2	4.98	6.19	1.16	1.45	1.07	1.19	2.61	28.9
a1cbab1	1.5	0.5	3.3	1750	0.90	1.00	4.9	9.8	3.1	0.90	1.02	4.8	5.9	6.5	6.8	7.2	5.6	5.8	6.0	6.4	9.1	1.00	3.8	3.0	3.42	3.88	0.31	0.43	0.38	0.46	1.16	56.6
a1cbab2	1.5	0.5	3.3	1770	1.07	1.25	7.6	14.1	3.1	1.08	1.22	7.3	9.1	10.0	10.5	11.1	8.6	8.9	9.3	9.9	14.5	1.00	4.0	3.1	3.33	3.76	1.19	1.51	0.6	0.76	2.11	31.7
a1cbab3	1.5	0.5	3.3	1800	1.20	1.40	10.2	19.9	3.3	1.20	1.40	9.7	11.9	13.0	13.6	14.3	11.3	11.7	12.2	12.9	18.5	0.96	4.3	3.2	3.21	3.74	1.33	1.61	0.8	0.99	2.85	37.0
a1cbab4	1.5	0.5	3.3	1850	1.31	1.80	12.0	21.8	3.0	1.31	1.60	11.5	14.1	15.4	16.1	16.9	13.5	14.0	14.5	15.2	20.3	0.97	4.3	2.9	3.22	3.93	1.52	1.78	1.03	1.15	3.46	55.8
a1cbab5	1.5	0.5	3.3	1850	1.44	1.70	14.7	25.4	3.3	1.43	1.77	13.8	16.7	18.0	18.7	19.4	16.1	16.6	17.2	17.9	22.6	0.97	4.3	2.8	3.21	3.97	1.69	1.97	1.14	1.24	3.87	49.1
a1cbac2	1.5	0.5	3.3	1620	0.87	0.95	7.0	11.8	5.0	0.90	1.00	6.8	8.0	8.8	9.3	9.8	7.5	7.8	8.1	8.6	12.5	0.95	5.2	4.2	2.92	3.24	0.47	0.86	0.46	0.54	1.65	38.1
a1cbac3	1.5	0.5	3.3	1700	0.97	1.10	9.4	18.0	5.0	1.01	1.10	8.9	10.9	12.0	12.7	13.5	10.2	10.6	11.1	11.7	17.1	0.99	5.6	4.7	2.82	3.07	1.11	1.41	0.47	0.57	2.54	39.4
a1cbac4	1.5	0.5	3.3	1750	1.08	1.25	12.0	21.6	4.9	1.11	1.25	11.2	13.7	14.9	15.5	16.1	13.0	13.4	14.0	14.6	19.7	0.95	5.8	4.6	2.76	3.11	1.6	1.87	0.82	1.16	3.06	47.7
a1cbac5	1.5	0.5	3.3	1800	1.16	1.35	13.9	23.8	4.9	1.19	1.35	12.8	15.6	17.0	17.8	18.7	14.9	15.4	16.0	16.8	25.8	0.97	5.8	4.5	2.77	3.14	1.72	1.95	1.09	1.18	3.64	31.9
c1abaa1	3	0.3	3.3	1880	1.44	1.77	5.0	9.1	1.0	1.44	1.77	4.8	5.8	6.3	6.6	7.0	5.5	5.7	6.0	6.3	9.8	1.01	1.5	1.0	2.74	3.36	0.28	0.48	0.25	0.32	1.11	43.6
c1abaa2	3	0.3	3.3	1930	1.70	2.15	7.5	14.1	1.0	1.70	2.10	7.3	8.9	9.6	10.0	10.4	8.6	8.8	9.2	9.6	12.9	0.98	1.6	1.1	2.62	3.24	0.87	1.1	0.74	0.88	1.92	68.7
c1abaa3	3	0.3	3.3	1960	1.89	2.40	10.3	20.4	1.1	1.92	2.40	9.9	12.3	13.3	13.8	14.2	11.8	12.2	12.7	13.2	17.8	0.99	1.7	1.1	2.54	3.18	0.88	1.15	0.67	0.81	2.32	74.3
c1abaa4	3	0.3	3.3	2100	2.00	2.73	15.0	32.0	1.3	2.03	2.75	13.1	15.0	15.8	16.3	16.7	14.7	15.0	15.4	15.9	19.8	0.91	2.0	1.1	2.34	3.16	0.75	0.99	0.59	0.69	3.02	63.7
c1abab1	3	0.3	3.3	1770	0.88	0.98	5.0	10.1	3.3	0.89	0.98	4.8	5.7	6.3	6.6	7.0	5.4	5.6	5.9	6.2	8.7	0.97	3.9	3.2	1.69	1.86	0.27	0.32	0.44	0.52	0.76	110.2
c1abab2	3	0.3	3.3	1820	1.05	1.25	7.4	14.2	3.0	1.06	1.25	6.9	8.4	9.2	9.6	10.1	8.1	8.3	8.7	9.1	12.3	0.98	3.9	2.8	1.68	1.98	0.42	0.56	0.38	0.44	1.44	60.9
c1abab3	3	0.3	3.3	1800	1.20	1.42	9.9	16.9	3.1	1.19	1.42	9.2	11.2	12.1	12.6	13.2	10.7	11.0	11.5	12.0	16.2	0.98	4.2	2.9	1.63	1.95	0.74	0.96	0.51	0.6	2.20	43.0
c1abab4	3	0.3	3.3	1880	1.30	1.60	11.8	20.0	3.0	1.30	1.60	10.8	12.9	13.8	14.2	14.7	12.5	12.8	13.2	13.7	17.5	0.95	4.1	2.7	1.65	2.03	1.33	1.54	0.81	0.92	2.51	54.2
c1abab5	3	0.3	3.3	1900	1.42	1.77	14.0	21.1	2.9	1.40	1.77	12.5	14.6	15.5	15.9	16.4	14.2	14.6	15.0	15.5	19.8	0.92	4.1	2.6	1.65	2.09	1.09	1.35	0.61	0.68	2.95	63.0
c1abac2	3	0.3	3.3	1700	0.85	0.98	6.8	11.4	4.5	0.88	1.00	6.2	7.6	8.4	8.7	9.2	7.1	7.4	7.7	8.2	12.2	0.99	5.1	4.0	1.47	1.67	0.29	0.34	0.32	0.34	1.13	75.0
c1abac3	3	0.3	3.3	1720	0.96	1.11	9.2	15.5	4.8	0.99	1.14	8.2	10.0	10.8	11.2	11.7	9.5	9.8	10.2	10.6	14.0	0.85	5.4	4.0	1.44	1.66	0.74	0.86	0.67	0.77	1.42	38.2
c1abac4	3	0.3	3.3	1780	1.06	1.28	11.7	18.8	4.6	1.10	1.25	10.3	12.3	13.2	13.6	14.2	11.8	12.1	12.5	13.1	16.4	0.83	5.5	4.2	1.43	1.62	0.74	0.95	0.48	0.53	2.24	54.5
c1abac5	3	0.3	3.3	1770	1.15	1.45	13.3	18.9	4.1	1.19	1.46	11.7	13.7	14.6	15.0	15.7	13.2	13.5	13.9	14.4	19.1	0.88	5.3	3.5	1.45	1.78	1.14	1.3	0.63	0.7	2.52	43.4
c1cbaa1	3	0.5	3.3	1880	1.43	1.70	5.0	9.7	1.1	1.43	1.70	4.8	5.8	6.3	6.6	7.0	5.5	5.7	6.0	6.3	9.2	1.00	1.5	1.1	2.72	3.23	0.21	0.3	0.2	0.23	1.30	65.3
c1cbaa2	3	0.5	3.3	1900	1.75	2.10	7.9	17.0	1.1	1.76	2.10	7.6	9.3	10.3	10.8	11.5	8.9	9.2	9.6	10.2	16.5	1.05	1.6	1.1	2.66	3.17	0.99	1.34	0.61	0.74	2.64	49.8
c1cbaa3	3	0.5	3.3	1950	1.98	2.50	10.1	18.7	1.0	2.00	2.50	9.6	11.8	12.9	13.4	14.1	11.4	11.8	12.2	12.8	17.8	1.02	1.5	1.0	2.69	3.36	1.23	1.54	0.7	0.77	2.91	41.4
c1cbaa4	3	0.5	3.3	1950	2.16	2.65	12.9	24.6	1.2	2.17	2.75	12.4	15.3	16.9	17.7	18.6	14.8	15.3	16.0	16.9	22.6	1.06	1.7	1.1	2.57	3.25	1.69	2.1	1.11	1.3	3.57	52.3
c1cbab1*	3	0.5	3.3	1800	0.89	0.98	5.0	8.7	3.3	0.89	0.95	4.7	5.8	6.2	6.4	6.6	5.5	5.7	5.9	6.2	7.2	0.96	3.8	3.3	1.71	1.83	0.31	0.37	0.3	0.35	0.63	84.9
c1cbab2	3	0.5	3.3	1800	1.07	1.25	7.5	15.1	3.1	1.05	1.25	7.1	8.7	9.6	10.0	10.6	8.3	8.6	8.9	9.4	14.1	1.00	4.1	2.9	1.64	1.95	0.43	0.58	0.39	0.48	1.37	65.8
c1cbab3	3	0.5	3.3	1800	1.18	1.50	9.8	17.1	2.8	1.18	1.50	9.2	11.3	12.4	13.0	13.6	10.8	11.2	11.6	12.3	21.0	1.00	4.2	2.8	1.62	2.06	0.78	1.07	0.53	0.66	2.19	47.2
c1cbab4	3	0.5	3.3	1850	1.31	1.60	12.0	24.1	3.0	1.31	1.55	11.5	14.0	15.5	16.3	17.2	13.4	13.9	14.5	15.3	22.0	1.00	4.3	3.1	1.61	1.90	1.34	1.58	0.84	1	2.85	25.2
c1cbab5	3	0.5	3.3	1850	1.45	1.75	14.6	29.1	3.1	1.48	1.83	13.9	16.8	18.2	19.0	19.9	16.1	16.6	17.2	18.1	24.6	0.99	4.1	2.7	1.65	2.04	1.45	1.76	0.88	1.1	3.47	21.6
c1cbac2	3	0.5	3.3	1650	0.85	1.00	7.0	12.1	4.5	0.90	1.00	6.5	7.8	8.5	8.9	9.4	7.3	7.6	7.9	8.3	11.4	0.92	5.1	4.2	1.47	1.63	0.43	0.52	0.44	0.52	0.98	69.4
c1cbac3	3	0.5	3.3	1700	0.98	1.14	9.5	15.5	4.7	1.01	1.14	8.6	10.6	11.7	12.3	13.0	10.0	10.4	10.8	11.4	18.3	1.01	5.4	4.2	1.43	1.62	0.5	0.64	0.43	0.52	1.56	50.1
c1cbac4	3	0.5	3.3	1800	1.07	1.25	11.6	21.0	4.8	1.10	1.25	10.5	12.8	14.1	14.7	15.4	12.2	12.6	13.1	13.8	18.1	0.98	5.6	4.3	1.41	1.61	0.71	0.99	0.47	0.53	2.10	63.2
c1cbac5	3	0.5	3.3	1800	1.15	1.35	13.8	23.2	4.8	1.20	1.42	12.3	14.9	16.1	16.8	17.6	14.2	14.7	15.2	15.9	22.4	0.9	5.5	3.9	1.43	1.69	1.23	1.56	0.77	0.89	2.49	31.0

TEST PROGRAMME FOR POSITION 3

Test ID	cot a	h	gamma	N	OFFSHORE WAVES Tm0	Tp0	Hs0	Hmax0	sm0	LOCAL WAVES Tm	Tp	Hs	H1/10	H1/20	H1/30	H1/50	H250	H200	H150	H100	Hmax	GF	sm	sp	Im	Ip	WAVE FORCES Normal: F1/25	F1/250	45 deg down: F1/25	F1/250	Peak: F1/25	Theta
b3aba2	2	0.3	3.3	1950	1.72	2.25	7.7	16.5	1.0	1.70	2.23	7.5	9.1	9.9	10.4	10.9	8.8	9.1	9.4	9.9	12.8	1.04	1.7	1.0	3.88	5.09	1.68	2.24	0	1.77	2.55	346.2
b3aba3	2	0.3	3.3	2000	1.90	2.50	10.3	20.3	1.1	1.86	2.50	8.9	12.1	13.2	13.8	14.5	11.8	12.2	12.7	13.3	18.5	1.01	1.8	1.0	3.69	4.98	0	2.45	0.41	0.59	2.71	1.4
b3aba4	2	0.3	3.3	2050	2.04	2.70	12.7	27.0	1.1	2.07	2.84	12.0	14.2	15.1	15.5	16.0	13.8	14.2	14.6	15.1	18.8	0.94	1.8	1.0	3.73	5.12	0	2.6	0.24	0.3	2.89	55.1
b3aba5	2	0.3	3.3	1900	1.78	2.35	9.5	17.7	3.0	1.72	2.30	8.1	10.1	10.6	10.9	11.3	9.3	9.6	9.9	10.4	13.0	1.04	1.7	1.0	3.64	4.91	0	2.41	0.31	0.4	2.68	8.4
b3aba4	2	0.3	3.3	1850	1.32	1.75	12.5	19.2	3.0	1.30	1.63	11.6	13.5	14.4	14.9	15.4	13.1	13.4	13.8	14.4	18.5	0.91	4.4	2.8	2.38	2.99	2.2	2.44	0.79	0.97	2.51	356.2
b3aba3	2	0.3	3.3	1700	0.97	1.08	9.4	15.3	5.2	1.00	1.64	12.7	14.6	15.5	16.0	16.5	14.3	14.6	15.0	15.5	19.7	0.92	4.2	2.4	2.45	3.23	2.45	2.64	0	1.44	2.78	14.9
b3aba2	2	0.3	3.3	1900	1.42	1.84	13.5	21.4	2.6	1.40	1.84	12.7	14.6	15.5	16.0	16.5	14.3	14.6	15.0	15.5	19.7	0.93	5.4	4.7	2.14	2.31	0.48	0.73	0.22	0.35	0.90	6.8
b3aba5	2	0.3	3.3	1750	1.16	1.40	13.1	19.2	4.3	1.19	1.40	11.8	14.0	15.1	15.6	16.2	13.4	13.8	14.2	14.9	18.4	0.90	5.3	3.9	2.14	2.53	0.47	1.22	0.4	0.48	1.44	3.9
b3cba2	2	0.5	3.3	2000	1.74	2.10	8.7	16.7	1.3	1.75	2.10	8.5	10.0	10.8	11.4	12.0	9.7	10.0	10.4	11.0	15.0	0.99	1.8	1.2	3.75	4.50	2.24	2.33	0	1.02	2.32	5
b3cba3	2	0.5	3.3	1950	1.97	2.50	10.2	19.4	1.0	1.97	2.50	9.8	11.8	12.9	13.4	14.0	11.4	11.8	12.3	12.9	15.2	0.98	1.6	1.0	3.93	4.68	1.18	2.39	0.38	0.49	2.45	8.3
b3cba4	2	0.5	3.3	1900	2.21	2.90	12.7	23.8	1.0	2.20	2.70	12.5	15.1	16.5	17.2	18.0	14.5	15.0	15.6	16.4	23.7	1.00	1.7	1.1	3.89	4.77	0	2.27	0.2	0.28	2.59	14.1
b3cbab3	2	0.5	3.3	1830	1.19	1.46	10.2	20.1	3.1	1.19	1.46	9.8	12.0	13.2	13.8	14.6	11.4	11.8	12.3	13.0	18.6	1.01	4.4	2.9	2.37	2.91	1.51	1.83	0.76	0.82	1.79	0.1
b3cbab4	2	0.5	3.3	1870	1.31	1.60	12.1	22.1	3.0	1.31	1.60	11.5	13.9	15.2	15.9	16.8	13.3	13.8	14.4	15.1	21.9	0.99	4.3	2.8	2.41	2.95	1.51	1.98	0.38	0.43	2.13	6.6
b3cbab5	2	0.5	3.3	1700	1.45	1.75	14.5	24.9	3.0	1.46	1.77	13.8	16.6	18.0	18.6	19.5	15.7	16.3	16.9	17.7	29.3	0.99	4.1	2.8	2.46	2.98	1.12	2.02	0.31	0.45	2.39	8.5
b3cbac3	2	0.5	3.3	1700	0.99	1.14	9.6	17.4	4.7	1.01	1.09	8.8	10.7	11.8	12.4	13.1	10.1	10.4	10.9	11.5	17.2	0.96	5.5	4.7	2.13	2.30	0.52	1.07	0.52	0.64	1.64	1.2
b3cbac4	2	0.5	3.3	1750	1.07	1.28	11.9	20.0	4.7	1.10	1.25	10.8	13.2	14.4	15.1	16.0	12.5	13.0	13.5	14.2	19.8	0.98	5.7	4.4	2.09	2.38	1.19	1.64	0.48	0.59	1.65	2.4
b3cbac5	2	0.5	3.3	1750	1.15	1.33	13.8	23.0	5.0	1.19	1.40	12.8	15.1	16.3	17.0	17.7	14.4	14.8	15.4	16.1	20.8	0.93	5.7	4.1	2.09	2.46	0.85	1.81	0.44	0.51	1.99	5.9

Enclosure 1

Wave Group Analysis

by means of

The Hilbert Transform Technique

WAVE GROUP ANALYSIS BY MEANS OF THE HILBERT TRANSFORM TECHNIQUE

Internal note
19.02.95

Tue Hald
Hydraulics & Coastal Engineering Laboratory
Aalborg University, Sohngaardsholmsvej 57, DK-9000 Aalborg, Denmark
tel: +45 96 35 80 80, fax: +45 98 14 25 55, e–mail: tue.hald@civil.auc.dk

1 Introduction

A wave group is generally defined as a sequence of consecutive high waves in a random wave train.

In sea wave recordings, group formations of high waves occur from time to time. This phenomenon corresponds to a non-zero correlation between successive waves. Information concerning this correlation is of importance when reproducing waves in the laboratory in order to determine the response of the modeled structure. Normally, irregular waves are reproduced in accordance with a specific energy spectrum solely defining the distribution of the variance. The grouping of waves is determined by the distribution of the phases. Hitherto, independence between successive waves have been applied and the phases are treated as independent random variables, each with a uniform probability density on the interval $[0;2\pi]$ leading to a sea surface that is Gaussian distributed. However, if the waves during wave propagation become more non-linear there will be some coupling and thus dependence of the phases of the component waves at different frequencies, which eventually will modify the wave grouping.

To illustrate the effect of randomly assigned phases two wave trains are generated from the same energy spectrum. These two wave conditions are depicted in Figure 1.

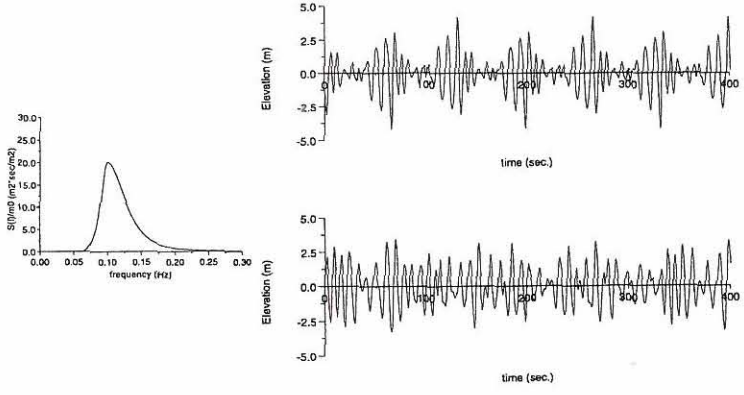

Figure 1: Wave energy spectrum and generated grouped and non-grouped wave trains.

Figure 1 shows different groupiness characteristics, and clearly it is important to have information on the wave grouping when coastal structures respond differ-

ently when exposed to the distinctive wave patterns. Especially, the stability of rubble mound structures appears to be significantly affected by the wave grouping, but also the slow drift oscillations of moored vessels is highly dependent on the wave grouping.

Burcharth (1979) and Johnson et al. (1978) found that the wave grouping significantly affects the stability of rubble mound breakwaters as well as the run-up. Johnson et al., (1978) compared the effects of a grouped and a non-grouped time series generated from the same energy spectrum, thus having the same statistical properties. Conclusively, the model tests showed that the breakwater response to the two different wave trains was quite different, with the grouped wave train causing severe damage and the non-grouped only causing minor rocking of the armour units. Similar significant influence on the wave grouping was found in the tests performed by Burcharth (1979).

In irregular seas, model tests by Spangenberg (1980) showed that the wave grouping has a significant influence on the slow drift motion of moored platforms and vessels. This influence might be explained by the fact that the period of the slow drift oscillations practically corresponds to the wave group period where the wave grouping is pronounced.

Both examples illustrate the importance of a correct modelling of natural sea waves in the laboratory if the structural responses are sensitive to the wave grouping. A characterization of the wave grouping seems therefore evident.

2 Description of wave groups

A measure of the wave grouping is obtained by defining the wave envelope to the time signal. Due to the presence of small waves in the signal the wave envelope is difficult to determine. However, if the time signal is squared, the squaring procedure will suppress the relative influence of the small waves present, and furthermore, a slowly varying part appears which may be interpreted as the square envelope.

Assuming that the sea surface elevation at a given point is a realization of a linear stationary Gaussian process defined by its one-sided spectrum $S_\eta(f)$, it can be represented by an ordinary sum of a finite number of waves

$$\eta(t) = \sum_{n=1}^{N} c_n \cos(\omega_n t + \varepsilon_n) \tag{1}$$

where c_n = amplitude, ω_n = cyclic frequency, and ε_n = phase angle. By squaring

the time signal following equation is obtained

$$\begin{aligned} \eta^2(t) &= \sum_{n=1}^{N}\sum_{m=1}^{N} c_n c_m \cos(\omega_n t + \varepsilon_n)\cos(\omega_m t + \varepsilon_m) && (2) \\ &= \sum_{n=1}^{N}\sum_{m=1}^{N} \{c_n c_m (\frac{1}{2}\cos((\omega_n + \omega_m)t + (\varepsilon_n + \varepsilon_m)) + \\ &\quad \frac{1}{2}\cos((\omega_n - \omega_m)t + (\varepsilon_n - \varepsilon_m)))\} && (3) \end{aligned}$$

Equation (3) represents a splitting of $\eta^2(t)$ into a slowly varying part (represented by the difference-frequencies) and a more rapid oscillating part (represented by the summation-frequencies).

By use of symmetry of the double summation, equation (3) can be expressed in terms of four separate contributions

$$\begin{aligned} \eta^2(t) &= \frac{1}{2}\sum_{n=1}^{N} c_n^2 + \frac{1}{2}\sum_{n=1}^{N} c_n^2 \cos(2\omega_n t + 2\varepsilon_n) \\ &\quad + \sum_{n=1}^{N}\sum_{m=n+1}^{N} c_n c_m \cos((\omega_n + \omega_m)t + (\varepsilon_n + \varepsilon_m)) \\ &\quad + \sum_{n=1}^{N}\sum_{m=n+1}^{N} c_n c_m \cos((\omega_n - \omega_m)t + (\varepsilon_n - \varepsilon_m))) \end{aligned} \tag{4}$$

The four terms on the right-hand side of equation (4) are identified as follows: The first term consists of a constant off-set component. The second and third term constitutes the superharmonic components, i.e. the summation-frequency terms, and the fourth term constitutes the subharmonic components, i.e. the difference-frequency terms. It is the latter that describes the slowly varying part of the squared time signal and the term which may be interpreted as the square envelope. By means of Bartlett filtering the superharmonic components on the right-hand side of equation (4) may be filtered out after subtraction of the constant off-set as done by Funke and Mansard (1979).

Funke and Mansard denoted the filtered square of the time signal the SIWEH (Smoothed Instantaneous Wave Energy History) function as the function provides a measure of the instantaneous wave energy in the time signal.

The effect of the Bartlett filtering corresponds to a digital low pass filtering and the efficiency of the SIWEH analysis can best be interpreted by examination of

the energy spectrum of the stochastic process in (1) and the energy spectrum of the squared process.

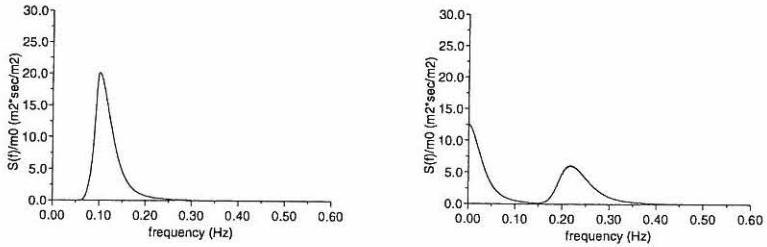

Figure 2: a) JONSWAP energy spectrum for a linear stochastic process and b) Energy spectrum for the squared process.

From Figure 2 it is understood that the SIWEH analysis does not exactly isolate the slowly varying part; also contributions from the superharmonic components occur and not the complete amount of energy from the subharmonic components is included. Only when the process is narrow-banded does the SIWEH analysis perform well but as the process becomes more and more broad-banded the SIWEH function is a poor estimator of the wave envelope, see Hudspeth and Medina (1988).

Instead of using a Bartlett window to isolate the subharmonic components, a wave envelope function defined on basis of the time series and its Hilbert transform isolates exactly the subharmonic components.

3 Hilbert transform technique

3.1 Theory

From the sea surface elevation $\eta(t)$ a conjugate signal $\hat{\eta}(t)$ is uniquely obtained by shifting the phase of each elementary harmonic component of $\eta(t)$ by $\pm\frac{\pi}{2}$. When the phase angles of all components of a given signal are shifted $\pm\frac{\pi}{2}$, the resulting function $\hat{\eta}(t)$ is known as the Hilbert transform of the original signal $\eta(t)$. The Hilbert transform is defined by

$$\hat{\eta}(t) = \frac{1}{\pi}\int_{-\infty}^{\infty}\frac{\eta(t)}{t-\tau}d\tau \tag{5}$$

From the definition of the Hilbert transform it is noted that $\hat{\eta}(t)$ is simply the convolution of $\eta(t)$ with a linear filter with the impulse response function $h(t) = \frac{1}{\pi t}$ [1]. Since a convolution of two functions in the time domain are transformed into a multiplication of their Fourier transforms in the frequency domain [2] a frequency response function $H(f)$ is related to the impulse response function. The frequency response function provides an equally characterization of the linear time-invariant input and output system in (5) and does furthermore visualize the effect of the Hilbert transform operation. Through the Fourier transform the frequency response of the Hilbert transformer becomes

$$H(f) = \mathcal{F}[\frac{1}{\pi t}] = -i\,\mathrm{sgn}(f) = \begin{cases} -i & f > 0 \\ 0 & f = 0 \\ i & f < 0 \end{cases} \tag{6}$$

The gain of this frequency response function is $\sqrt{\mathrm{re}^2(H(f)) + \mathrm{im}^2(H(f))}$ resulting in unity in magnitude, and thus, the amplitudes of the signal does not change. The phase angle is $\arctan(\frac{\mathrm{im}(H(f))}{\mathrm{re}(H(f))})$ resulting in a phase angle of $-\frac{\pi}{2}$ for $f > 0$ and $+\frac{\pi}{2}$ for $f < 0$. Such a system is denoted an ideal 90-degree phase shifter.

Consequently, applying the Hilbert transform operation to the sea surface eleva-

[1] The convolution of two functions, denoted $g(t) * h(t)$, is defined

$$g(t) * h(t) \equiv \int_{-\infty}^{\infty} g(\tau)h(t-\tau)d\tau$$

[2] The convolution theorem

$$g(t) * h(t) \Leftrightarrow G(f)H(f)$$

tion in (1) the cosine function simply shifts to the sine function

$$\hat{\eta}(t) = \sum_{n=1}^{N} c_n \sin(\omega_n t + \varepsilon_n) \tag{7}$$

Associated with the Hilbert transform is the complex analytical signal defined from the original signal $\eta(t)$ and the Hilbert transform $\hat{\eta}(t)$

$$\begin{aligned} \tilde{\eta}(t) &= \mid \tilde{\eta}(t) \mid \exp(i\psi(t)) = \mid \tilde{\eta}(t) \mid \cos(\psi(t)) + i \mid \tilde{\eta}(t) \mid \sin(\psi(t)) \\ &= \eta(t) + i\hat{\eta}(t) \end{aligned} \tag{8}$$

where the envelope or the modulation $\mid \tilde{\eta}(t) \mid = \sqrt{\eta^2(t) + \hat{\eta}^2(t)}$ and the associated phase $\psi(t) = \arctan(\frac{\hat{\eta}(t)}{\eta(t)})$. The properties of the Hilbert transform operation entail that the slowly varying difference-frequency terms in the second order expression $\eta^2(t)$ are separated mathematically by the expression

$$E(t) \equiv \mathrm{re}(\tilde{\eta}^*(t)\tilde{\eta}(t)) = \mid \tilde{\eta}(t) \mid^2 \tag{9}$$

where $\tilde{\eta}^*(t)$ = the complex conjugate and $E(t)$ = the square wave envelope function.

In order to visualize the effect of the defined envelope function the Hilbert transform of the sea surface elevation is squared and rewritten by use of trigonometry and symmetry of the double summation similar to $\eta^2(t)$

$$\hat{\eta}^2(t) = \sum_{n=1}^{N}\sum_{m=1}^{N} c_n c_m \sin(\omega_n t + \varepsilon_n)\sin(\omega_m t + \varepsilon_m) \tag{10}$$

$$= \sum_{n=1}^{N}\sum_{m=1}^{N} \{c_n c_m (\frac{1}{2}\cos((\omega_n - \omega_m)t + (\varepsilon_n - \varepsilon_m)) - \frac{1}{2}\cos((\omega_n + \omega_m)t + (\varepsilon_n + \varepsilon_m)))\} \tag{11}$$

$$= \frac{1}{2}\sum_{n=1}^{N} c_n^2 - \frac{1}{2}\sum_{n=1}^{N} c_n^2 \cos(2\omega_n t + 2\varepsilon_n) - \sum_{n=1}^{N}\sum_{m=n+1}^{N} c_n c_m \cos((\omega_n + \omega_m)t + (\varepsilon_n + \varepsilon_m)) + \sum_{n=1}^{N}\sum_{m=n+1}^{N} c_n c_m \cos((\omega_n - \omega_m)t + (\varepsilon_n - \varepsilon_m)) \tag{12}$$

Remembering that the squared time signal is given by (4), the square wave envelope function, according to (9), then becomes

$$E(t) = \sum_{n=1}^{N} c_n^2 + 2\sum_{n=1}^{N}\sum_{m=n+1}^{N} c_n c_m \cos((\omega_n - \omega_m)t + (\varepsilon_n - \varepsilon_m)) \tag{13}$$

Introducing $\frac{1}{\sqrt{2}}$ in the complex analytical signal $\tilde{\eta}(t) = \frac{1}{\sqrt{2}}(\eta(t) + i\hat{\eta}(t))$ leads to the definition of an envelope function which may be interpreted as half the square envelope.

$$E(t) = \mid \tilde{\eta}(t) \mid^2 = \frac{1}{2}(\eta^2(t) + \hat{\eta}^2(t)) \tag{14}$$

This envelope function isolates exactly the slowly varying part of the squared time signal plus the constant off-set similar to what approximately is achieved by the SIWEH analysis.

The present method seems to be more convenient than the SIWEH analysis and it does not require the narrow-band spectrum assumption. The disadvantage of this method is however that the sea surface must be described by a linear model.

3.2 Computation of half the square envelope

To compute the Hilbert transform numerically the continuous-time convolution integral in (5) is approximated by a discrete-time Hilbert transformation. Furthermore, as the Hilbert transformation is non-banded, approximations limiting the impulse response function are made. A tool to handle the ideal Hilbert transformation of the sea surface elevation is by using FIR approximations. In such approximations the 90-degree phase shift is conserved exactly.

The principle in the FIR approximation is that the convolution integral in (5) is represented by a summation over a finite number of coefficients where the coefficients are fitted to represent the impulse response function. Taking an even number of coefficients, easily extended to an odd number, the non-causal FIR approximation can be written

$$\hat{\eta}_j = \sum_{k=-N_c/2}^{N_c/2-1} c_k \eta_{j-k} = \sum_{k=0}^{N_c-1} c_k \eta_{j+k-N_c/2} \tag{15}$$

where c_k = the k'th coefficient, N_c = number of coefficients or filter length, $\hat{\eta}_j$ is the Hilbert transform corresponding to the time step j, and $\eta_{j+k-N_c/2}$

are the input elevations to the filter system. The reason why the index on the filter coefficients remain unchanged is that the coefficients are mirrored in the Nyquist frequency, i.e. the frequency corresponding to half the filter length. The coefficients are derived from the frequency response function by FFT to obtain a least-square fit of the coefficients. Opposite the centered format definition of the Fourier transformation, the FFT is based on a one-sided format

$$c_k = \frac{1}{N_c} \sum_{j=0}^{N_c-1} X_j \exp(i\omega_j k\Delta t) = \frac{1}{N_c} \sum_{j=0}^{N_c-1} X_j \exp(i\frac{2\pi jk}{N_c}) \tag{16}$$

where ω_j is the cyclic frequency corresponding to the j'th coefficient and X_j is the desired sampled frequency response of the system. By using the one-sided format a time delay corresponding to half the filter length is introduced

$$\tau = \frac{N_c}{2}\Delta t \tag{17}$$

The corresponding phase delay may then be found as

$$\psi_\tau = \tau\omega_j = \tau\frac{2\pi j}{N_c\Delta t} = \pi j \tag{18}$$

To compensate for the phase delay the original frequency response function given by (6) only needs to be multiplied by a linear phase shift operator $\exp(-i\pi k)$ and X_j might be interpreted as

$$X_j = H(f_j)\exp(-i\pi j) = G(f_j)\cos(\psi_j - \pi j) + iG(f_j)\sin(\psi_j - \pi j) \tag{19}$$

where $G(f_j)$ is the gain of the input amplitude to equal the output amplitude and $\psi_j - \pi j$ is the phase difference between the input and the output signal.

To sample the frequency response function the frequency band is subdivided into N_c discrete frequencies where $f_j = j\frac{f_s}{N_c}$ and f_s is the sample frequency. Since the phase $\psi_j = -\frac{\pi}{2}$ for $0 < f_j < f_{Nq}$ and $\psi_j = \frac{\pi}{2}$ for $f_{Nq} < f_j < 2f_{Nq}$ the sampled discrete frequency response function becomes

$$H(f_j) = \begin{cases} G(f_j)\cos(-\frac{\pi}{2} - \pi j) + iG(f_j)\sin(-\frac{\pi}{2} - \pi j) & 0 < f_j < f_{Nq} \\ 0 & f_j = 0, f_{Nq} \\ G(f_j)\cos(-\frac{\pi}{2} - \pi j) - iG(f_j)\sin(-\frac{\pi}{2} - \pi j) & f_{Nq} < f_j < 2f_{Nq} \end{cases} \tag{20}$$

Due to the truncation of the Fourier transformation, the filter frequency response will differ from the desired frequency response. To illustrate the effect of the

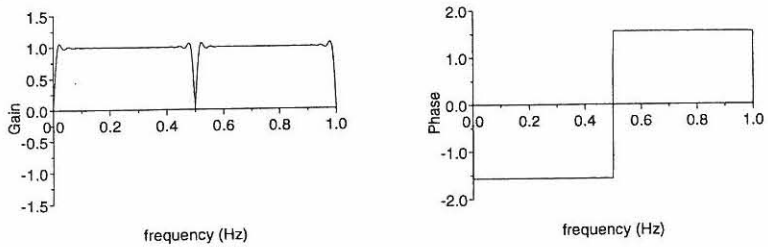

Figure 3: Gain and phase characteristic of linear FIR Hilbert filter with a filter length $N_c = 64$ and $f_s = 1.0$ Hz.

least-square fit, both the gain and phase characteristic of a linear FIR Hilbert filter are plotted in Figure 3.

To compare the FIR approximated Hilbert transform with the theoretical Hilbert transform an irregular time signal is generated from the JONSWAP spectrum and the two transforms are depicted in Figure 4. Generally very good accordance is observed also at the edges where a zone of half the filter length normally is disturbed.

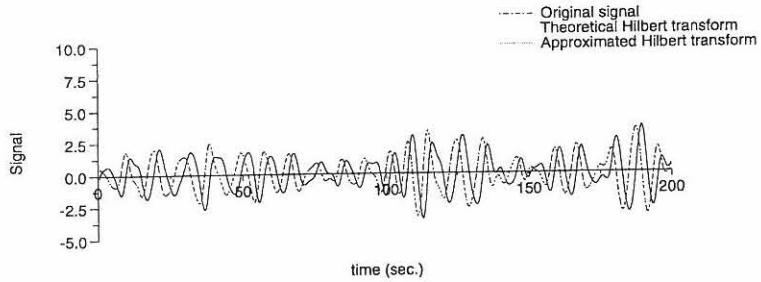

Figure 4: Comparison of theoretical and FIR approximated, $N_c = 64$, Hilbert transform. The signal is generated from the JONSWAP spectrum, $f_p = 0.1$ Hz and $\gamma = 3.3$.

To illustrate the envelope function, $E(t)$ is plotted together with half the squared elevation in Figure 5 for a time signal generated from the JONSWAP spectrum.

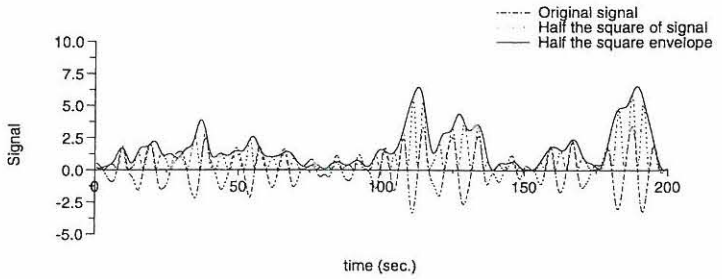

Figure 5: Comparison of half the square envelope $E(t)$ and $\frac{1}{2}\eta^2(t)$ for signal generated from a JONSWAP spectrum, $f_p = 0.1$ Hz, $\gamma = 3.3$, and $N_c = 64$.

4 Groupiness factor

To characterize the actual groupiness of a wave train the energy spectrum $S_{\hat{\eta}}(f)$ of half the square envelope function can be evaluated. However, a simpler measure is the groupiness factor that is defined as the standard deviation of half the square envelope relative to the variance of the original time signal

$$GF = \frac{\sigma[E(t)]}{\sigma^2[\eta(t)]} \tag{21}$$

For a monochromatic (sinusoidal) signal the envelope function $E(t)$ is constant leading to a groupiness factor $GF = 0$. Taking a completely Gaussian signal the expected value of the groupiness factor can be shown to be equal to 1.0 independent of the spectrum shape. The actual values for time signals generated from a JONSWAP spectrum including approximately 500 periods are approximately 1.0 in mean with a standard deviation of approximately $\sigma = 0.13$.

Instead of computing one value of the groupiness factor over the complete length of the time signal, the groupiness factor can be evaluated as instantaneous values by computing an average groupiness factor over a time moving window. The length of the window in time is dependent on the desired degree of smoothing of the computed groupiness factor function.

In Figure 6 to Figure 9 the groupiness factor function is plotted for both a narrow-banded and a broad-banded JONSWAP spectrum for two different window sizes.

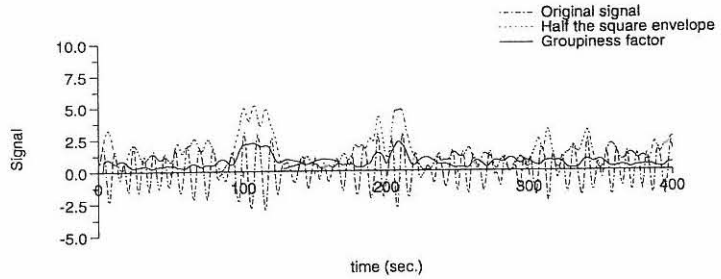

Figure 6: Groupiness factor function GF(t) for signal generated from JONSWAP spectrum, $f_p = 0.1$ Hz, $f_s = 1.0$ Hz, $\gamma = 10.0$, $N_c = 64$, and window size = T_m.

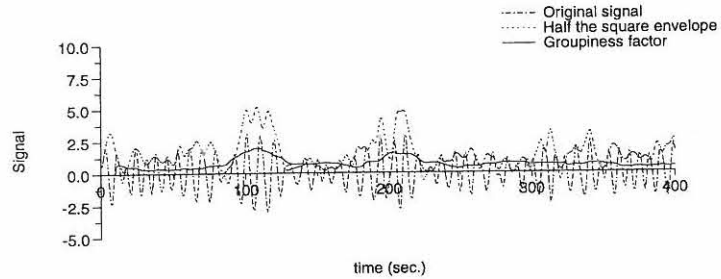

Figure 7: Groupiness factor function GF(t) for signal generated from JONSWAP spectrum, $f_p = 0.1$ Hz, $f_s = 1.0$ Hz, $\gamma = 10.0$, $N_c = 64$, and window size = $3T_m$.

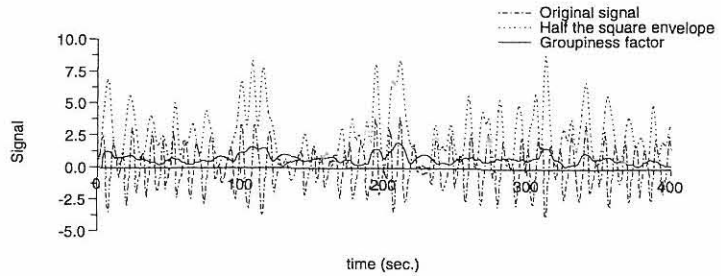

Figure 8: Groupiness factor function GF(t) for signal generated from JONSWAP spectrum, $f_p = 0.1$ Hz, $f_s = 1.0$ Hz, $\gamma = 1.0$, $N_c = 64$, and window size = T_m.

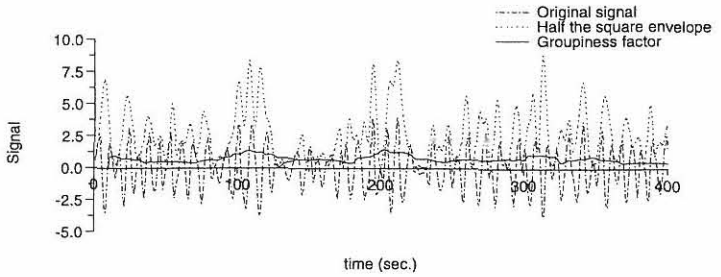

Figure 9: Groupiness factor function GF(t) for signal generated from JONSWAP spectrum, $f_p = 0.1$ Hz, $f_s = 1.0$ Hz, $\gamma = 1.0$, $N_c = 64$, and window size = $3T_m$.

Generally, a more smooth groupiness factor function is obtained for a window size of 3 mean periods and only the largest wave groups are separated as high and smooth peaks. It should though be noted that the sample frequency is 1.0 Hz and that a higher sample frequency eventually will lead to smoother groupiness factor function for smaller window sizes.

5 Conclusions and further use

Based on a linear assumption a method for calculating the instantaneous wave energy history and the groupiness factor function has been presented. The method is based on a temporal Hilbert filter and this approach enables an exact isolation of the 2nd order subharmonics which describe the slowly varying part of the time signal. This Hilbert filter approach is thus more efficient than the SIWEH analysis. The groupiness factor has proven to be ineffective in describing Gaussian distributed sea surfaces and the groupiness factor function is defined. Also discussions regarding the implementation of the Hilbert filter using FIR approximations and choice of window sizes for computing the groupiness factor functions are made.

The method can easily be extended to a three-dimensional motion but a physical interpretation of the more slowly varying part must then be revised.

The groupiness factor function enables computations of instantaneous groupiness factors in time and hence, the function is suitable for comparing the correlation between the damage development of e.g. a breakwater and the wave grouping in the wave train causing the damage.

A further application is the possibility to evaluate the change in wave grouping due to shoaling and thus also the change in phase distribution from deep to shallow water.

6 References

Bose, N.K., (1985), *Digital Filters; Theory and Applications*, Elsevier Science Publishing B.V., The NetherLands, 1985.

Burcharth, H.F. (1979), *The Effect of Wave Grouping on On-Shore Structures*, Coastal Engineering, No. 2, pp. 189-199.

Funke, E.R., Mansard, E.P.D. (1979), *On The Synthesis of Realistic Sea States in a Laboratory Flume*, Technical Report, LTR-HY-66, National Research Council of Canada, Hydraulics Laboratory, Ottawa, 1979.

Hudspeth, R.T., Medina, J.R. (1988), *Wave Group Analysis by the Hilbert Transform*, Proceedings, 21st ICCE, 1988, Torremolinos, pp. 884-898.

Johnson, R.R., Mansard, E.P.D., Ploeg, J. (1978), *Effects of Wave Grouping on Breakwater Stability*, Proceedings, 16th ICCE, 1978, Hamburg, pp. 2228-2243.

Karl, J.H. (1989), *An Introduction to Digital Signal Processing*, Academic Press Ltd., 1989.

Oppenheim, A.V., Schafer, R.W. (1989), *Discrete-Time Signal Processing*, Prentice-Hall International, Inc., 1989.

Rye, H. (1982), *Ocean Wave Groups*, Report UR-82-18, Department of Marine Technology, Norwegian Institute of Technology, 1982.

Spangenberg, S. (1980), *The Effect of Wave Grouping on Slow Drift Oscillations of an Offshore Structure*, Bulletin No. 46, Danish Ship Research Laboratory, 1980.

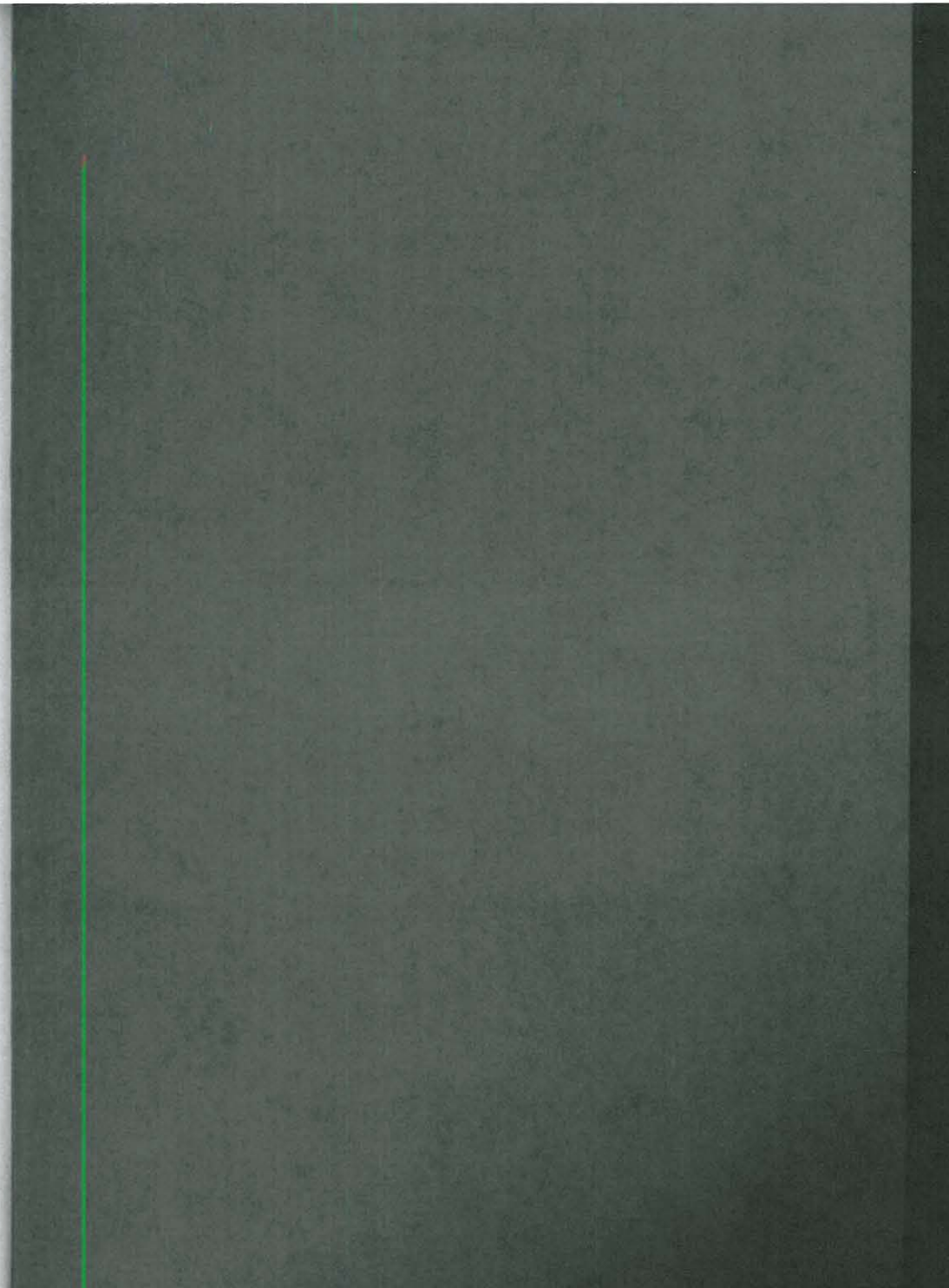

Hydraulics & Coastal Engineering Laboratory
Aalborg University
Series Paper No. 18
ISSN 0909-4296